

Electronic Theses and Dissertations, 2004-2019

2013

Design Optimization Of Llc Topology And Phase Skipping Control Of Three Phase Inverter For Pv Applications

Utsav Somani
University of Central Florida

 Part of the [Electrical and Electronics Commons](#)
Find similar works at: <https://stars.library.ucf.edu/etd>
University of Central Florida Libraries <http://library.ucf.edu>

This Masters Thesis (Open Access) is brought to you for free and open access by STARS. It has been accepted for inclusion in Electronic Theses and Dissertations, 2004-2019 by an authorized administrator of STARS. For more information, please contact STARS@ucf.edu.

STARS Citation

Somani, Utsav, "Design Optimization Of Llc Topology And Phase Skipping Control Of Three Phase Inverter For Pv Applications" (2013). *Electronic Theses and Dissertations, 2004-2019*. 2885.
<https://stars.library.ucf.edu/etd/2885>

DESIGN OPTIMIZATION OF LLC TOPOLOGY AND PHASE SKIPPING
CONTROL OF THREE PHASE INVERTER FOR PV APPLICATIONS

by

UTSAV SOMANI
B.S. University of Pune, India, 2010

A thesis submitted in partial fulfillment of the requirements
for the degree of Master of Science
in the Department of Electrical Engineering and Computer Science
in the College of Engineering and Computer Science
at the University of Central Florida
Orlando, Florida

Summer Term
2013

Major Professor: John Shen and Issa Batarseh

© 2013 Utsav Somani

ABSTRACT

The world is heading towards an energy crisis and desperate efforts are being made to find an alternative, reliable and clean source of energy. Solar Energy is one of the most clean and reliable source of renewable energy on earth. Conventionally, extraction of solar power for electricity generation was limited to PV farms, however lately Distributed Generation form of Solar Power has emerged in the form of residential and commercial *Grid Tied Micro-Inverters*. Grid Tied Micro-Inverters are costly when compared to their string type counterparts because one inverter module is required for every single or every two PV panels whereas a string type micro-inverter utilizes a single inverter module over a string of PV panels. Since in micro-inverter every panel has a dedicated inverter module, more power per panel can be extracted by performing optimal maximum power tracking over single panel rather than over an entire string of panels. Power per panel extracted by string inverters may be lower than its maximum value as few of the panels in the string may or may not be shaded and thereby forming the weaker links of the system.

In order to justify the higher costs of Micro-Inverters, it is of utmost importance to convert the available power with maximum possible efficiency. Typically, a micro-inverter consists of two important blocks; a Front End DC-DC Converter and Output DC-AC Inverter. This thesis proposes efficiency optimization techniques for both the blocks of the micro-inverter.

Efficiency Optimization of Front End DC-DC Converter

This thesis aims to optimize the efficiency of the front end stage by proposing optimal design procedure for resonant parameters of LLC Topology as a Front End DC-DC Converter for PV Applications. It exploits the I-V characteristics of a solar panel to design the resonant parameters such that resonant LLC topology operates near its resonant frequency operating point which is the highest efficiency operating point of LLC Converter.

Efficiency Optimization of Output DC-AC Inverter

Due to continuously variable irradiance levels of solar energy, available power for extraction is constantly varying which causes the PV Inverter operates at its peak load capacity for less than 15% of the day time. Every typical power converter suffers through poor light load efficiency performance because of the load independent losses present in a power converter. In order to improve the light load efficiency performance of Three Phase Inverters, this thesis proposes *Phase Skipping Control* technique for Three Phase Grid Tied Micro-Inverters. The proposed technique is a generic control technique and can be applied to any inverter topology, however, in order to establish the proof of concept this control technique has been implemented on Three Phase Half Bridge PWM Inverter and its analysis is provided. Improving light load efficiency helps to improve the CEC efficiency of the inverter.

Dedicated to my Late Grandfather

Shri. Nandlal Jechand Somani

ACKNOWLEDGMENTS

I have always believed that whatever we have; is what we have earned. It is our hard work that would help us grow and nothing else. However, my experience during my days at Florida Power Electronics Center has led me to make an amendment in my beliefs which is that apart from one's hard work and initiative, it is the support from your family, friends, colleagues and teachers that helps you achieve different milestones in life. I would like to use this space to express my gratitude to all those people who directly or indirectly have helped me to achieve on of the milestones of my life.

First of all, I would like to thank Dr. John Zheng Shen & Dr. Issa Batarseh for giving me an opportunity to contribute to this highly distinguished research group. I am deeply grateful to my seniors, Lin Chen and Dr. Haibing Hu, whose positive recommendations helped me secure a position of Research Assistant at Florida Power Electronics Center. It was a great honor to be a part of such an elite research group.

I am highly grateful to my other senior colleagues Anna Grishina, Ahmadreza Amirahmadi, Dr. Qian Zhang and Dr. Xiang Fang for being patient and helping me throughout my time at FPEC. All the skills that I have acquired at FPEC; my colleagues have played a major role in helping me acquire them. I would also like to thank my supervisor Jesus Barrios for helping me to learn different lab equipment and develop the right laboratory practices while performing experiments.

I am thankful to my committee members Dr. Issa Batarseh, Dr. Thomas Wu and Dr. Alireza Seyedi who gave me their guidance, support and their expert judgment during the completion of my thesis.

Of all the people we meet in our lifetime, there are only a handful people to whom you can give the title *Guru*. I have been very fortunate to meet one such person at FPEC in such an early phase of my life, my true mentor, Charles Jourdan. I cannot thank him enough for being ridiculously patient with me during the course of my *Master's Thesis*. Everything I learnt about Power Electronics Design at FPEC, I owe it to him.

Another such a pair of *Gurus* which I was endowed with by birth is my parents. All of my achievements are the culmination of qualities like honesty, perseverance and sincerity which I tried to inherit from my parents. No words can measure the sacrifice and hard work of theirs in making me the person who I am today.

Finally, I am grateful to family, friends, *special* friends and every single person who has nurtured, educated and supported me.

TABLE OF CONTENTS

LIST OF FIGURES.....	xii
LIST OF TABLES.....	xvi
CHAPTER 1: INTRODUCTION.....	1
1.1 Global Energy Trends	1
1.2 Renewable Energy Trends.....	4
1.3 Solar Power Trends	5
1.4 Types of PV Systems.....	7
1.4.1 Off Grid PV Systems (Standalone PV Systems).....	7
1.4.2 Grid Tied PV Systems	8
1.5 Grid Tie Inverter Architectures	10
1.5.1 Central Type Inverters	10
1.5.2 String Type Inverter	12
1.5.3 Multi-String Type Inverter	14
1.5.4 AC Module Type Inverter – Micro-Inverters.....	15
1.6 Comparative Review of Existing Single Phase Micro-Inverters in the market ..	17
1.7 Micro-Inverters for Three Phase Applications	19
1.7.1 Existing 3 Phase Configurations using Single Phase Micro-inverters.....	19
1.8 Three Phase Micro-Inverter	21

1.9	Objective and Outline of the Thesis	23
1.10	References	25
CHAPTER 2: DESIGN OPTIMIZATION OF LLC TOPOLOGY FOR PV APPLICATIONS		
.....		27
2.1	PV Panel Characteristics	28
2.1.1	Observations from Solar Panel's I-V and P-V Curves:	33
2.2	Full Bridge LLC Resonant Converter:	33
2.2.1	LLC Converter FHA Analysis.....	35
2.2.2	Operating Modes of LLC Converter.....	39
2.2.3	Discussion on Design considerations of LLC Converter as front end DC-DC Converter of Micro-Inverter	48
2.3	Design Procedure for Resonant Parameters of LLC Converter as Front End DC-DC Converter of Micro-inverter.....	50
2.3.1	Deriving the Design Specifications	50
2.3.2	Calculating Resonant Parameters	51
2.3.3	Design Example	54
2.4	References.....	58
CHAPTER 3: LIGHT LOAD EFFICIENCY IMPROVEMENT OF THREE PHASE GRID TIED INVERTERS.....		60

3.1	Daily Solar Irradiance Pattern	60
3.2	Significance of Weighted Efficiency for PV Inverters.....	64
3.3	Efficiency Behavior in Power Converters	66
3.4	Half Bridge PWM Inverter	69
3.4.1	Half Bridge Inverter Operation:.....	71
3.4.2	Loss Analysis of Half Bridge Inverter:.....	78
3.4.3	Loss Model of Half Bridge Inverter:	84
3.4.4	Verification of Loss Model.....	87
3.5	Phase Skipping Control of Three Phase Micro-Inverter	91
3.5.1	Concept	91
3.5.2	Implementation of Phase Skipping Control for Three Phase Grid Tied Micro-Inverters	93
3.5.3	Experimental Results of Phase Skipping Control	95
3.5.4	Avoiding Phase Power Imbalance due to Phase Skipping	98
3.6	References.....	100
CHAPTER 4: CHAPTER FOUR: CONCLUSIONS AND FUTURE WORK.....		103
4.1	Conclusions.....	103
4.2	Future Work	107
4.2.1	Future Work for LLC Converter as front end DC-DC Converter	107

4.2.2 Future Work for Phase Skipping Control 108

LIST OF FIGURES

Figure 1-1 Impact of Population and GDP on Global Energy Demand	2
Figure 1-2 Trends of Shares of World Primary Energy	3
Figure 1-3 Global New Investment in Renewable Energy: Developed vs Developing Countries, 2004-2011, \$BN Source: Bloomberg New Energy Finance	4
Figure 1-4 Global New Investment in Renewable Energy by Sector, 2011, And Growth on 2010, \$BN.	5
Figure 1-5 Off Grid PV System Architecture.....	7
Figure 1-6 Grid Tie PV System	9
Figure 1-7 Central Type PV Inverter Architecture	11
Figure 1-8 String Type Inverter Architecture	13
Figure 1-9 Multi-String Type Inverter.....	14
Figure 1-10 AC Module Type Inverter Architecture	15
Figure 1-11 Single Phase Micro-Inverter Connected to Three Phase Grid	20
Figure 1-12 Block Diagram of Three Phase Micro-Inverter	21
Figure 2-1 Block Diagram - Grid Tied Micro-Inverter.....	27
Figure 2-2 Single Diode Equivalent Model of PV Panel	29
Figure 2-3 I-V & PV Characteristics of PV Panel.....	30
Figure 2-4 I-V Curves of Solar Panel with Varying Temperature and Irradiance Level .	31
Figure 2-5 P-V Curves of Solar Panel with Varying Temperature and Irradiance Level	32
Figure 2-6 Block Diagram of Resonant Converter Topology	34
Figure 2-7 Full Bridge LLC Converter.....	35

Figure 2-8 AC Equivalent Circuit of LLC Converter	36
Figure 2-9 Derivation of AC Equivalent Impedance	36
Figure 2-10 LLC Converter Gain Curves ($L_n=2$)	38
Figure 2-11 Waveforms for Zone 1- $f_{co} \leq f_{sw} \leq f_o$	41
Figure 2-12 Equivalent Circuits of Operation Modes of LLC Converter in Zone 1 - $f_{co} \leq f_{sw} \leq f_o$	42
Figure 2-13 Waveforms of Zone 2- $f_{sw} = f_o$	44
Figure 2-14 Waveforms of Zone 3 – $f_{sw} > f_o$	46
Figure 2-15 Equivalent Circuits of Operation Modes of LLC Converter in Zone 3 - $f_{sw} > f_o$	47
Figure 2-16 Optimal Design Consideration for LLC Converter as front DC-DC converter of Micro-Inverter	49
Figure 2-17 Normalized Gain, M vs Quality Factor, Q_e	52
Figure 2-18 Gain vs Switching Frequency-Fixed Q_e -Variable L_n	53
Figure 2-19 Full Bridge LLC Converter as Front End DC-DC Converter for Micro- Inverter	54
Figure 2-20 Gain vs. Switching Frequency, Design Example.....	56
Figure 2-21 PV Panel Power vs. Switching Frequency for LLC Converter as front end DC-DC Converter, design example	57
Figure 2-22 Experimental Results - Efficiency, design example.....	57
Figure 3-1 Solar Irradiance Pattern on a Typical Day.....	60
Figure 3-2 Solar Irradiance Patterns – Clear Days.....	62

Figure 3-3 Solar Irradiance Curves – Cloudy Days	63
Figure 3-4 Efficiency Curve of a Typical Power Converter	66
Figure 3-5 Impact of Losses as a Function of Load Current on Efficiency	68
Figure 3-6 Comparison of Synchronous Buck Converter and Half Bridge Inverter	69
Figure 3-7 Gate Drive Signal for Half Bridge Inverter	70
Figure 3-8 Half Bridge Inverter - Operation Modes - Topology.....	75
Figure 3-9 Half Bridge Inverter - Operation Mode Waveforms - Positive Half Cycle	76
Figure 3-10 Half Bridge Inverter - Operation Mode Waveforms- Negative Half Cycle...	77
Figure 3-11 Half Bridge Inverter - With Drive Circuit	78
Figure 3-12 MOSFET Switching Waveform	80
Figure 3-13 Diode Reverse Recovery Waveforms	81
Figure 3-14 Load Independent Losses based on Loss Model, design example	88
Figure 3-15 Load Dependent Losses based on Loss Model, design example.	89
Figure 3-16 Losses in Half Bridge Inverter, design example	89
Figure 3-17 Efficiency of Half Bridge Inverter - Loss Model Calculated vs. Experimental	90
Figure 3-18 Half Bridge Three Phase PWM Inverter	90
Figure 3-19 Conceptual Diagram - Normal Mode - Phase Skipping Mode.....	92
Figure 3-20 Implementation of Phase Skipping Control Scheme- Single Stage	94
Figure 3-21 Flow Chart of Phase Skipping Control Algorithm-Single Stage.....	94
Figure 3-22 Prototype of 400W Three Phase Micro-Inverter	96
Figure 3-23 Schematic of Three Phase Micro-Inverter	96

Figure 3-25 Operational Waveforms of Phase Skipping Control 97

Figure 3-26 Three Phase Half Bridge Inverter Efficiency with Phase Skipping Control *
..... 98

Figure 3-27 Avoiding Power Imbalance amongst Phases due to Phase Skipping Control
– Concept..... 100

LIST OF TABLES

Table 1-1 Specifications of the existing Single Phase Micro-Inverters	1-18
---	------

CHAPTER 1: INTRODUCTION

The biggest quest on which mankind has embarked upon in the 21st Century is to identify cheap and reliable source of energy. Industrialization has led to an exponential increase in global energy demands. Since the dawn of industrial revolution, fossil fuels have been a dominant source of energy. However, the limited availability of fossil fuels and the environmental hazards caused due to CO₂ emissions due to burning of these fossil fuels has further propelled mankind to identify alternative cleaner and sustainable sources of energy.

1.1 Global Energy Trends

The two key drivers of global energy demand are rise in *Population* and *Income*. British Petroleum in their annual energy outlook [1.1], predict that by 2030 the global population will increase by 1.3 Billion and thereby making the total global population of 8.3 Billion. The global GDP is expected to roughly double the 2011 level in real terms by 2030. Due to this increase in population and GDP, the world energy demand is projected to grow by 1.6% p.a. from the year 2011 to 2030 thereby leading to 36% increase in global energy consumption by 2030. Figure 1-1 [1.1], shows that global population and GDP have similar trend as of global energy demand. In this figure, the statistics are presented from the countries belonging to set of groups.

1. OECD (Organization for Economic Co-operation and Development)
2. Non-OECD.

90% of the total population growth will be contributed by low and medium income economies outside the OECD. The non OECD economies will undergo rapid industrialization, urbanization and motorization which will lead them to contribute to 70% of the total GDP growth and over 90% of the global energy demand growth by the year 2030 [1.1].

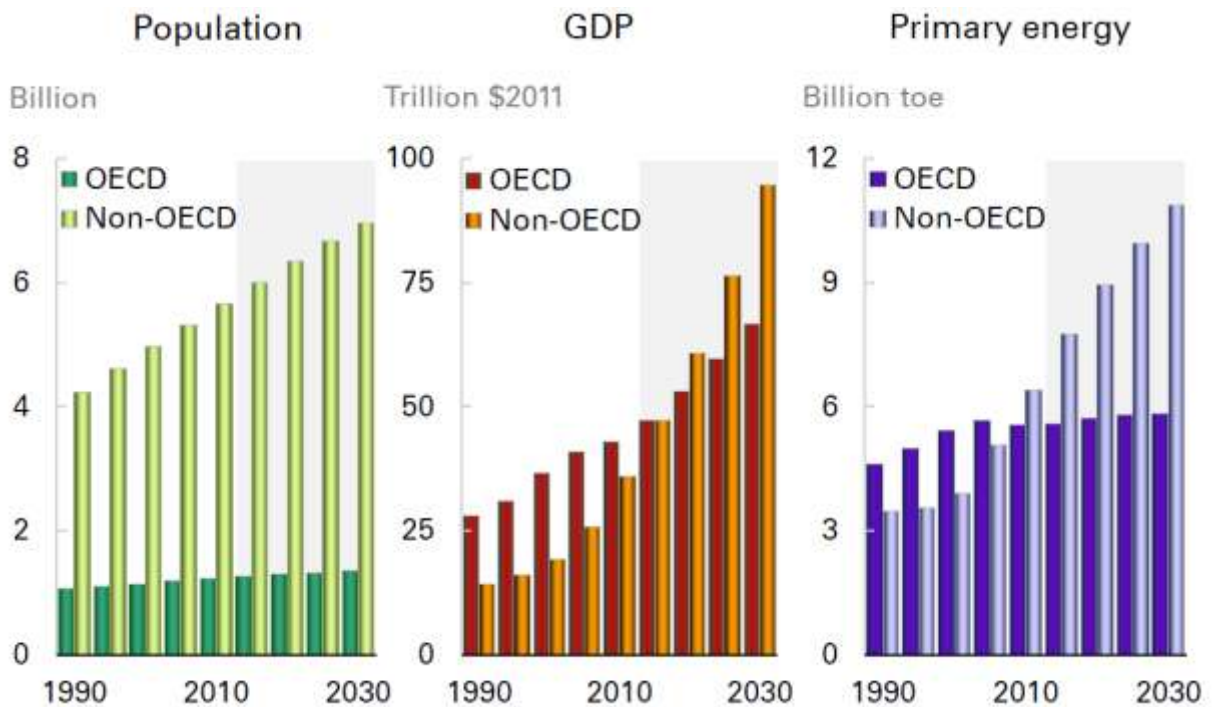


Figure 1-1 Impact of Population and GDP on Global Energy Demand

In order to achieve the goal of limiting global warming to 2°C, the consumption of fossil fuels prior to 2050 should not be more than one third of proven reserves of fossil fuels [1.2]. This leaves the world only with two choices viz. *Nuclear Energy* and *Renewable Energy* in order to meet their energy demands. The *Fukushima Nuclear Plant Disaster* which occurred in Japan in 2011 has led many countries to review their policies towards nuclear energy due to their safety concerns.

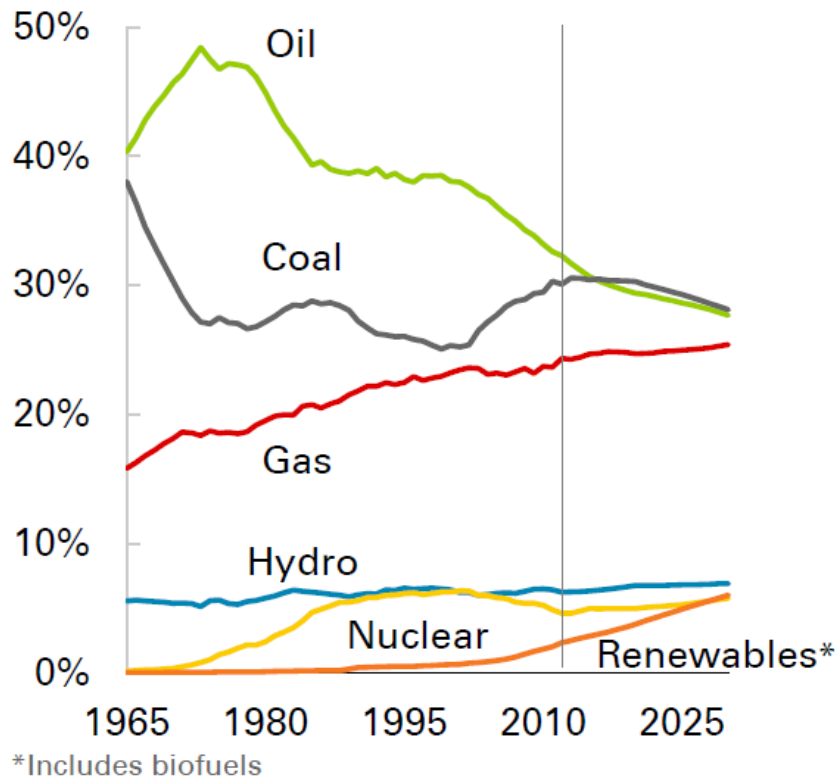


Figure 1-2 Trends of Shares of World Primary Energy

From Figure 1-2 it can be concluded that consumption of fossil fuels with high CO₂ emissions like coal and oil are predicted to fall. The trend of nuclear energy shows that it has crossed a tipping point and is expected to observe a growth with caution due to their safety concerns. The trends project Renewable Energy to have the highest growth rate in the share of World Primary Energy.

1.2 Renewable Energy Trends

Renewable energy is the forerunner in the search of a cleaner and safer source of energy. A steady rise in the hydropower, wind and solar installations has made renewable energy an essential contributor in meeting the global energy demand. International Energy Agency estimates that by 2035 renewable energy would account for almost 1/3rd of the total electricity production. This speedy rise in renewable energy is further propelled by increasing prices of fossil fuels and carbon pricing, falling technology costs of renewable energy and most importantly, by the subsidies offered. Global subsidies for renewable energy are expected to rise from \$88 billion in 2011 to a staggering \$240 billion by 2035[1.2].

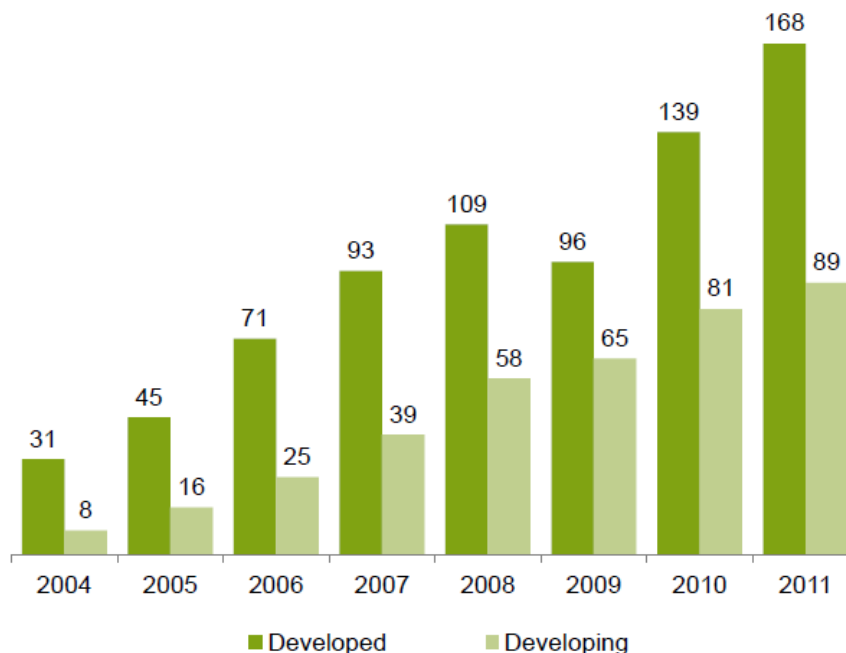


Figure 1-3 Global New Investment in Renewable Energy: Developed vs Developing Countries, 2004-2011, \$BN
Source: Bloomberg New Energy Finance

1.3 Solar Power Trends

Solar Energy is emerging to be the fastest growing source of renewable energy. Wind energy was considered to be one of the most mature renewable power technologies. However in 2011, solar took a lead in the race by attracting twice as much investment as wind. Investment in solar power observed an increase by 52% to \$147 billion whereas investment in wind power grew by only 12% to \$84 billion [1.4].

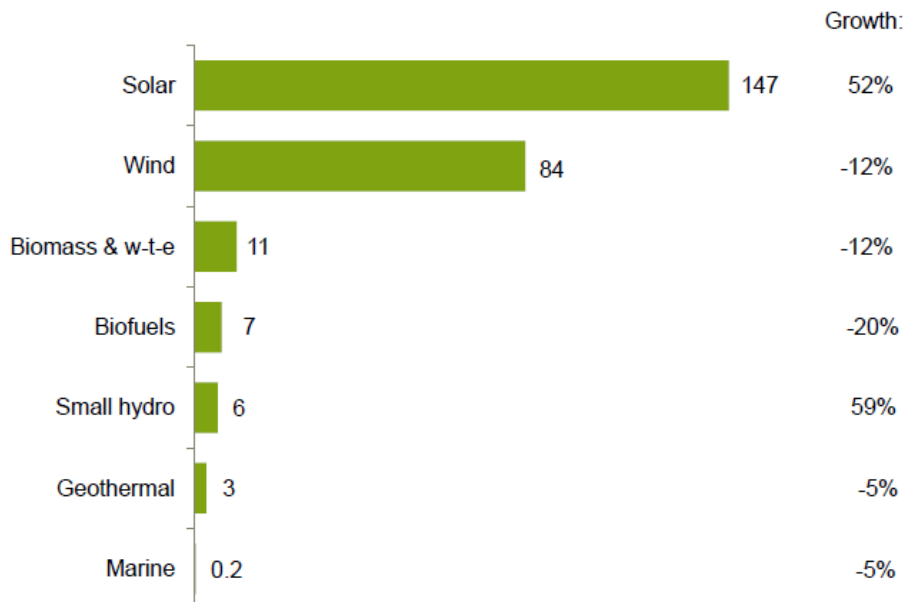


Figure 1-4 Global New Investment in Renewable Energy by Sector, 2011, And Growth on 2010, \$BN.

New investment volume adjusts for re-invested equity. Total values include estimates of undisclosed deals.

Source: Bloomberg New Energy Finance, UNEP

One of the key economic factors which led to growth in investment in solar power is the falling in technology costs of solar power. Photovoltaic module prices fell by almost 50% in the year 2011[1.3]. By the end of 2011, the PV modules prices were dropped

between \$1 and \$1.20 per watt which was approximately 76% below their prices during summer of 2008. Apart from the economic benefits, the other factors which makes solar energy more investment friendly according to [1.4][1.5] are:

- No moving parts hence low maintenance.
- No water need.
- Noiseless operation.
- No hazardous emissions.
- Scalable for any capacity of power requirement.
- Flat construction allowing them to be implemented the building rooftops.
- Long Lifetimes.
- Highly suitable for distributed power generation.
- Peak solar power generation coincides with peak energy demanded.

1.4 Types of PV Systems

PV systems are classified based on their power delivery system, type of load driven and the storage elements present in the PV system. The type of PV system adopted also depends on the functional requirements of the power delivery system. PV systems are broadly classified into following 2 categories.

1. Off Grid PV Systems (Standalone PV Systems).
2. Grid Tie PV Systems.

1.4.1 Off Grid PV Systems (Standalone PV Systems).

Off Grid PV System invert the DC solar power into AC power to drive the AC loads connected. They are equipped with battery storage. This battery storage is used to store the surplus power available during the day. This stored power is used to drive the loads during low light conditions or night time. Figure1- 5 shows the architecture of Off Grid PV System.

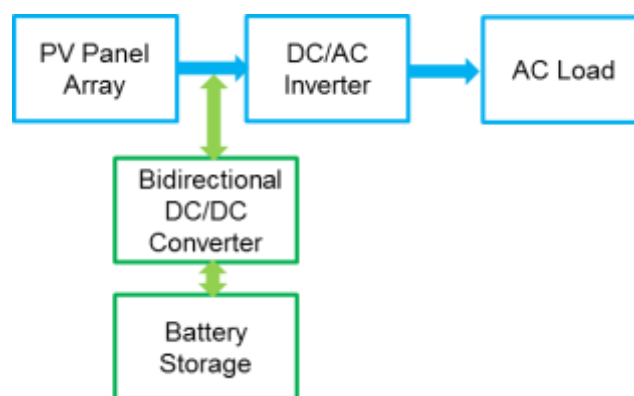


Figure 1-5 Off Grid PV System Architecture

Advantages:

- Independent of Grid.
- No need to inject power in sync with utility grid.
- Does not inject any instability in the utility grid.
- No anti-islanding issues.
- Able to provide power to rural areas where there is no utility grid.

Disadvantages:

- Cost of battery makes the system expensive.
- Additional cost of battery charger.
- No incentives or tax credits.
- Once the batteries are fully charged, the excess available power is wasted.
- Power conversion losses occur while storing the power in batteries and while converting the stored power back into AC power.

1.4.2 Grid Tied PV Systems

Grid Tied PV systems inject the solar power into utility grid which in turn drives the load connected on the grid. It is one of the key power sources in Distributed Generation (DG) Power System. Grid Tie PV system is the most popular and widely adopted PV system. It eliminates the need of storage unit thereby reducing the cost dramatically. This PV system is most suitable for residential, commercial and PV farm applications. Figure 1-6 shows the architecture of Grid Tie PV system.

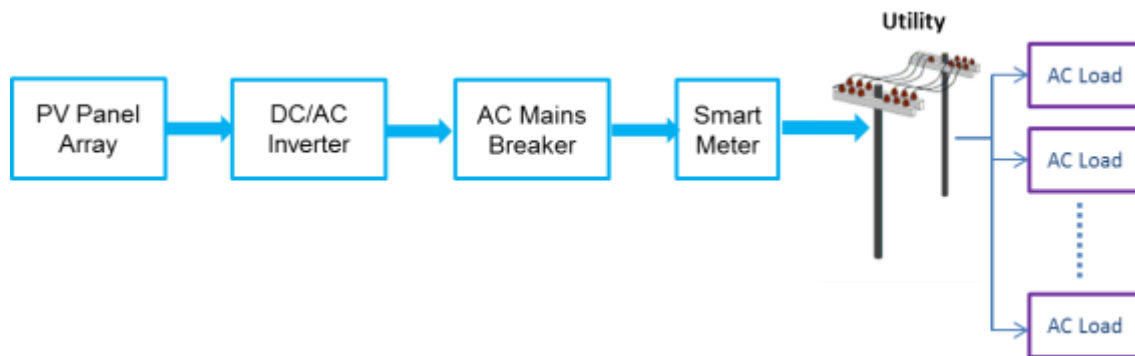


Figure 1-6 Grid Tie PV System

Advantages:

- No need of energy storage.
- Amount of excess power injected into grid is accounted for and credited into utility bill.
- No storage losses.
- Easy installation.
- Higher Power density due to absence of energy storage.

Disadvantages:

- Requires synchronization with the grid.
- Requires anti-islanding.
- Grid operators need to achieve balance between load and generated power.
- Varying injected power tends to create instability into the grid.

1.5 Grid Tie Inverter Architectures

Grid Tie Inverters can be classified into different architectures depending upon the manner in which the power is processed from solar panels to the utility grid. Grid Tie PV Inverter architecture is classified as follows [1.6]:

1. Central Type Inverters.
2. String Type Inverters.
3. Multi-String Type Inverters.
4. AC Module Type Inverter / Micro-Inverter

1.5.1 Central Type Inverters

In this architecture large number of PV panels are interfaced together in a series to form a string. The number of PV panels in this string is selected such that total series DC voltage at the output of each string is high enough that no further amplification is needed. Many such strings are connected together in parallel using series using blocking diodes and fed to a central DC-AC inverter. Figure 1-7 shows the architecture of Central Type PV Inverter. The central inverter performs the maximum power point tracking for all the panels collectively.

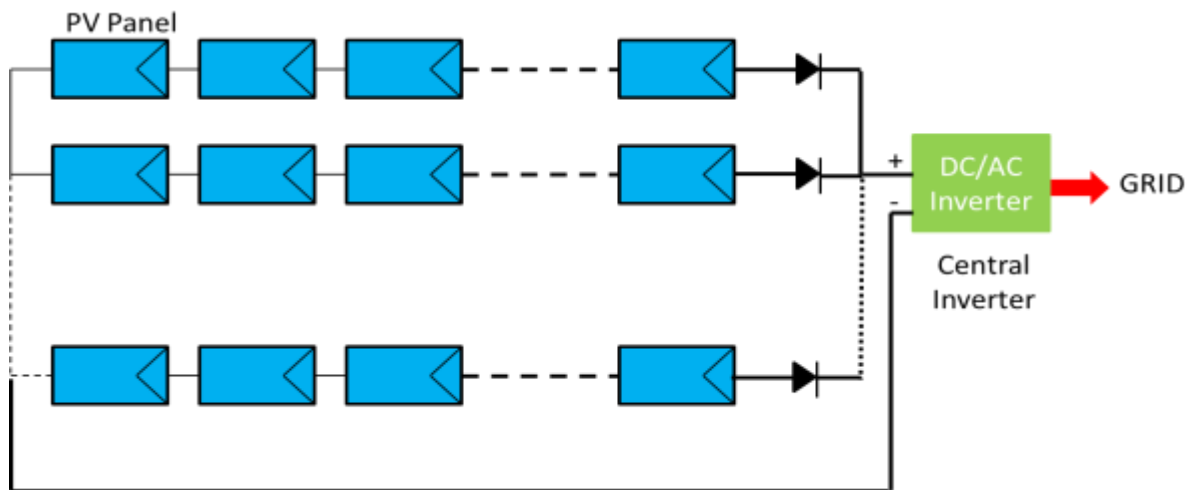


Figure 1-7 Central Type PV Inverter Architecture

Advantages:

- Economical architecture for large PV farms.
- Higher weighted efficiency of central inverter due to high input voltage levels.

Disadvantages [1.7]:

- High voltage DC cables PV Panels and inverter.
- High DC voltages may lead to arcing.
- Losses due to mismatch between PV panels
- Centralized maximum power point tracking (MPPT) leads to power losses.
- Losses in string blocking diodes.
- Non flexible design due to which cost effectiveness of mass production cannot be attained.
- Grid connected stage is usually line commutated by thyristors which lead to generation of current harmonics and thereby poor power quality.

- Lack of redundancy - Failure of the central inverter brings down the entire PV farm.
- Central inverter needs to be kept in a protected environment due to large power capacity which further increases the cost.
- Central Type inverters are not easily scalable thereby each PV farm needs a custom design depending upon its power capacity.

1.5.2 String Type Inverter

String Type inverter architecture can be considered to be the modular version of Central Type Inverter. A large numbers of PV panels are connected in series to form a string. Each of these string are fed to an individual DC-AC inverter which performs maximum power point tracking and inverts the DC power from PV panel string into AC power and injects into the utility grid. Similar to central type inverter, in string inverter each string generates DC voltage high enough such that no further need of amplification is needed. Figure 1-8 shows the architecture of String Inverter.

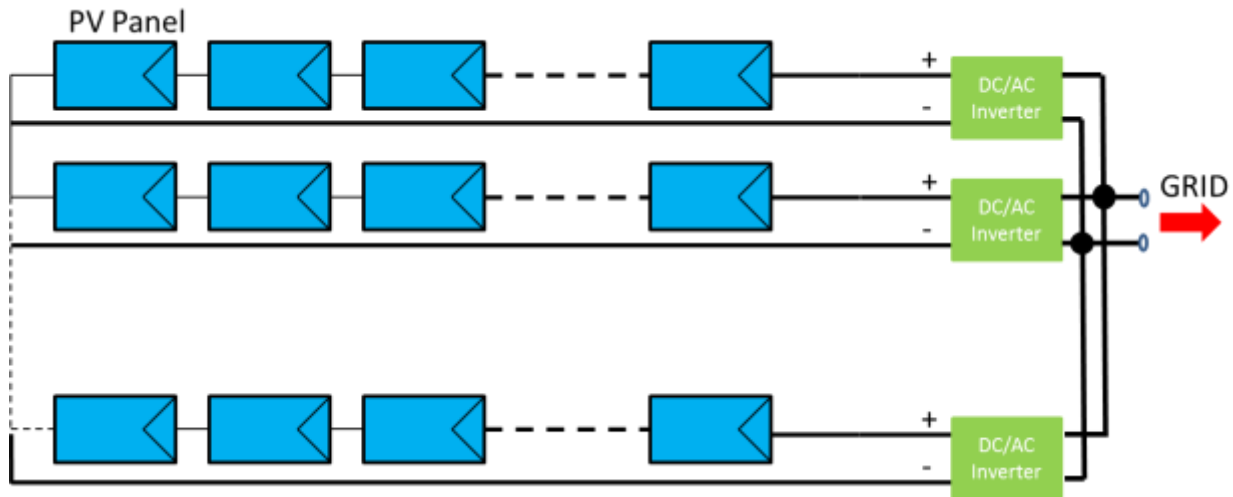


Figure 1-8 String Type Inverter Architecture

Advantages:

- Modular design at string level which enables standard design of DC-AC inverter.
- String level modularity provides this architecture some scalability in steps of power capacity of each string.
- String level MPPT is achieved.
- Redundancy is achieved at string level. If DC-AC inverter of one of the strings fails then still the other still will continue injecting power thereby increasing the power reliability of the PV farm.
- No blocking diode power loss.

Disadvantages:

- High level of DC voltage continues to pose safety hazard and higher cost of cabling.
- String level MPPT is still lower than individual panel level MPPT.
- Needs protected environment due to high power capacity.

1.5.3 Multi-String Type Inverter

Multi-String Type Inverter consists of a DC-DC converter which performs the MPPT and voltage amplification for each string. This permits lower number of PV panels connected in series in one string. This architecture has a higher degree of modularity than Central type and String type architecture. Multi-string type architecture is shown in figure 1-9

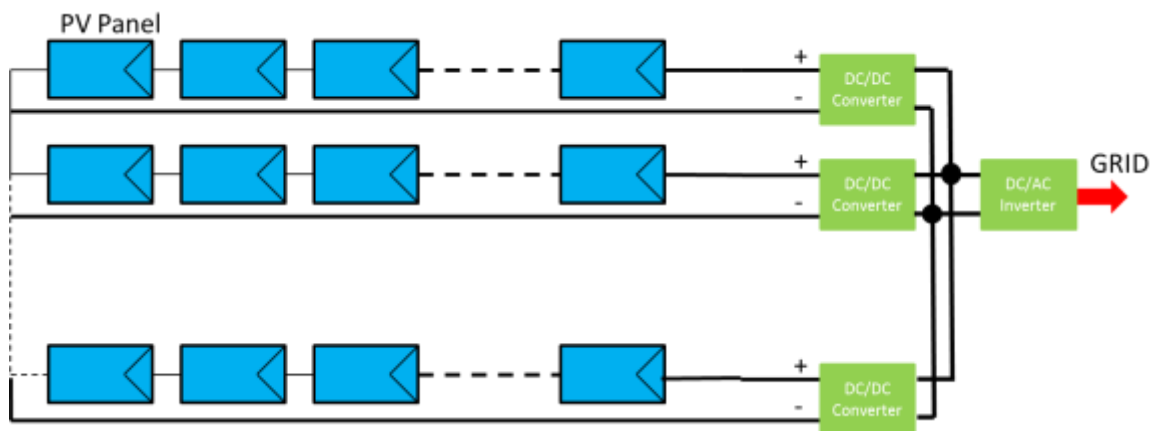


Figure 1-9 Multi-String Type Inverter

Advantages:

- Lower panel mismatch losses.
- Optimal MPPT performed on each string due to lower number of PV panels.
- String level redundancy is achieved. If one string is down, other strings continue to inject power.
- Finer modularity than Central and String type inverter helps to achieve benefit of mass production.
- No blocking diode losses.

Disadvantages:

- Although the size of string is reduced, still the DC output voltage of each string is high enough to be considered to be hazardous.
- MPPT is still lower than individual panel level MPPT.

1.5.4 AC Module Type Inverter – Micro-Inverters

AC Module Type Inverter is an integration of PV Panel with an inverter. In this architecture each PV panel has a dedicated AC module which performs MPPT, DC voltage amplification and inversion. AC Module Type Inverter is the smallest grid connected PV system unit [1.8] hence, it is also known as *Micro-Inverter*. Due to high level of modularity which can be achieved in this architecture, installation of these inverters does not require any knowledge of electrical installations. AC Module Type Inverter architecture is shown in Figure 1-10.

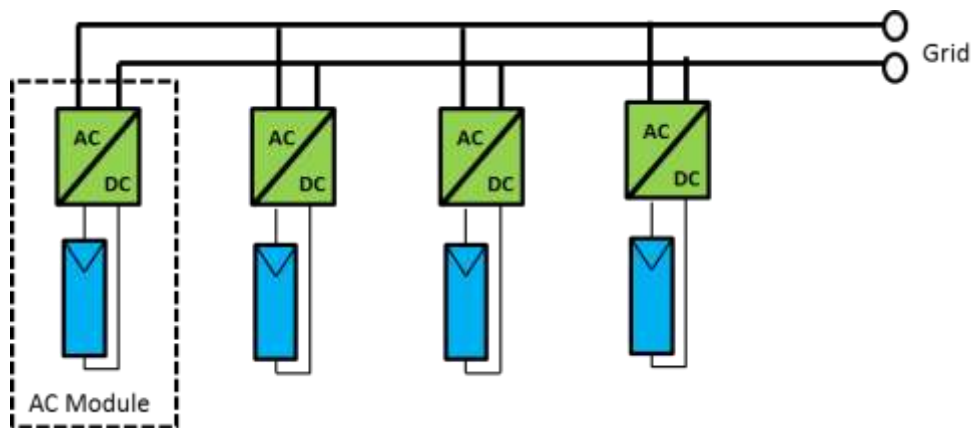


Figure 1-10 AC Module Type Inverter Architecture

Advantages [1.6] [1.7]:

- Lower cost per unit achieved due to benefits of mass production.
- High Reliability - As each PV panel has its independent inverter, if one of the inverter fails then all the other inverter continues to power the PV farm without any significant loss of power.
- Minimum Down Time – Once a faulty module is identified, it can be easily replaced by a new module due to its Plug N Play nature, thereby reducing down time.
- Simpler System Design.
- Mismatch losses between PV modules are completely eliminated as there is only one panel per inverter.
- Optimal MPPT is achieved as each PV panel has its dedicated MPPT controller.
- High Scalability – Due to modular nature of the AC Module Type Inverter, this architecture can be easily scaled to the required power capacity.
- Higher Safety – There are no hazardous high voltage cables.

Disadvantages:

- High voltage amplification required at every panel reduces the overall efficiency.
- Increase in price per watt due to more complex circuit topologies performing MPPT, DC voltage amplification and inversion.

1.6 Comparative Review of Existing Single Phase Micro-Inverters in the market

In order to understand the existing trends in the micro-inverter designs; side by side comparison of micro-inverters from leading manufacturers based on their specifications were done. Table 1-1 summarizes the design specifications of the micro-inverters manufactured by the following six major manufacturers based on the public data:

1. Solar Bridge.
2. Enecsys.
3. Enphase.
4. Power One.
5. SMA.
6. Petra Solar.

By comparing the design specifications of Table 1, following observations can be made about the current trends of the micro-inverters.

1. Most of the micro-inverters have power ratings of 200~300W as wide number of PV panel manufacturers have PV panels in this power range. Enecsys SMI-D240W-60-UL which consists of two PV panels connected in parallel at the input of the micro-inverter has a power rating of 450W.
2. Nominal output voltage and frequency ratings vary according to the regional standards.
3. Weighted efficiency is higher than 93%.
4. Micro-inverters incorporate communication capability with a central server for diagnostics and monitoring purposes.

Table 1-1 Specifications of the existing Single Phase Micro-Inverters

	Solar Bridge- Pantheon2		Enecsys						Enphase	Power One		SMA	Petra Solar
	60Hz	50Hz(P 250LV- 230AU)	SMI- S240W- 60-UL	SMI- D240W-60- UL	240-60-MP		300-60-MP			0.25-I- OUTD	0.3-I- OUTD	Sunny Boy 240 US	SEM120
Output Power - Active- (Watts)	238	238	225	450	240		300		215	250	300	240	200
Output Power- Reactive- (VAR)	NA		NA						NA	NA		NA	+/-200
Nominal Output Voltage (V)	240	230	240	240	230	240	230	240	240/208	240/208		240	120
Nominal Output Frequency(Hz)	60	50	60	60	50	60	50	60	60	60		60	60
Power Factor	>0.99	>0.99	>0.95	>0.95	>0.95	>0.95			>0.95	>0.95		NA	NA
Peak Efficiency (%)	95.7	95.6	95	96	96.4	96.5	96.4	96.5	96.3	96.5		95.5	NA
Weighted Efficiency (%)	95 (CEC)	93.2(E URO)	93(CEC)	94.5(CEC)	95(EUR O)	96(CEC)	95(EUR O)	96(CEC)	96(CEC)	96(CEC)		95(CEC)	93 (CEC)
Communication	Power Line	Power Line	Zigbee IEEE 802.15.4						Power Line	Web Based		Web Based	Zigbee IEEE 802.15.4

1.7 Micro-Inverters for Three Phase Applications

Currently, micro-inverters are highly popular amongst residential and low power commercial rooftop applications. However, due to the advantages of micro-inverter over string inverter like optimal maximum power point tracking, high redundancy, scalability, safety as there are no high voltage DC cables and ease in fault identification; micro-inverters are also becoming popular for high power residential, commercial rooftop applications and low power PV farm applications. For these applications, the utility grid is 3 Phase.

1.7.1 Existing 3 Phase Configurations using Single Phase Micro-inverters

Presently, only single phase micro-inverters are commercially available. Figure 1-11 shows the arrangement to connect these single phase micro-inverters to three phase grid for high power residential, commercial rooftop applications and low power PV farms. Single Phase Inverters in US are designed to operate with split phase configurations which exist in most of the households in the country. Hence, when single phase micro-inverters are connected to three phase grid systems in US, they are connected between two phases. From the arrangement shown in figure 1-11[1.8-1.9] following conclusions can be made:

1. Systematic planning is required before installing the micro-inverters in order to balance the power injection levels into all three phases.
2. Micro-inverter needs to be installed in multiples of three to avoid power imbalance which makes the scalability of power less granular.

3. Increased cost of installation and cabling as the numbers of units to be installed are in multiples of three.
4. Failure of any single micro-inverter tends to create power imbalance amongst the phases. Thus, failure of one unit would necessitate shutting down of two more micro-inverters in the other corresponding phases to ensure power balance.

Based on the above observations, it can be concluded that for high power residential, commercial rooftop applications and low power PV farm applications, it is advantageous to use true three phase micro-inverter.

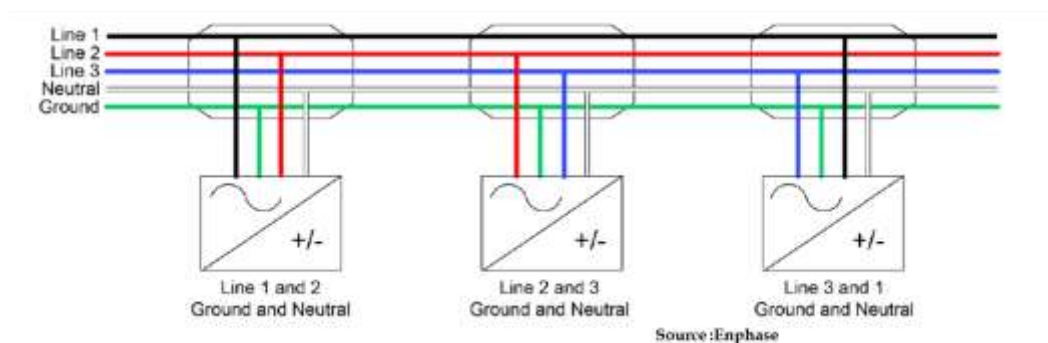
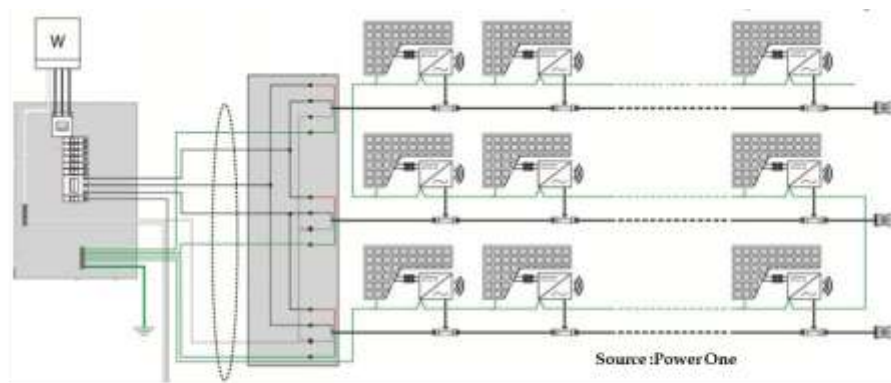


Figure 1-11 Single Phase Micro-Inverter Connected to Three Phase Grid

1.8 Three Phase Micro-Inverter

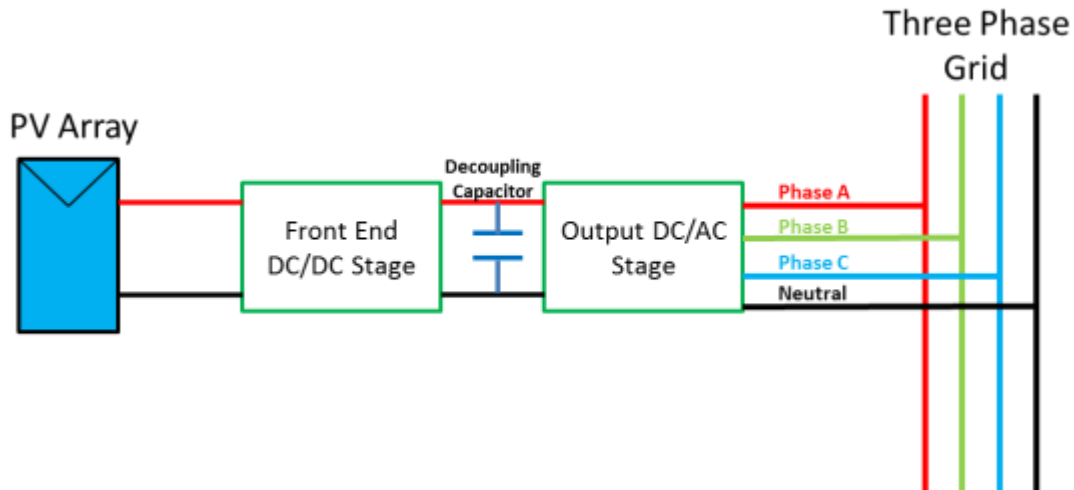


Figure 1-12 Block Diagram of Three Phase Micro-Inverter

A true Three Phase Micro-Inverter is shown in the figure 1-12 above. Three phase micro-inverter is identical to single phase micro-inverter except the DC-AC stage is three phase instead of single phase.

Front End DC-DC Converter acts as MPPT controller and also boosts the PV panel voltage high enough for the DC-AC Stage to be able to invert it into AC power.

DC-AC Inverter performs couple of more functions apart from inversion of power as stated below:

1. DC Bus Voltage Regulation: As the front end DC-DC Converter acts as an MPPT Controller, the task of regulating the DC Bus voltage across the decoupling capacitor falls upon the DC-AC Stage. DC-AC Stage regulates the variation in

the Bus voltages occurring due to varying maximum power point voltages of PV panel by varying the injected power into the grid.

2. Grid Monitoring: In order to be able to inject Real or Reactive power, the inverter must be in synchronous with the AC Grid. Also, the micro-inverter should stop injecting power under conditions like fault on the grid or when grid is turned OFF for maintenance by the utility company. For the above mentioned purposes, there is a constant need to monitor the 3 Phase Grid which is done the by the DC-AC Stage.

Advantages of True Three Phase Micro-Inverter:

1. Low ripple voltage on DC Bus: As the inverter is a 3 Phase System, the ripple voltage on the DC Bus is lower and has a frequency of 360Hz as compared to 60 Hz on a single phase micro-inverter. This helps to reduce the required bus capacitor value. As the required capacitor value is low, high reliability film capacitors can be used instead of low reliability electrolytic capacitors, thereby increasing the reliability of the micro-inverter.
2. No need of multiple units to achieve power balance amongst three phases: As each unit is a true three phase micro-inverter, power is injected simultaneously into all three phases. Thus, eliminating need of installing multiple units in order to achieve power balance amongst three phases as needed when single phase micro-inverters are used in three phase systems.
3. Reduction in \$/W costs: A single unit of Three Phase Micro-Inverter replaces three units of single phase micro-inverter when connected in a three phase

system. Thus, cost of DC-DC Stage, controller for DC-AC stage, communication module and installation for Three Phase Micro-inverter is $1/3^{\text{rd}}$ of the cost of Single Phase Micro-inverter for the same amount of power injection capacity in three phase power systems.

4. Multiple Panels per Micro-Inverter: As a three phase micro-inverter has high power injection capacity, multiple panels can be connected to a single micro-inverter. This configuration can help to reduce the number of micro-inverters considerably in low power PV farm.

1.9 Objective and Outline of the Thesis

Primary objective of this thesis is to:

1. Optimize the design of LLC converter in order to achieve higher efficiency for PV applications.
2. Propose analysis and implementation of light load efficiency optimization control technique for Three Phase Micro-Inverters.

This thesis is divided into 4 chapters, which are organized as follows.

First chapter summarizes the current energy scenario and its predicted trends. Promising future of Solar Energy amongst other sources of renewable energy is established. Furthermore, the dichotomy of PV systems is explained with focus on Grid Tied PV systems. This chapter covers the existing Grid Tied PV System Architectures and focuses on the AC Module type / Micro-Inverters. In Micro-Inverters, this thesis

gives a comparative review of existing micro-inverters in the market and thereby identifying the trends in the micro-inverter industry. As the existing micro-inverters are primarily designed for single phase systems, their applicability in three phase systems are analyzed based on which a need of Three Phase Micro-inverters is established. The block diagram of three phase micro-inverters is introduced and its advantages over single phase micro-inverters in a three phase power systems are stated.

Chapter 2 focuses on optimal design of resonant parameters of LLC converter when used as a front end converter for PV applications. This chapter identifies mutually benefitting characteristics of PV panel and LLC converter and based on these characteristics a design procedure for the resonant parameters of the LLC converter is proposed.

Chapter 3 proposes a control technique to improve the light load efficiency of Three Phase Inverters for grid tied PV applications. This chapter begins with establishing the need of light load efficiency improvement in PV micro-inverters by analyzing the solar irradiance patterns. Furthermore, it identifies the factors causing lower light load efficiency in half bridge PWM inverters by developing its loss model. The accuracy of the loss model is proved by experimental results. Having identified the need of improving light load efficiency, *Phase Skipping Control* technique is proposed to improve the same in three phase micro-inverters Improvement in efficiency with the

proposed control technique is proved using experimental results obtained from Three Phase Half Bridge PWM Inverter.

Chapter 4 summarizes and concludes the findings presented in chapter 2 and chapter 3. Based on the conclusions, future research opportunities are reported.

1.10 References

- 1.1 British Petroleum (2013). *BP Energy Outlook 2030*. Retrieved from http://www.bp.com/liveassets/bp_internet/globalbp/globalbp_uk_english/reports_and_publications/statistical_energy_review_2011/STAGING/local_assets/pdf/BP_World_Energy_Outlook_booklet_2013.pdf
- 1.2 International Energy Agency (2012). *World Energy Outlook 2012 - Executive Summary*. Retrieved from <http://www.iea.org/publications/freepublications/publication/name,33339,en.html>
- 1.3 Frankfurt School UNEP Collaborating Centre for Climate & Sustainable Energy Finance (2012). *Global Trends in Energy Investment 2012*. Retrieved from <http://fs-unep-centre.org/publications/global-trends-renewable-energy-investment-2012>
- 1.4 Karabanov, S.; Kukhmistrov, Y.; Miedzinski, B.; Okraszewski, Z., "Photovoltaic systems," *Modern Electric Power Systems (MEPS)*, 2010

Proceedings of the International Symposium , vol., no., pp.1,5, 20-22
Sept. 2010.

- 1.5 Green, Dino. (2012, June 13). *Pros and Cons of Photovoltaic (PV) panels – solar energy*.www.greenenergysavingtips.com. Retrieved from <http://www.greenenergysavingtips.com/pros-and-cons-of-photovoltaic-pv-panels-solar-energy/>
- 1.6 Kjaer, S.B.; Pedersen, J.K.; Blaabjerg, F., "A review of single-phase grid-connected inverters for photovoltaic modules," *Industry Applications, IEEE Transactions on* , vol.41, no.5, pp.1292,1306, Sept.-Oct. 2005.
- 1.7 Myrzik, J. M A; Calais, M., "String and module integrated inverters for single-phase grid connected photovoltaic systems - a review," *Power Tech Conference Proceedings, 2003 IEEE Bologna* , vol.2, no., pp.8 pp. Vol.2., 23-26 June 2003
- 1.8 Power One (2013), *Aurora Micro Grid Tied Inverters – Technical Manual*. Retrieved from <http://www.power-one.com/renewable-energy/products/solar/string-inverters/panel-products/aurora-micro/series-0>
- 1.9 Enphase Energy (2013), *Enphase Microinverter Model M215 – Installation and operation manual*. Retrieved from <http://enphase.com/products/m215/>

CHAPTER 2: DESIGN OPTIMIZATION OF LLC TOPOLOGY FOR PV APPLICATIONS

PV panel market is dominated by Mono-crystalline and Polycrystalline types of PV panels. Typically, the output voltages of these panels lie in the range 25V-50V depending upon their power capacity. In order to invert the available DC power into AC Power, the DC output of the solar panel needs to be boosted before it is fed to the DC-AC Inverter. Figure 2-1 shows the blocks in a typical Grid Tied Micro-Inverter.

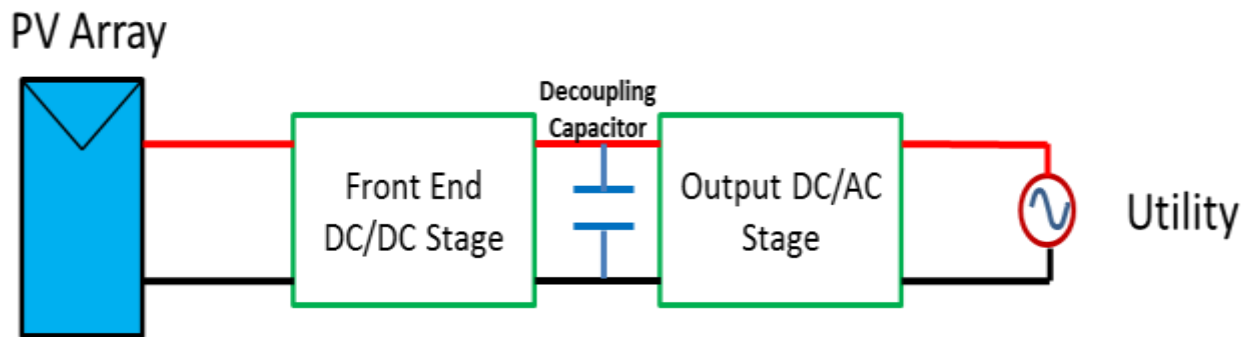


Figure 2-1 Block Diagram - Grid Tied Micro-Inverter

Front End DC-DC stage performs a dual role of Maximum Point Power Tracking as well as amplification of DC voltage. Due to safety concerns, isolated DC-DC stage topologies are preferred as a Front End DC-DC Converter for Grid Tied Micro-Inverter.

Following are few isolated DC-DC Converter topologies are suitable for Grid Tied Micro-Inverter.

1. Fly-back Converter.
2. Isolated SEPIC Converter.
3. Forward Converter.
4. Half Bridge Converter.

5. Full Bridge Converter.
6. Push Pull Converter.
7. LCC Converter.- Half Bridge and Full Bridge.
8. LLC Converter- Half Bridge and Full Bridge.

Recently, LLC resonant topology has gained a lot of popularity due to their low component count, soft switching capability of input switches as well as output rectifier diodes. PV panel I-V characteristics have a unique feature which complements LLC topology thereby making it a preferred topology for PV applications.

This chapter discusses the complementing features of PV panel which benefits LLC topology. Based on this mutually benefit behavior, resonant parameters of LLC topology can be designed such that converter operates at highest possible efficiency.

2.1 PV Panel Characteristics

An equivalent PV panel model is illustrated in figure 2-2 and mathematical equations to model PV Panel as voltage controlled current source [2.1] are given as follows:

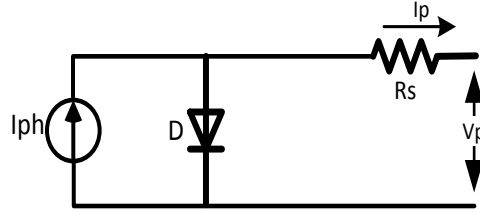


Figure 2-2 Single Diode Equivalent Model of PV Panel

$$I_p = I_{sc} \left[1 - C_1 \cdot \left(e^{\frac{V_p}{C_2 V_{oc}}} - 1 \right) \right] \quad (2.1)$$

Where

$$C_1 = \left(1 - \left(\frac{I_{MPP}}{I_{sc}} \right) \right) e^{-\frac{V_{MPP}}{C_2 V_{oc}}} \quad (2.2)$$

$$C_2 = \frac{\frac{V_{MPP}-1}{V_{oc}}}{\ln\left(1 - \frac{I_{MPP}}{I_{sc}}\right)} \quad (2.3)$$

Coefficients C_1 and C_2 depends on the following module parameters:

- I_{sc} – Short Circuit Current.
- V_{oc} – Open Circuit Voltage.
- V_{MPP} – Maximum Power Point Voltage
- I_{MPP} – Maximum Power Point Current.

Based on the above equivalent model, I-V and P-V characteristics of the PV panel at different temperature and irradiance levels can be plotted as shown in figure 2-3 [2.2].

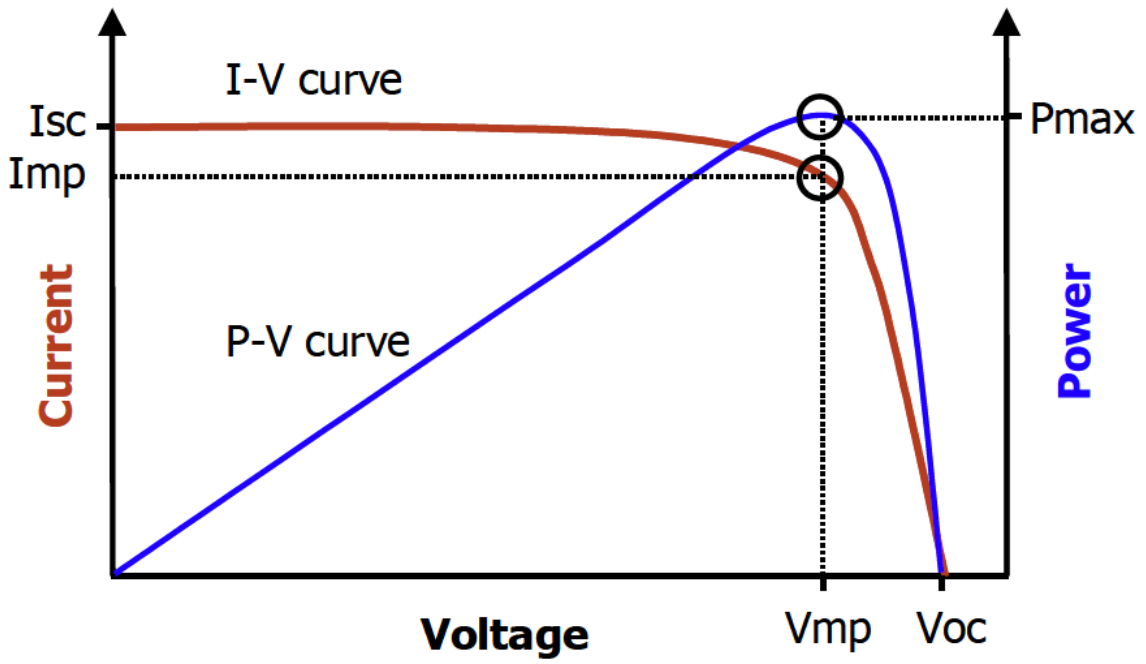
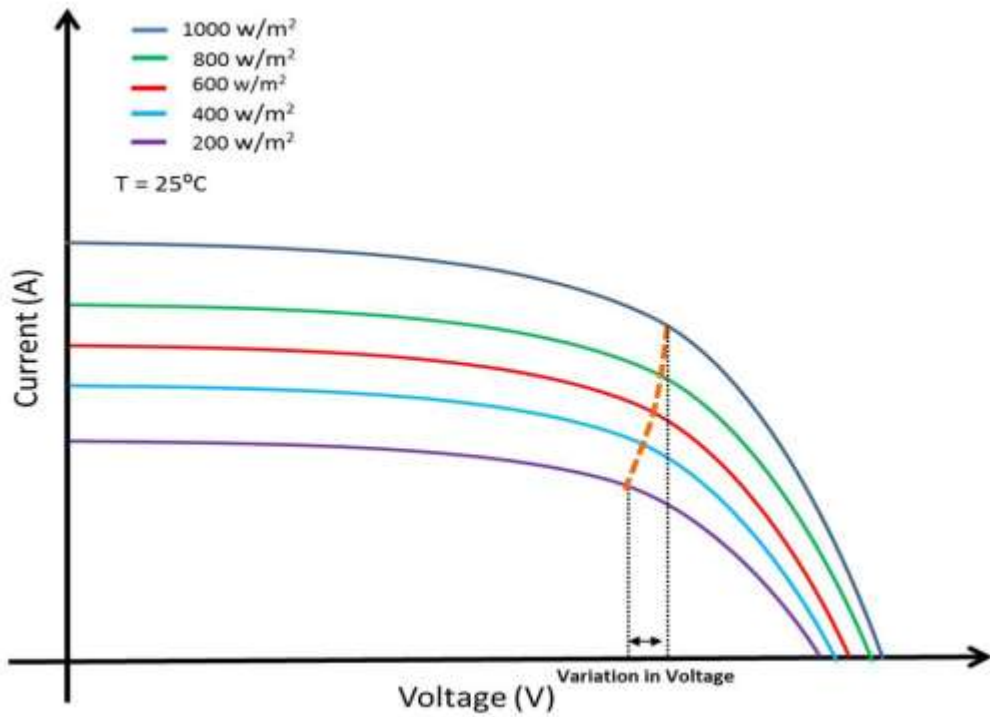
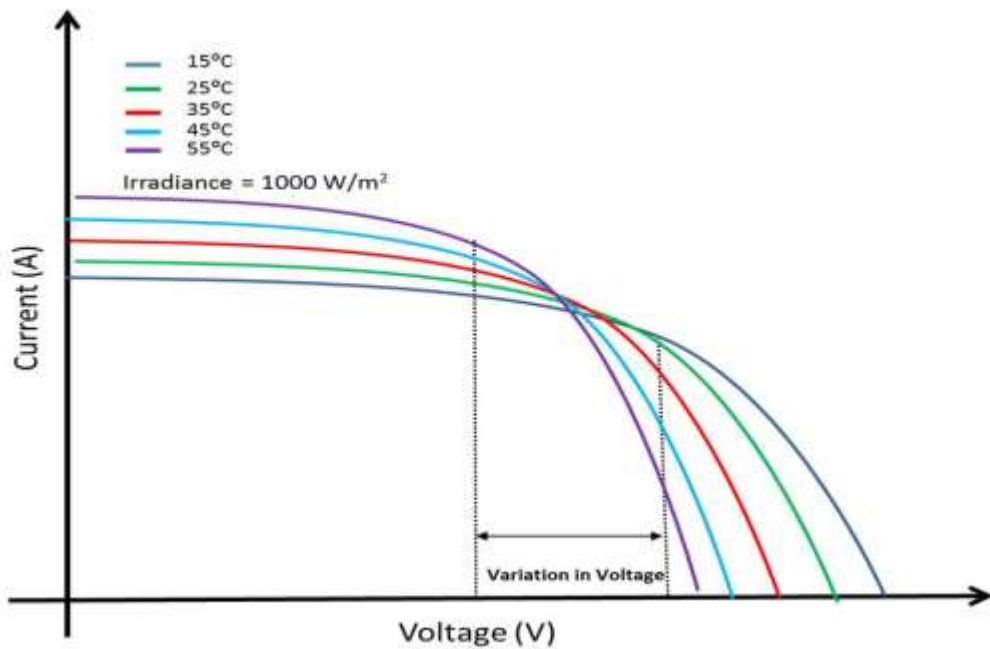


Figure 2-3 I-V & PV Characteristics of PV Panel

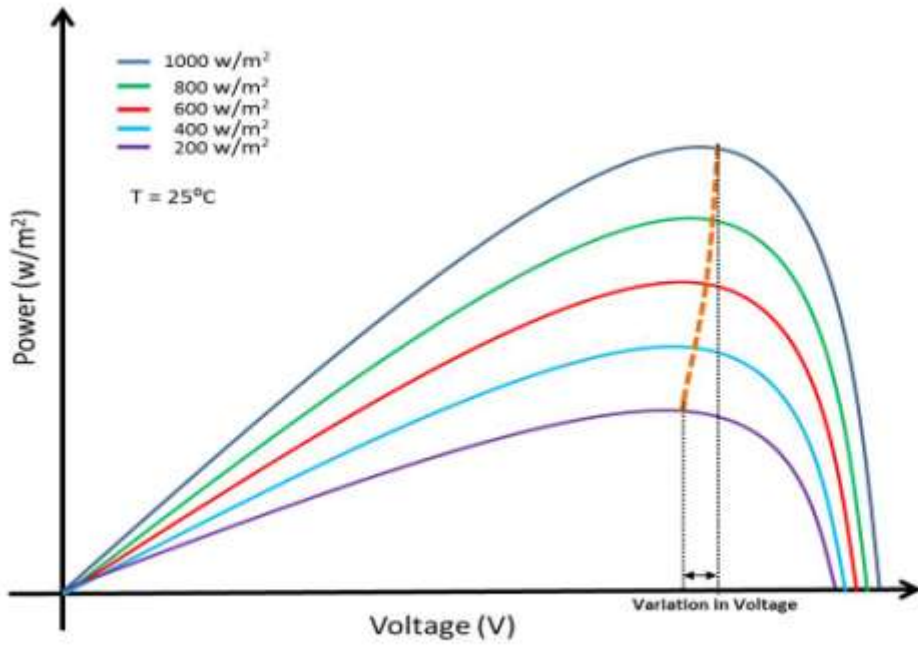


(a) I-V Curve for Solar Panel – Constant Temperature – Varying Irradiance Level

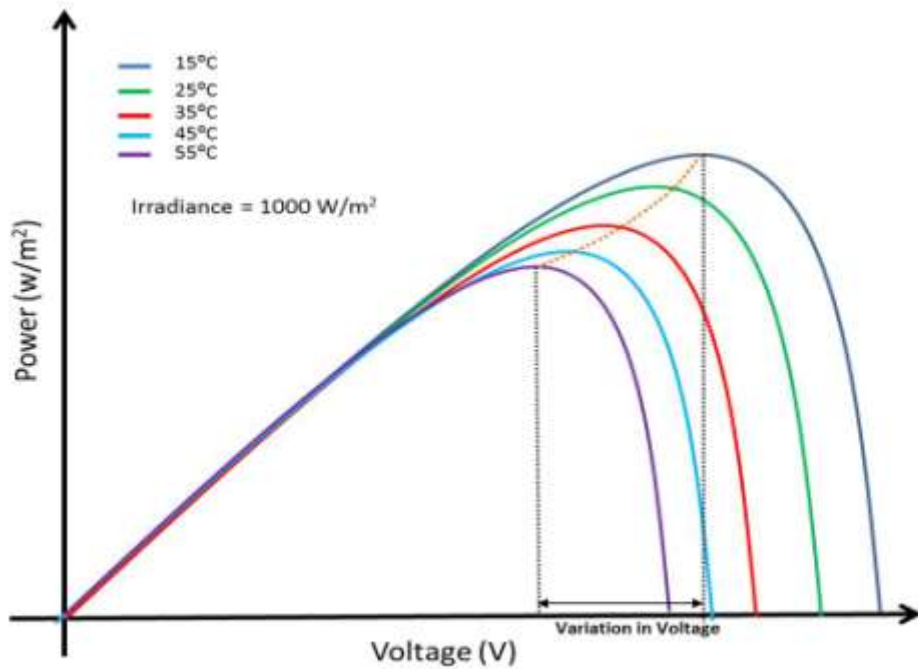


(b) I-V Curve for Solar Panel – Varying Temperature – Constant Irradiance Level

Figure 2-4 I-V Curves of Solar Panel with Varying Temperature and Irradiance Level



(a) P-V Curve for Solar Panel – Constant Temperature – Varying Irradiance Levels



(b) P-V Curve for Solar Panel – Varying Temperature – Constant Irradiance Level

Figure 2-5 P-V Curves of Solar Panel with Varying Temperature and Irradiance Level

2.1.1 Observations from Solar Panel's I-V and P-V Curves:

- V_{MPP} (Maximum Power Point Voltage) variation due to change in irradiance levels is very small.
- V_{MPP} varies inversely with temperature (negative temperature coefficient).
- Increase in temperature reduces V_{MPP} which in turn reduces maximum power available.

One key conclusion that can be arrived at from the above observations is that under standard test conditions i.e. 25°C, V_{MPP} is nearly constant. This unique feature of PV panel enables to maintain the gain of Front End DC-DC Converter fairly constant at room temperature. This constant gain requirement for PV panels helps in optimal design of the Front End DC-DC Converter. The DC-DC Converter can be designed such that its highest efficiency gain point intersects with the gain requirement for the PV panel at Standard Test Conditions.

2.2 Full Bridge LLC Resonant Converter:

LLC Converter is a resonant converter topology. Like any other resonant converters, LLC Converter has three key blocks in its topology as shown in figure 2-6[2.4].

1. Switching Network:

Switching network chops the input voltage or current into symmetric (in time domain) high frequency square pulse and applies it across the resonant network. Depending upon the gain requirement, the switching network may be half-bridge or full bridge switching network.

2. Resonant Network:

Resonant network consists of a series and or parallel combination of Inductor and Capacitor depending upon type of resonant converter. The energy applied across the resonant tank by the switching network is circulated in the tank network and some of it is delivered to the output either in the same or the next switching cycle.

3. Rectifier Network:

Output of resonant tank is either stepped up or stepped down depending upon the need of conversion ratio and applied across the Rectifier Network. The rectifier network rectifies the high frequency AC and converts into the DC. For converters with higher load current, the diode rectifier network can be replaced by synchronous rectifier to reduce the conduction losses in rectifier diodes.

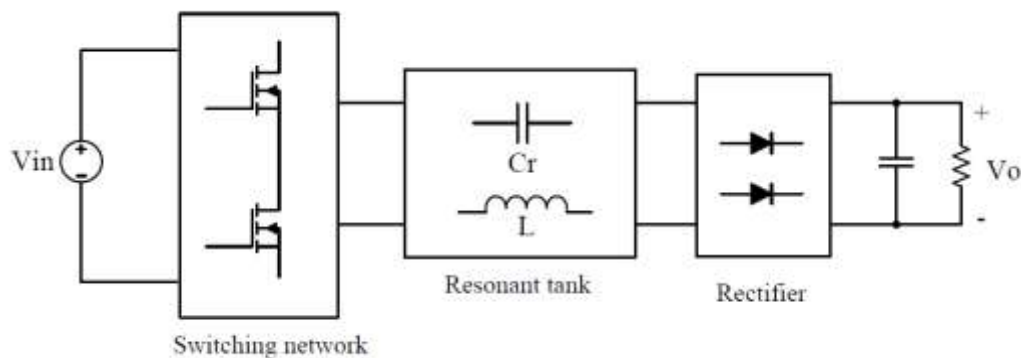


Figure 2-6 Block Diagram of Resonant Converter Topology

LLC Resonant converter is a series-parallel type resonant converter. The series resonant tank consists of a series combination of L_r and C_r . This series network is in

parallel with L_m which forms the parallel tank circuit. Figure 2-7 illustrates a Full Bridge LLC Resonant Converter. Parallel Inductor L_m is implemented as the magnetizing inductance of the power transformer. This transformer is a step-up or step-down depending upon the DC gain requirement.

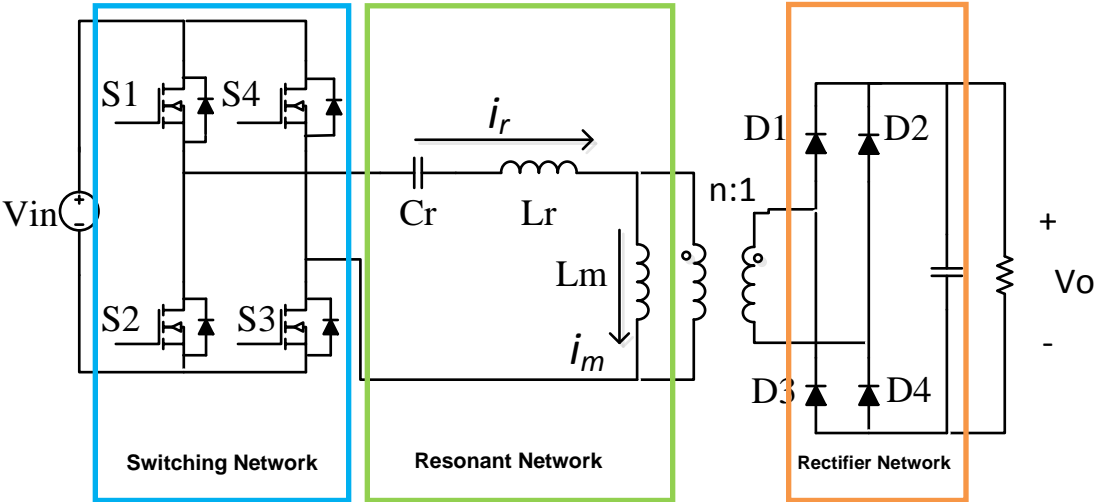


Figure 2-7 Full Bridge LLC Converter

2.2.1 LLC Converter FHA Analysis

Fundamental Harmonic Analysis [2.4] is widely used method to obtain DC gain curve for LLC converter. This method simplifies the analysis by ignoring the higher order harmonics of the square wave input voltage and treats the input purely sinusoidal. Although this method is not very accurate but it greatly reduces the complexity of the analysis. The transfer function of the LLC converter is obtained by applying FHA to AC equivalent circuit of LLC Converter shown in figure 2-8. The resonant tank of LLC can be divided into two impedances i.e. Series and Parallel.

$$Z_s = j\omega L_r + \frac{1}{j\omega C_r} \quad (2.4)$$

$$Z_p = j\omega L_m \quad (2.5)$$

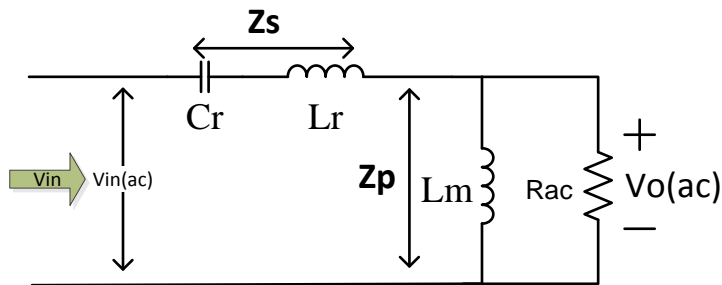


Figure 2-8 AC Equivalent Circuit of LLC Converter

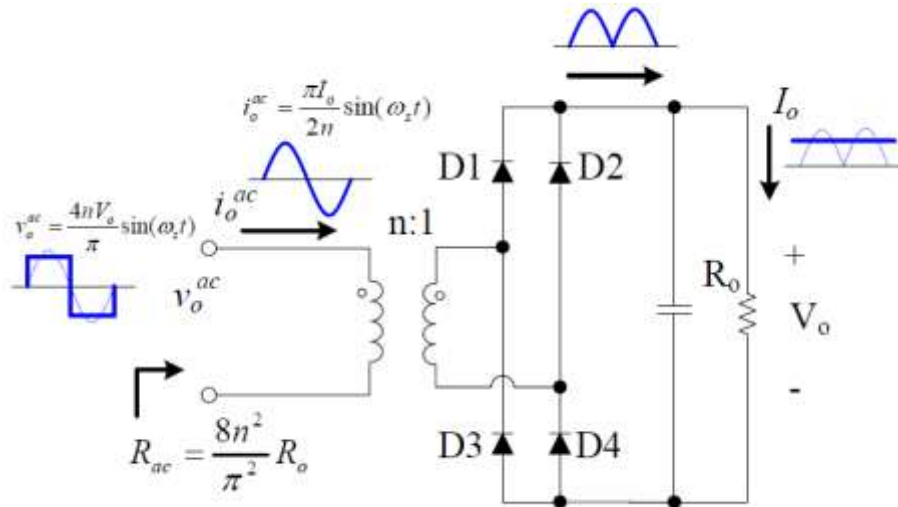


Figure 2-9 Derivation of AC Equivalent Impedance

R_{ac} in the AC equivalent circuit shown above is the AC impedance of the output load resistance reflected on the primary side of the transformer as shown in figure 2-9[2.4].

Assuming the output voltage V_o to be constant, the fundamental component of the primary side voltage of the transformer can be calculated as

$$V_o^{ac} = \frac{4nV_o}{\pi} \sin(\omega_s t) \quad (2.6)$$

Assuming that the current at the input of the output rectifier network is sinusoidal in nature, thereby output current I_o is average of the sinusoidal current at the input of the rectifier. Thus, the current at the primary side of the transformer can be calculated as

$$i_o^{ac} = \frac{(\pi * I_o)}{2n} * \sin(\omega_s t) \quad (2.7)$$

Thus, AC equivalent impedance can be calculated from (13) and (14) as

$$R_{ac} = \frac{V_o^{ac}}{i_o^{ac}} = \frac{8n^2 R_o}{\pi^2} = \frac{8n^2 V_o}{\pi^2 I_o} \quad (2.8)$$

The normalized DC gain as a function of switching frequency as given in [2.6]:

$$M = \frac{nV_o}{V_{in}} = \frac{\frac{4}{\pi} nV_o \sin(\omega_s t)}{\frac{4}{\pi} V_{in} \sin(\omega_s t)} = \left| \frac{L_n f_n^2}{[(L_n + 1)f_n^2 - 1] + j[(f_n^2 - 1)f_n Q_e L_n]} \right| \quad (2.9)$$

$$\text{where } L_n = \frac{L_m}{L_r}, f_n = \frac{f_s}{f_o}, f_o = \frac{1}{2\pi\sqrt{L_r C_r}}, Q_e = \frac{\sqrt{L_r}}{R_{ac}}$$

Figure 2-10 plots the gain curves using equation (2.9) for different load values which is reflected by Q_e . Maximum achievable peak gain reduces with increase in load for a fixed value of L_m , L_r and C_r . Also the frequency at which peak gain occurs is shifted towards resonant switching frequency with increase in load.

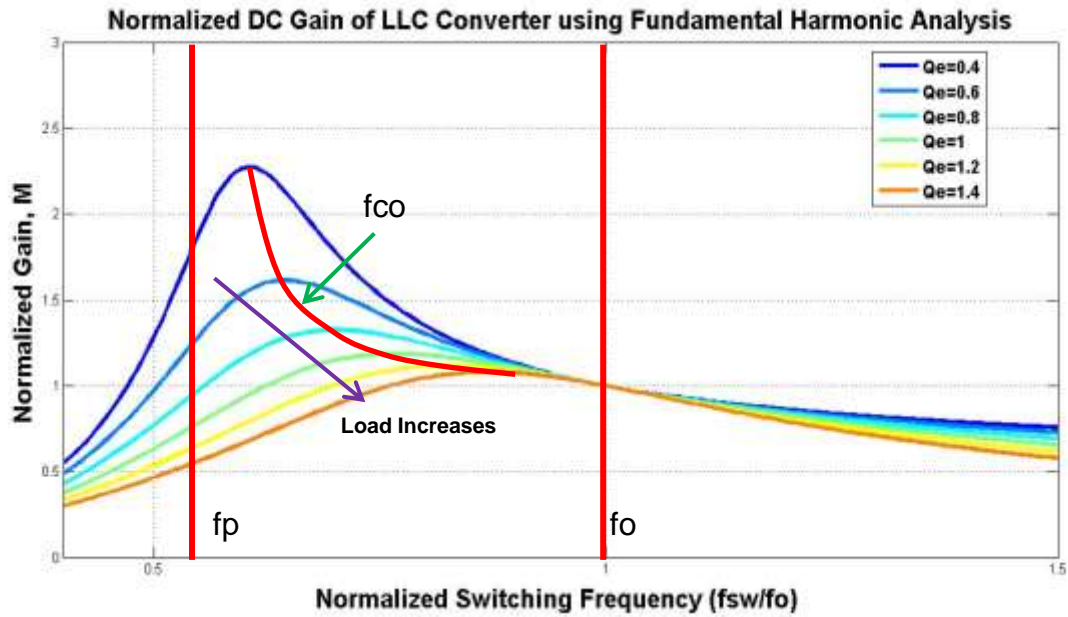


Figure 2-10 LLC Converter Gain Curves (Ln=2)

LLC Converter has three characteristic frequencies:

1. Resonant Frequency (f_o): This frequency is the function of Series tank components. At this frequency, Z_s is purely resistive and thus no circulating power in the tank circuit..

$$f_o = \frac{1}{2 * \pi * \sqrt{L_r * C_r}} \quad (2.10)$$

2. Pole Frequency (f_p): This frequency is the function of all the resonant parameters of the tank circuit.

$$f_p = \frac{1}{2 * \pi * \sqrt{(L_m + L_r) C_r}} \quad (2.11)$$

3. Peak Gain Frequency (f_{co}): DC gain of the LLC converter is at its maximum at this frequency. f_{co} is load dependent; $f_p \leq f_{co} \leq f_o$. At no load, $f_{co} = f_p$; when output is short-circuited, $f_{co} = f_o$.

In order to maintain control loop stability and to achieve Turn ON ZVS for the switches, it is essential that switching frequency $(f_{sw}) > f_{co}$.

Depending upon the switching frequency (f_{sw}) , the LLC converter has three major operating zones [2.5].

2.2.2 Operating Modes of LLC Converter

Zone 1- $f_{co} \leq f_{sw} \leq f_o$:

Figure 2-11 describe the waveforms of LLC Converter while operating in Zone 1. The operation of the LLC converter in Zone 1 can be divided into 6 modes. Equivalent circuits for each mode are shown in figure 2-12. For the sake of simplicity, parasitic capacitances for the MOSFETs are not shown.

Mode 1(t_0-t_1):

At $t=t_0$, S2 and S4 turns OFF. t_0-t_1 is the dead-time period, hence S1 and S3 are also OFF. During this mode, the lagging current i_r freewheels through body diodes of S1 and S3. Since L_m is clamped by reflected output voltage, the resonance occurs in L_r and C_r only.

Mode 2 (t_1-t_2):

At $t=t_2$, S1 and S3 are turned ON at zero voltages across them due to freewheeling of i_r through their respective bypass diodes in Mode 1. The resonant current i_r continues to drop to zero and reverses its direction. The magnetizing current i_m , increases linearly from negative peak to positive peak during this mode. The difference between resonant

current i_r and magnetizing current i_m flows through output rectifier diodes D1 and D3 during this mode.

Mode 3 (t_2-t_3):

During this mode, L_r , C_r and L_m enter into resonance. Since $L_m+L_r>L_r$, the resonant period of this resonance is longer than the switching period, thereby, i_r and i_m can be regarded as constant during this mode. As $i_r=i_m$, there is no net current flowing into the transformer, thereby, causing the diode D1 and D3 to turn OFF. Thus in this zone, diodes are Zero Current Switched.

Since duty cycle of the switching network is 50%, operation in Mode 4, Mode 5 and Mode 6 is similar as in Mode 1, Mode 2 and Mode 3 respectively. The waveforms in these three modes are symmetrical with waveforms in Mode 1, Mode 2 and Mode 3.

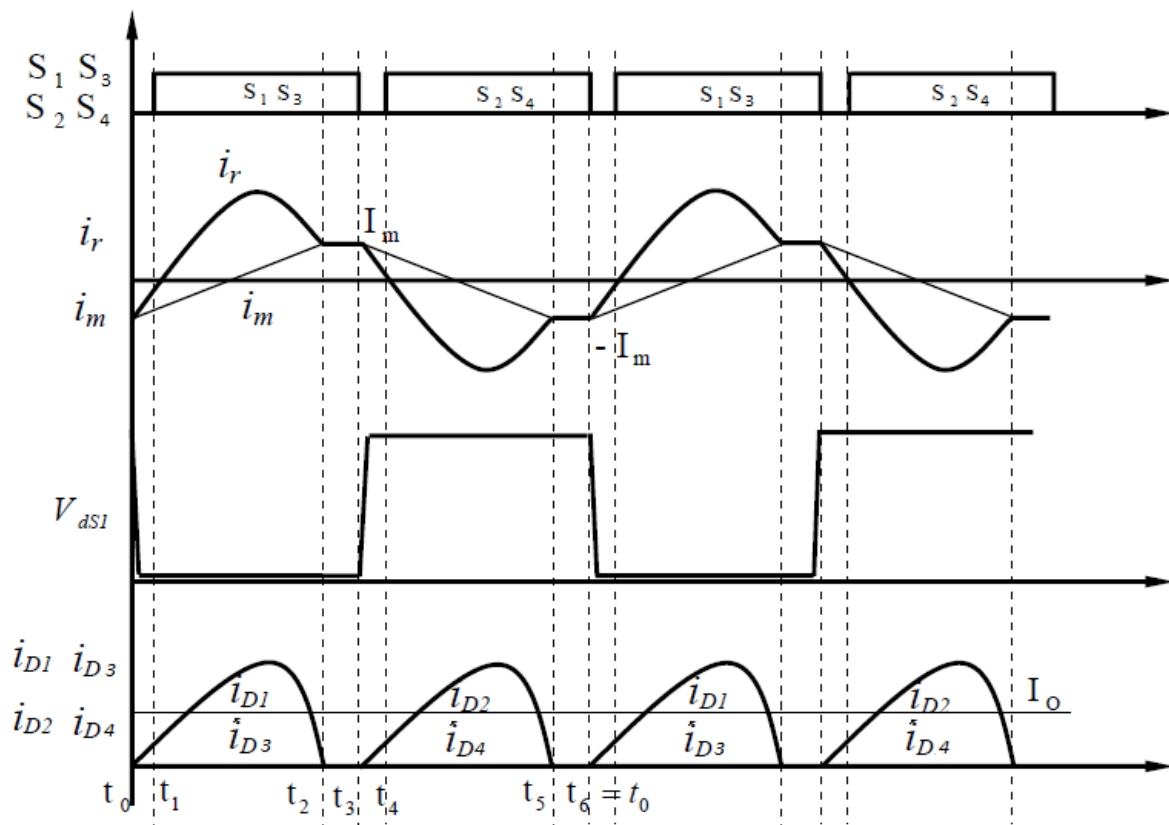


Figure 2-11 Waveforms for Zone 1- $f_{co} \leq f_{sw} \leq f_o$

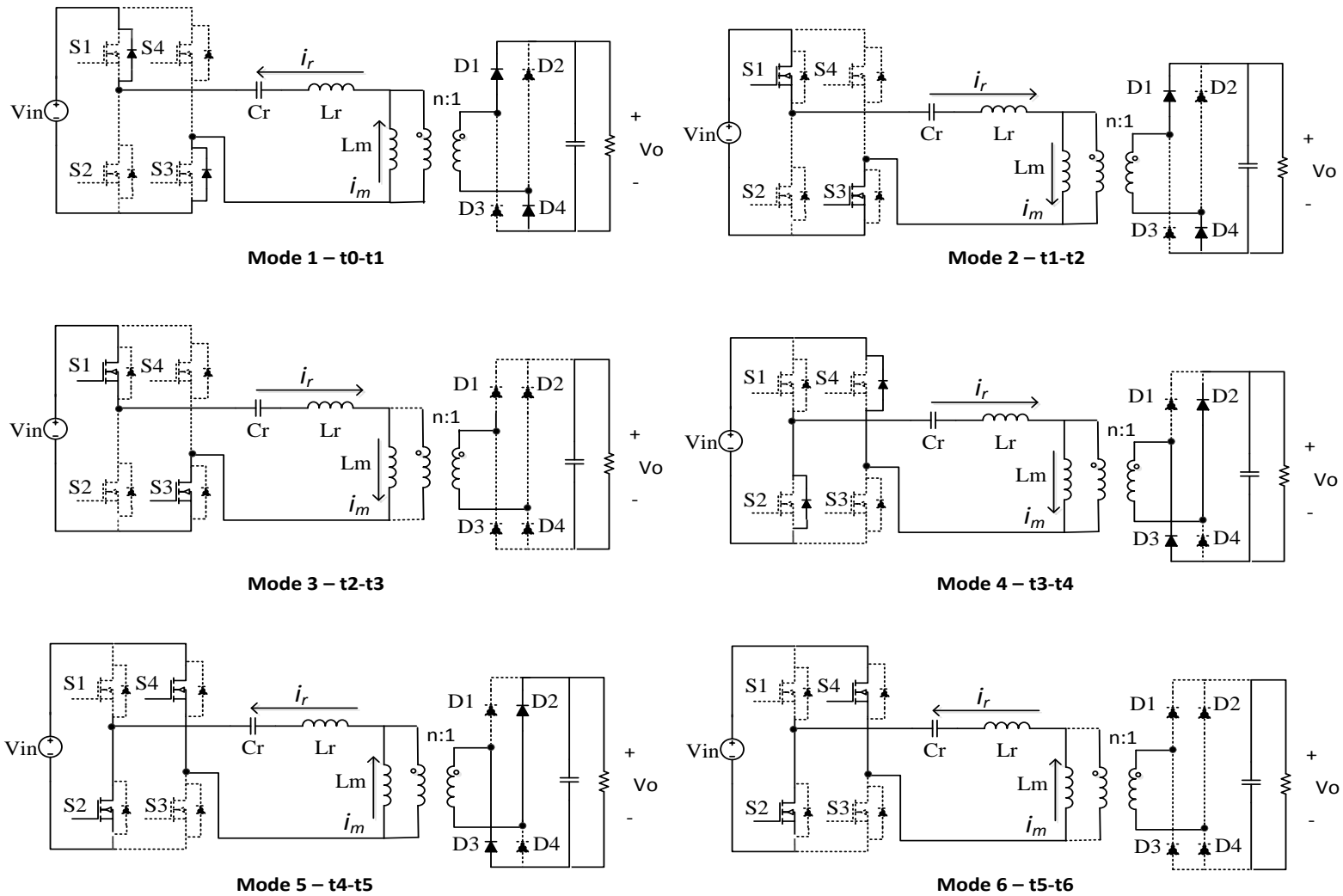


Figure 2-12 Equivalent Circuits of Operation Modes of LLC Converter in Zone 1 - $f_{co} \leq f_{sw} \leq f_o$

Zone 2- $f_{sw}=f_o$:

LLC converter enters this zone when the switching frequency of the switching network is exactly same as resonance frequency. In this zone, there is only one resonance occurring in L_r and C_r . Operation modes in this zone is similar to zone 1 except, there is no Mode 3 and Mode 6. Figure 2-13 shows the waveforms during this zone. The gain in this zone is unity, hence the only voltage conversion ratio available in this zone is provided by the turns-ratio of the transformer. This is the most efficient operating point of the LLC converter because of two reasons:

1. During the entire switching cycle, L_r and C_r are in resonance thereby, no circulating current and hence no conduction losses in the tank circuit.
2. Due to resonance, the current is sinusoidal in nature. Due to sinusoidal nature of the current, the RMS value of the operation current is low thereby less losses.

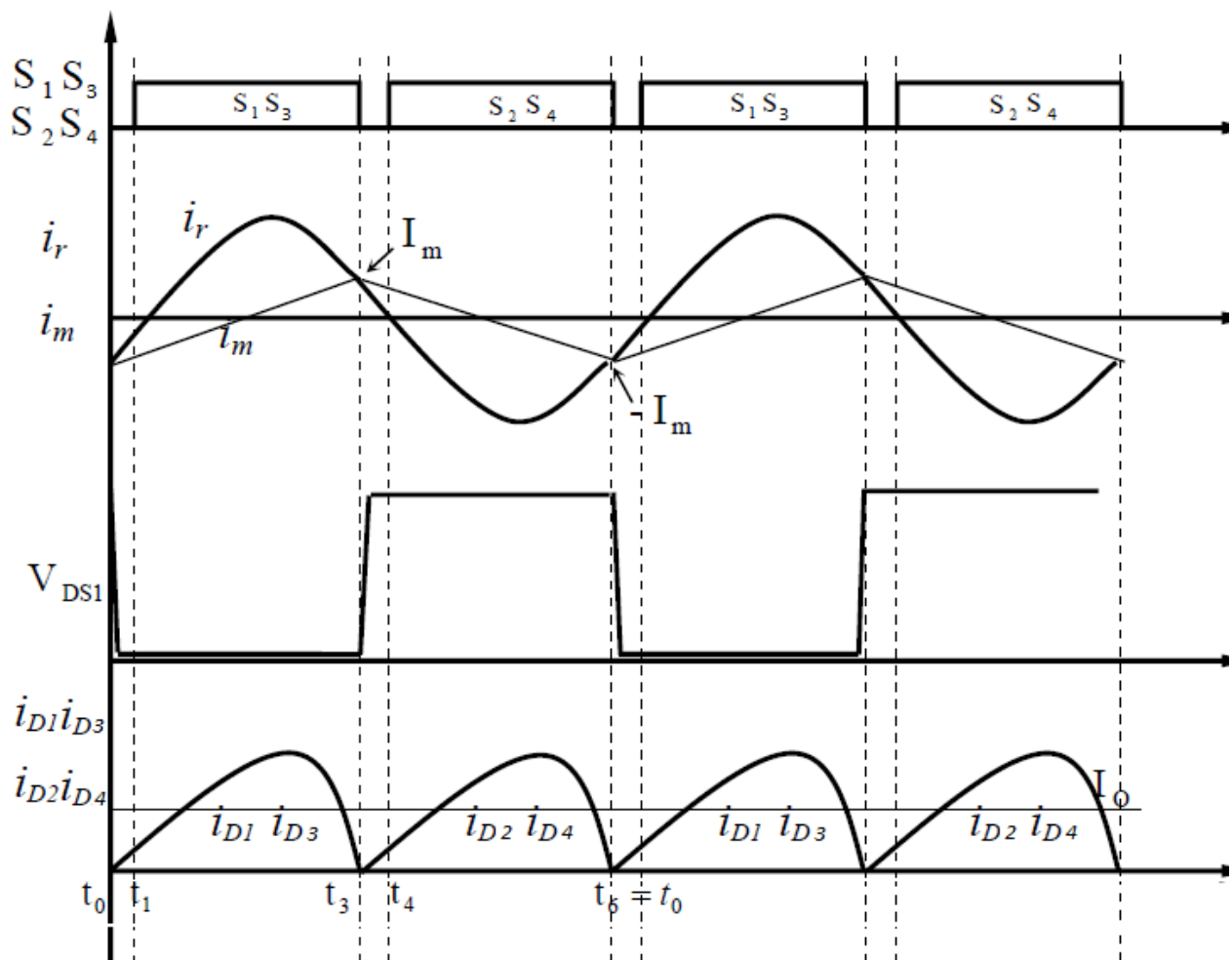


Figure 2-13 Waveforms of Zone 2- $f_{sw}=f_o$

Zone 3 – $f_{sw} > f_o$:

LLC Converter enters into Zone 3 once the switching frequency of the switching network $> f_o$. Figure 2-14 illustrates the waveforms in this zone. The converter goes through 6 modes while operating in this zone. Equivalent circuits for all 6 modes are shown in figure 2-15.

Mode 1- (t_0-t_1):

At $t=t_0$, S1 and S3 are turned ON. At the start of this mode, i_r and i_m are equal. The input voltage applied across the resonant network; causes L_r and C_r to undergo resonance. Due to resonance, i_r starts increasing sinusoidally. Since L_m does not undergo resonance, i_r and i_m begin to diverge. Difference between i_r and i_m causes D1 and D3 to go into conduction and is delivered to the load. Turning ON of D1 and D3 clamps L_m to reflected output voltage. This clamped voltage causes the current i_m to linearly increase from its negative peak to positive peak.

Mode 2 (t_1-t_2):

At $t=t_1$, S1 and S3 are turned OFF. This is the dead-time period of the switching cycle. Since S1 and S3 are turned OFF before the end of resonance period, $i_r > i_m$. This difference in the resonant and magnetizing currents keeps D1 and D3 conducting. Thus, the reflected output voltage clamped across L_m and no input voltage, blocks the resonant current i_r and causes it reduce further rapidly. At the same time, the clamped voltage across L_m keeps increasing i_m linearly.

Mode 3 (t_2-t_3):

At $t=t_2$, S2 and S4 are turned ON which cause the resonant current i_r to further drop. D1 and D3 are still conducting, which causes the L_m to be clamped at the reflected output voltage. This clamped voltage also adds to the decay of i_r and cause i_m to linearly increase. This mode ends at $t=t_3$, at which $i_r=i_m$ causing diodes D1 and D3 to turn OFF.

Since the switching network is switched at 50% duty cycle, Mode 4, Mode 5 and Mode 6 are similar to Mode 1, Mode 2 and Mode 3 respectively. The waveforms during Mode 4, Mode 5 and Mode 6 are symmetrical to that of Mode 1, Mode 2 and Mode 3 respectively.

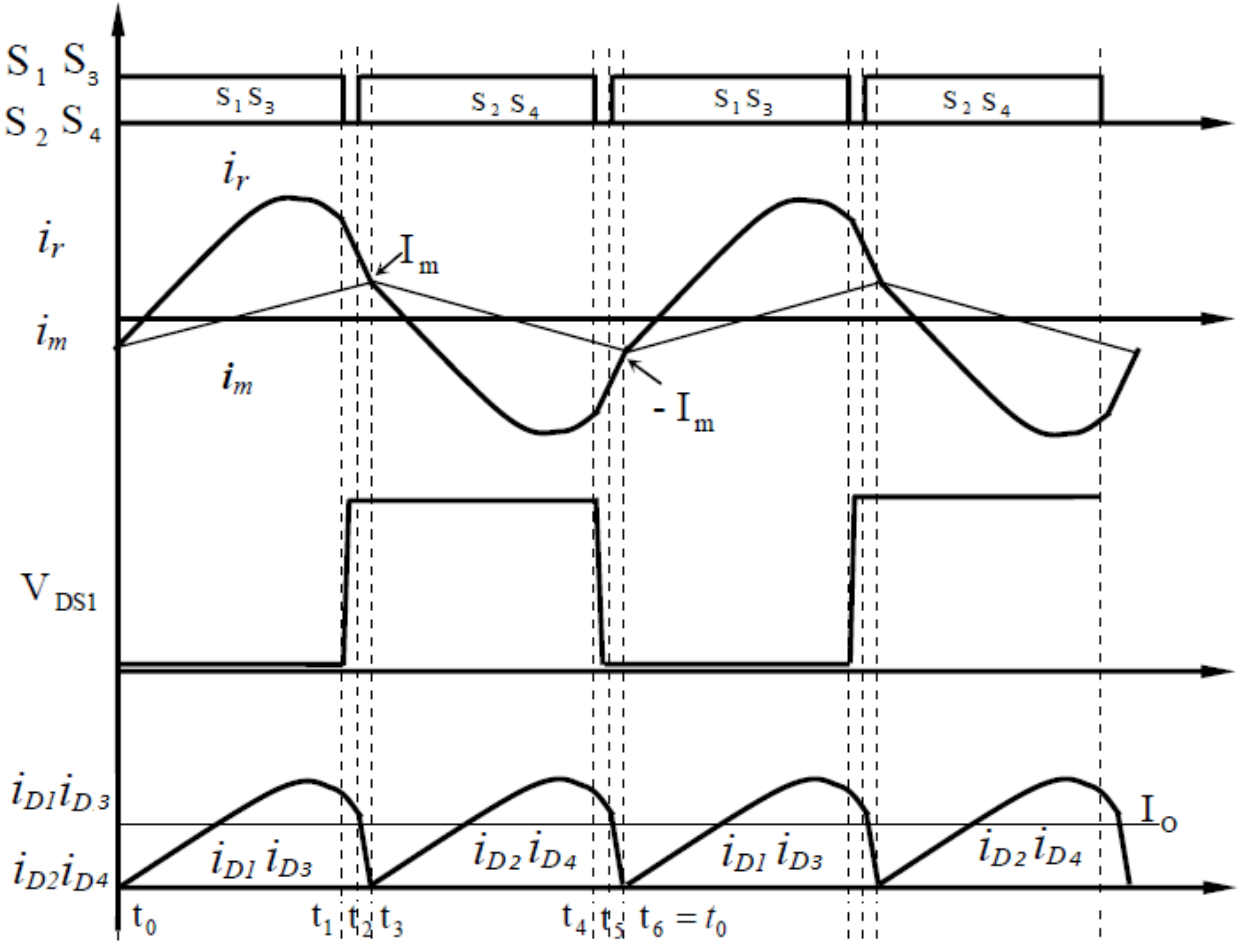


Figure 2-14 Waveforms of Zone 3 – $f_{sw} > f_o$

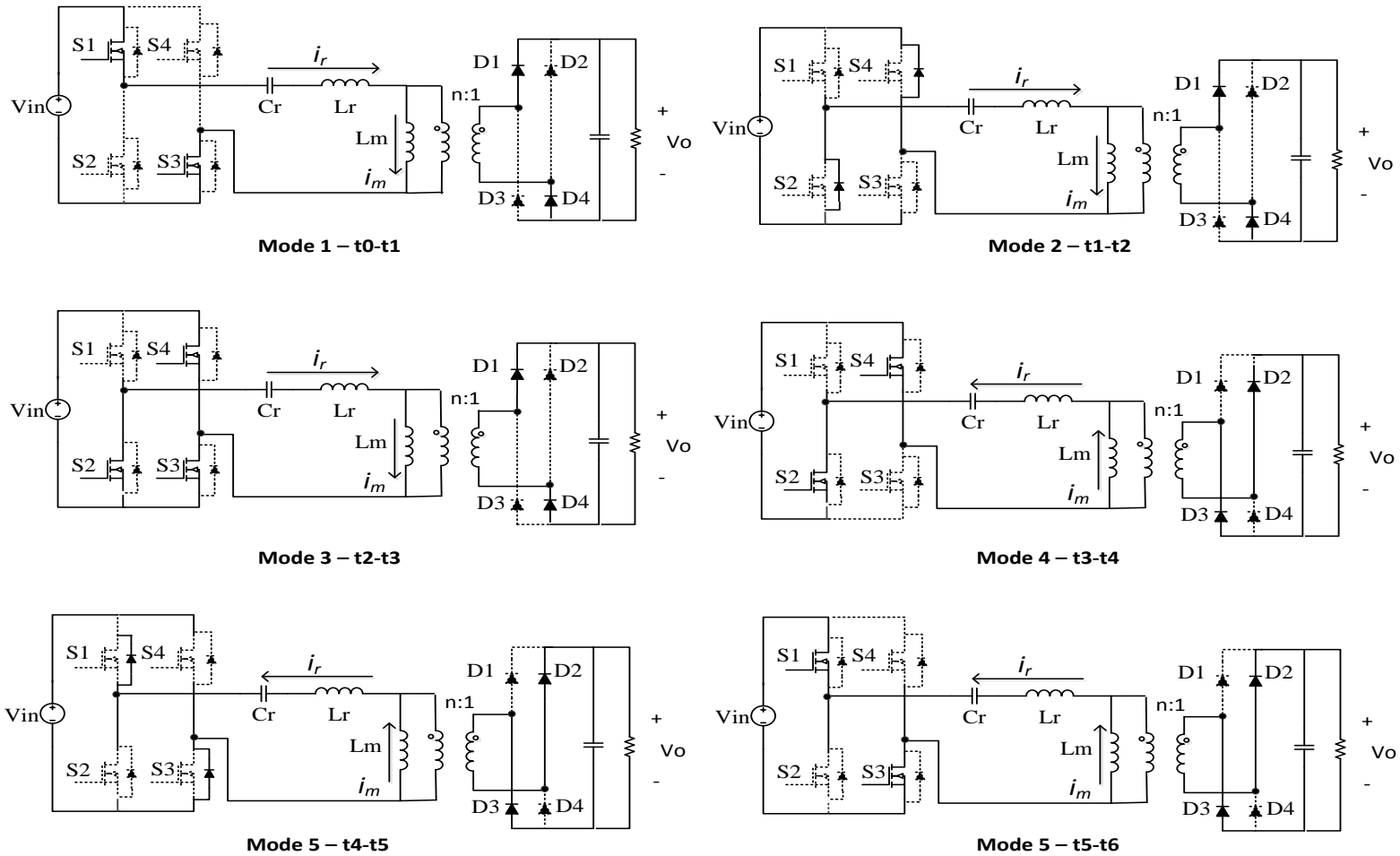


Figure 2-15 Equivalent Circuits of Operation Modes of LLC Converter in Zone 3 - $f_{sw} > f_o$

2.2.3 Discussion on Design considerations of LLC Converter as front end DC-DC Converter of Micro-Inverter

Front End DC-DC Converter of a micro-inverter has two primary functions.

1. Boost Converter: A typical 200W PV Panel delivers power at DC voltage level of 25-38V. This voltage level is not enough to invert the power at line voltage levels. Hence, there is a need to boost the DC voltage output of the PV Panel.
2. MPPT Controller: As seen in figure 2-13, a PV panel has an optimal operating point at which it delivers maximum power. This operating point varies with temperature and irradiance levels. Front End converter needs to make sure that the power is extracted from the PV panel at this maximum power point.

LLC topology is a highly suitable candidate to be used as front end DC-DC converter for micro-inverter for following reasons [2.7-2.9]:

1. Wide input voltage range.
2. High gain range.
3. Low component count.
4. Soft-Switching capability.

Apart from the advantages mentioned above, LLC converter has a unique feature which complements well with certain features of the PV panel.

As explained in operating modes of LLC resonant converter, the highest operating efficiency is obtained in Zone 2 i.e. $f_{sw} = f_o$. Also in this zone, the voltage gain is independent of load. As mentioned in section 2.1.1, at a constant temperature the

variance is V_{MPP} with respect to irradiance levels is very low. Hence, LLC Converter can be designed such that it operates in zone 2 when PV panel is operating at room temperature. As the voltage gain in zone 2 is independent of load and in case of PV panel as the input source, voltage gain is independent of irradiance levels; the LLC converter operates at its highest efficiency point for entire load range. As show in figure 2-16, zone 2 of LLC converter coincides with Maximum Power Point of PV Panel at room temperature.

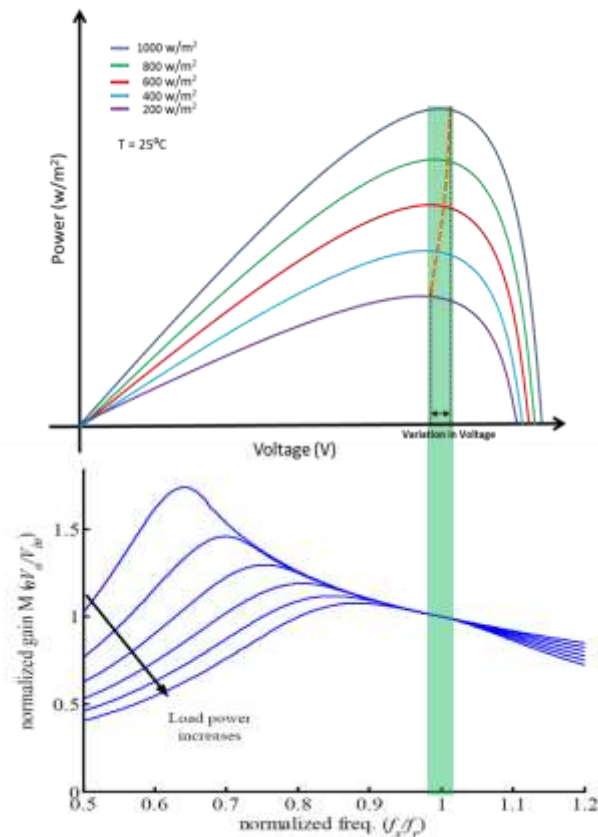


Figure 2-16 Optimal Design Consideration for LLC Converter as front DC-DC converter of Micro-Inverter

2.3 Design Procedure for Resonant Parameters of LLC Converter as Front End DC-DC Converter of Micro-inverter

This section provides the design procedure for calculating resonant parameters for LLC converter. In order to design the LLC converter first the design specifications needs to be derived with the help of PV Panel Datasheet.

2.3.1 Deriving the Design Specifications

In this design example, the input PV panel is 410W PV panel from Advanced Solar Photonics and the rectifier network is a voltage doubler.

- Desired output voltage = 400V.
- Maximum output power = 400W.

1. Turns Ratio:

In order to operate LLC Converter at highest efficiency point at room temperature, the LLC converter should operate in zone 2. In this operation zone, the gain of the LLC converter is unity. Hence the required gain to boost PV panel voltage to 400V should be achieved from the turns-ratio of the transformer.

$$n = \frac{V_{MPP(25^{\circ}C)}}{V_{OUT}} \quad (2.12)$$

2. Gain Range:

Gain range can be calculated from the operating temperature range of the micro-inverter. PV Panel V_{MPP} has a negative temperature coefficient i.e. V_{MPP} decreases with increase in temperature.

$$M_{MAX} = \frac{nV_{OUT}}{V_{MPP(MaxTemp)}} \quad (2.13)$$

$$M_{MIN} = \frac{nV_{OUT}}{V_{MPP}(Min Temp)} \quad (2.14)$$

2.3.2 Calculating Resonant Parameters

Once the turns ratio and gain range is obtained, the resonant parameters i.e. Lr, Cr and Lm are calculated using procedure shown in [2.6]

DC gain curve of LLC converter is a function of two dummy variables i.e. Ln and Qe as defined by equation (2.9) respectively. Behavior of DC gain with variance in Ln and Qe can be summarized as follows:

1. As shown in figure 2-10, the gain reduces with increase in Qe i.e. gain reduces with increase in load current.
2. Lower Qe increases the maximum achievable gain but the associated gain curves require large frequency variation for a given gain adjustment.
3. For a fixed value of Qe, maximum achievable gain varies inversely with Ln. This phenomenon can be observed in figure 2-17. However, lower value of Ln cause Lm to reduce which in turn increases the magnetizing current. Increase in magnetizing current leads to increase in circulating current, thereby increasing the losses.
4. From figure 2-17, it can also be concluded that a particular value of gain can be achieved by more than one combination of Ln and Qe values.
5. It can be seen from figure 2-18 that for a fixed Qe (load current), increase in Ln leads to an increase in frequency variation for a given gain adjustment.

As the required gain can be achieved using different combinations of L_n and Q_e , $L_n = 5$ and $Q_e = 0.5$ is considered to be a good starting point [2.6]. From this starting point, further reiteration is necessary to achieve an optimal combination of L_n and Q_e such that required gain is obtained with minimum losses.

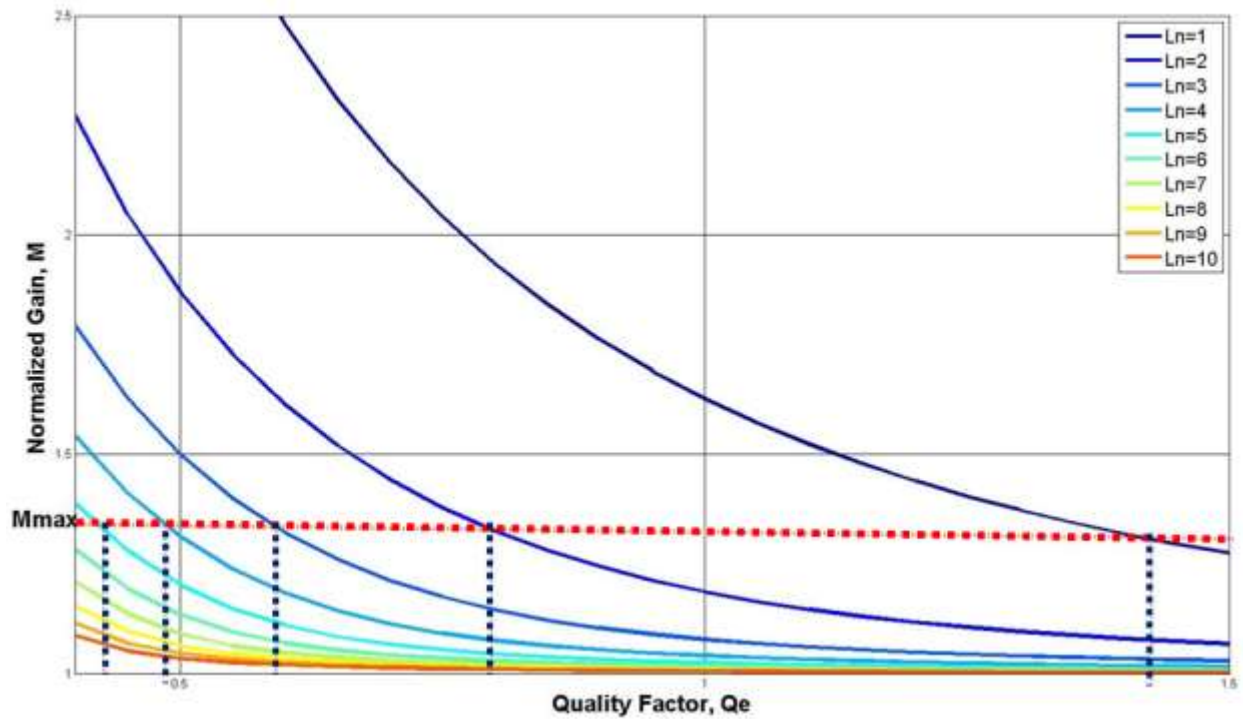


Figure 2-17 Normalized Gain, M vs Quality Factor, Q_e

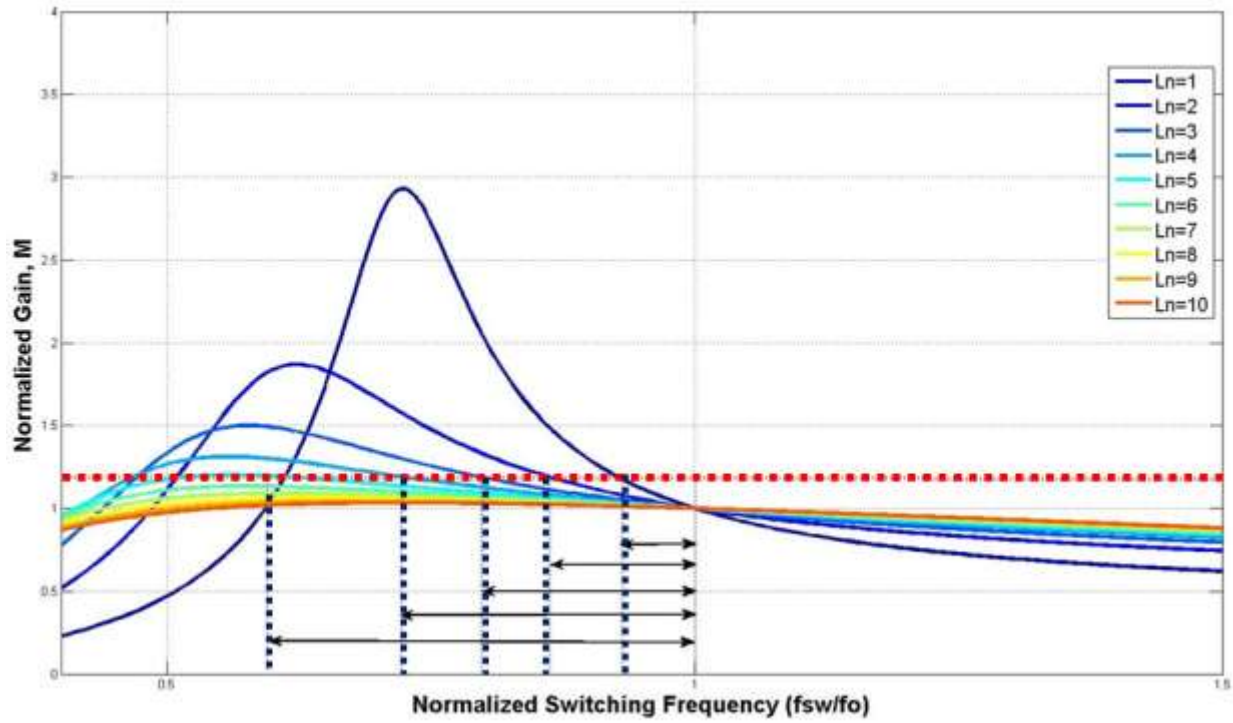


Figure 2-18 Gain vs Switching Frequency-Fixed Qe-Variable Ln

Once the values of L_n and Q_e are obtained, resonant parameters can be calculated using following equations.

$$C_r = \frac{1}{2\pi f_o R_e Q_e} \quad (2.15)$$

$$L_r = \frac{1}{(2\pi f_o)^2 C_r} \quad (2.16)$$

$$L_m = L_n L_r \quad (2.17)$$

2.3.3 Design Example

This design example considers a 410W mono-crystalline PV panel from Advanced Solar Photonics at the input of a full bridge LLC Converter with voltage doubler as the output rectifier network as shown in figure 2-19

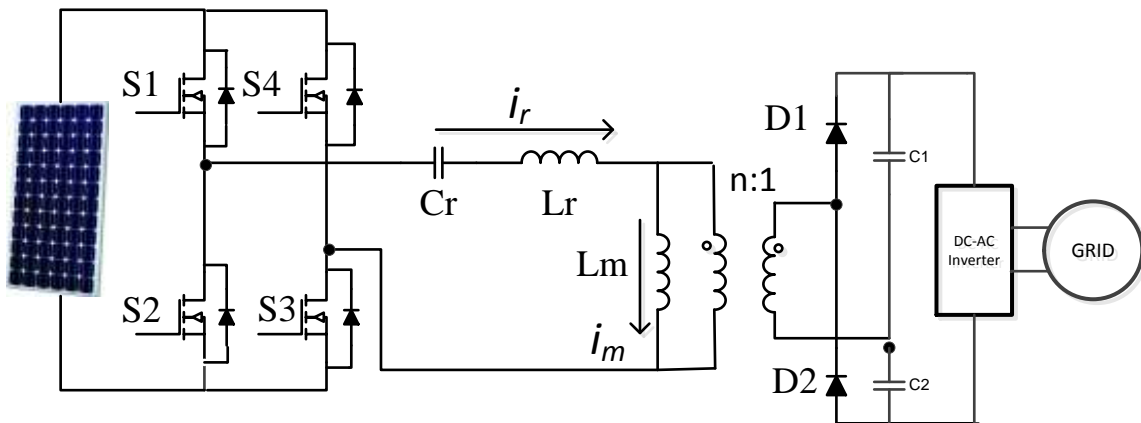


Figure 2-19 Full Bridge LLC Converter as Front End DC-DC Converter for Micro-Inverter

The above mentioned PV Panel has following specifications at standard test conditions:

- $P_{max} = 410W$
- $V_{MPP} = 50.34V$.
- $I_{MPP} = 8.15A$.
- Temperature Coefficients:
 - Power ($\%/^{\circ}C$) = -0.49.
 - V_{MPP} ($\%/^{\circ}C$) = -0.40.

Input specifications for a temperature range of $-40^{\circ}C$ to $65^{\circ}C$ can be derived as:

$$n = \frac{V_{MPP(25^{\circ}C)}}{\frac{V_{OUT}}{2}} = \frac{50.34}{200} = 0.2517$$

In the above equation output voltage is divided by 2 to compensate the voltage gain provided by voltage-doubler.

$$M_{MAX} = \frac{\frac{nV_{OUT}}{2}}{V_{MPP(65^{\circ}C)}} = \frac{50.34}{42.285} = 1.19$$

$$M_{MIN} = \frac{\frac{nV_{OUT}}{2}}{V_{MPP(-40^{\circ}C)}} = \frac{50.34}{63.428} = 0.793$$

Based on the calculation method described in previous section, after certain design iterations; following are the final resonant parameters.

$$**fr = 140kHz**$$

$$**Qe = 0.002 for 10% load and Qe = 0.08 for 100% load.**$$

$$**Ln = 10.52**$$

$$**Lr = 1.9\mu H**$$

$$**Cr = 680nF**$$

$$**Lm = 20\mu H**$$

Gain curve for the above design is shown in figure 2-20. From the figure it can be seen that the design is able to meet Mmax requirement, however, it does not meet Mmin requirements at maximum frequency. In order to achieve the Mmin requirement, the converter must be operated in half bridge mode at higher input voltages i.e. at lower temperatures.

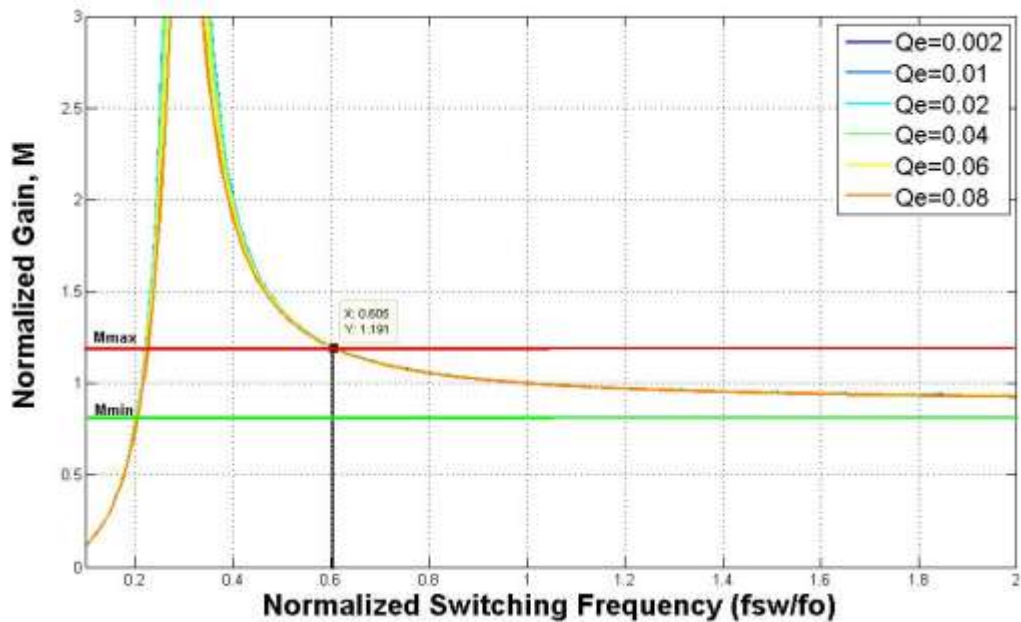


Figure 2-20 Gain vs. Switching Frequency, Design Example

Figure 2-21 shows the power drawn from the 410W PV Panel. From the figure, it can be observed that when the designed LLC converter is used as the front end converter DC-DC converter for the micro-inverter; the maximum power is tracked at $f_{sw} = 140$ kHz which is the resonant frequency for this design. Thus, the converter operates in high efficiency operating zone i.e. zone 2 while tracking maximum power. Figure 2-22 shows the experimental results of the efficiency performance of the designed LLC converter @ 51.8V input. This design yields a peak efficiency of 98.2% at input voltage of 51.8V.

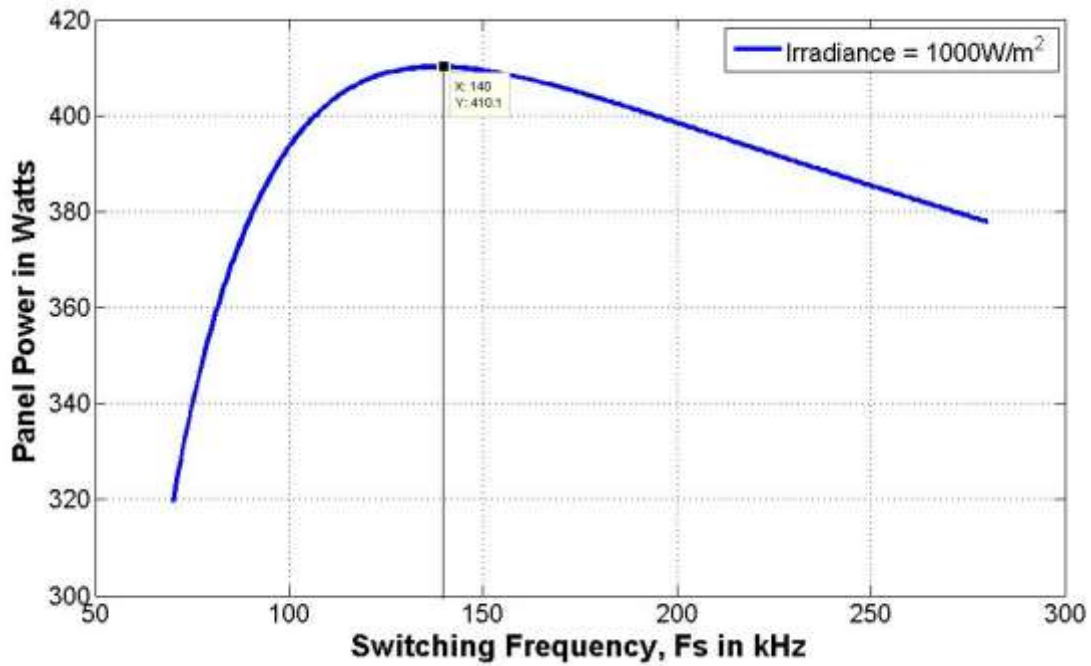


Figure 2-21 PV Panel Power vs. Switching Frequency for LLC Converter as front end DC-DC Converter, design example

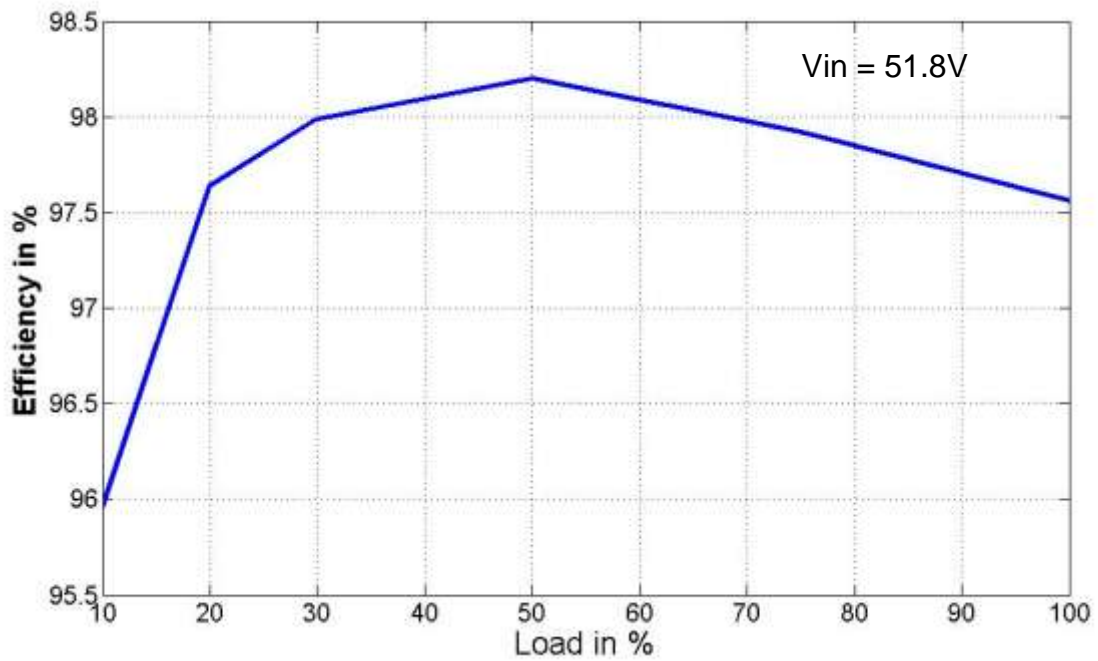


Figure 2-22 Experimental Results - Efficiency, design example

2.4 References

- 2.1 Bellini, A.; Bifaretti, S.; Iacovone, V.; Cornaro, C., "Simplified model of a photovoltaic module," *Applied Electronics, 2009. AE 2009* , vol., no., pp.47,51, 9-10 Sept. 2009
- 2.2 Solmetric. *Guide to Interpreting I-V Curve Measurements of PV Arrays – Application Note PVA-600-1.*
- 2.3 Florida Solar Energy Centre (2002), *Photovoltaic Modules and Arrays*. Retrieved from
http://www.pttrenenergy.upc.edu/index2.php?option=com_docman&task=doc_view&qid=213&Itemid=35
- 2.4 Fang, X. (2012). *Analysis and Design Optimization of Resonant DC-DC Converters* (Doctoral Dissertation). Retrieved from UCF Libraries Database.
- 2.5 Huang, Guisong; Gu, Yilei (2000), Delta Power Electronics Center. *Half Bridge LLC Converter* (Technical Report).
- 2.6 Huang, Hong ;. *Designing an LLC Converter Half-Bridge Power Converter* Texas Instruments Design Application Note.
- 2.7 Jee-Hoon Jung; Joong-Gi Kwon, "Theoretical analysis and optimal design of LLC resonant converter," *Power Electronics and Applications, 2007 European Conference on* , vol., no., pp.1,10, 2-5 Sept. 2007.
- 2.8 Chun-An Cheng; Hung-Wen Chen; En-Chih Chang; Chun-Hsien Yen; Kun-Jheng Lin, "Efficiency study for a 150W LLC resonant

converter," *Power Electronics and Drive Systems, 2009. PEDS 2009.*

International Conference on , vol., no., pp.1261,1265, 2-5 Nov. 2009

2.9 Pawellek, A.; Oeder, C.; Duerbaum, T., "Comparison of resonant LLC

and LCC converters for low-profile applications," *Power Electronics and*

Applications (EPE 2011), Proceedings of the 2011-14th European

Conference on , vol., no., pp.1,10, Aug. 30 2011-Sept. 1 2011.

CHAPTER 3: LIGHT LOAD EFFICIENCY IMPROVEMENT OF THREE PHASE GRID TIED INVERTERS

3.1 Daily Solar Irradiance Pattern

Incident solar power on a PV panel is function of time of day, time of year, shading, cloud cover and the location co-ordinates. On a typical day in a non-polar region, with clear sky and no partial shading, the incident power reaches its maximum during the day at noon and its minimum at night. The solar irradiance profile on a typical day appears like a Gaussian curve as shown in figure 3-1 below.

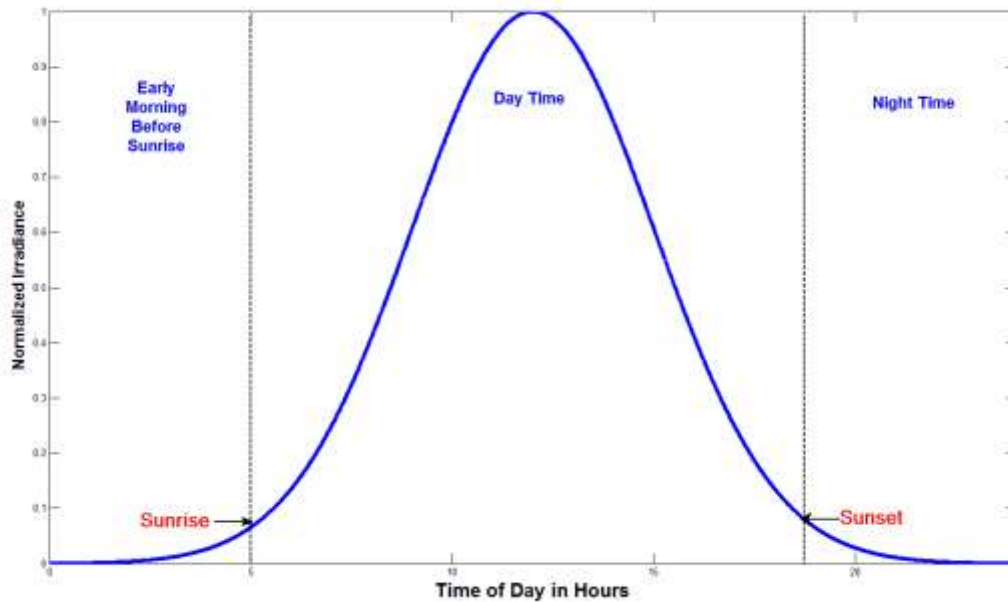


Figure 3-1 Solar Irradiance Pattern on a Typical Day

The N point Gaussian curve can be represented in a discrete form using the following equation from [3.1]:

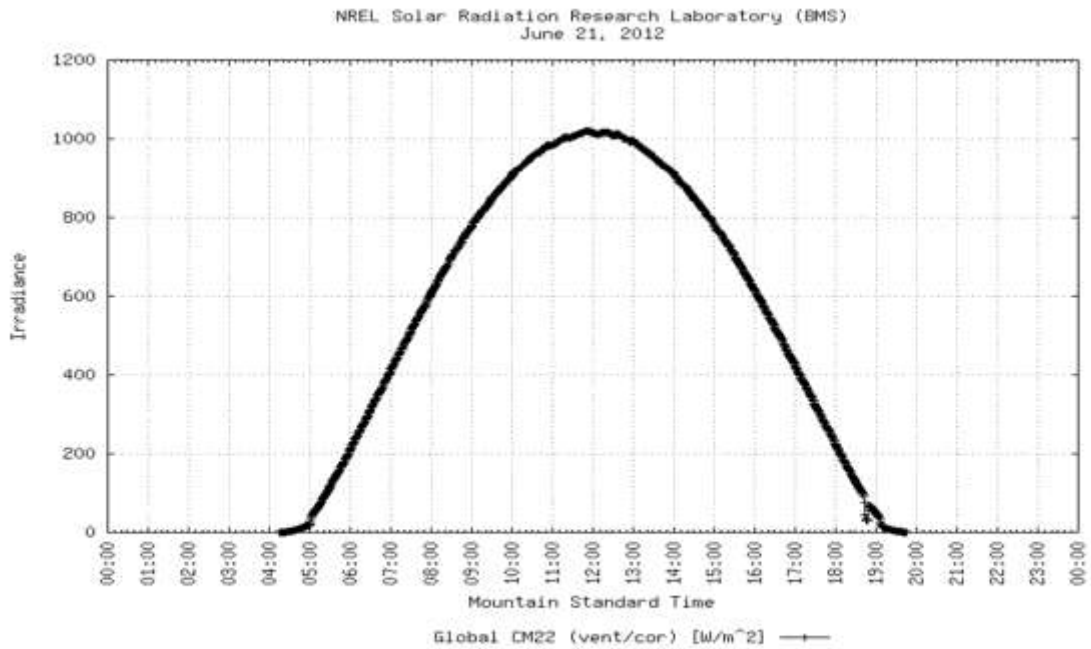
$$f(n) = e^{-\frac{1}{2}\left(\frac{2\alpha n}{N}\right)^2} \text{ where } -\frac{(N-1)}{2} \leq n \leq \frac{(N-1)}{2} \quad (3.1)$$

$$\alpha = \frac{N}{2\sigma} \text{ where } \sigma = \text{Standard Deviation} \quad (3.2)$$

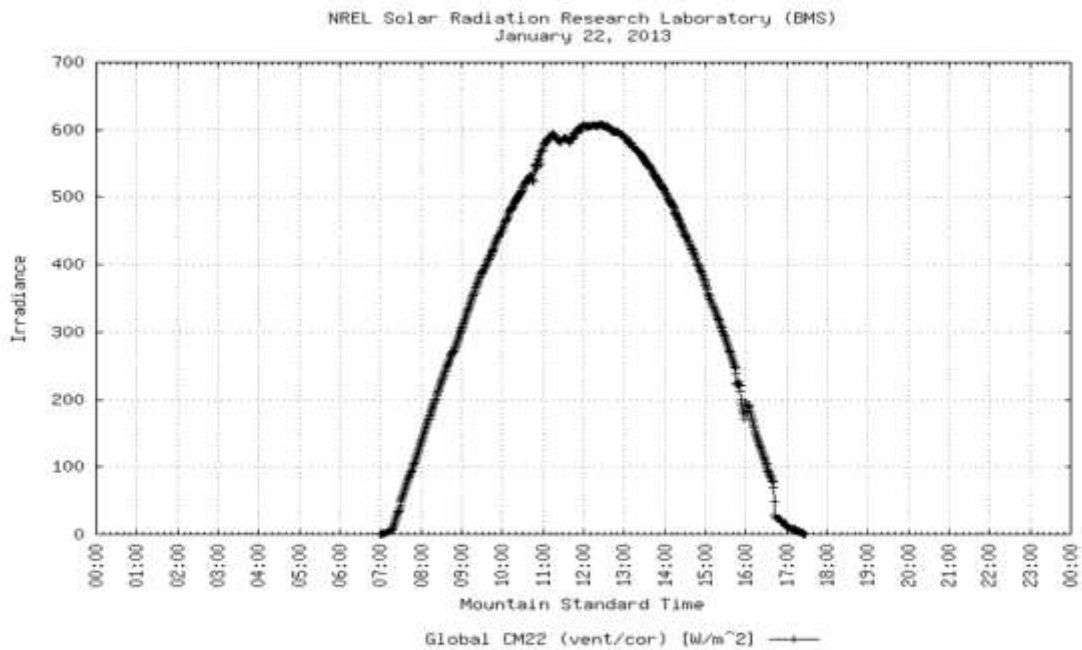
The width of Gaussian curve is inversely proportional to α . Thus, for solar irradiance pattern α is an indirect function of *length of day* i.e. the time between sunrise and sunset. During summer time, the *length of day* is longer than the *length of day* during winter, thereby the irradiance curve during summer time are wider than the ones during winter.

NREL's Solar Radiation Research Laboratory located at Golden, Colorado, US continuously measures solar radiation components. From their measured solar irradiance pattern shown in figure 3-2 it can be verified that on a typical day the solar irradiance pattern follows a Gaussian curve. The figure 3-2 below shows irradiance pattern of a typical day during summer time and winter time. It can be concluded by observation that during summer time when the *length of day* is longer, the width of irradiance curve is wider. Figure 3-3 shows irradiance patterns of a cloudy day. From the irradiance curves of cloudy days, it can be deduced that, the available solar power is at its peak for less than 10% of the day time.

Due to highly variable nature of available solar power, it is essential for a PV inverter to have flat efficiency response over its entire load range. In order to have more realistic efficiency index, PV inverters are evaluated according to their *weighted efficiency* and not at *peak efficiency*.



(a) Solar Irradiance Curve – Summer



(b) Solar Irradiance Curve – Winter

Figure 3-2 Solar Irradiance Patterns – Clear Days

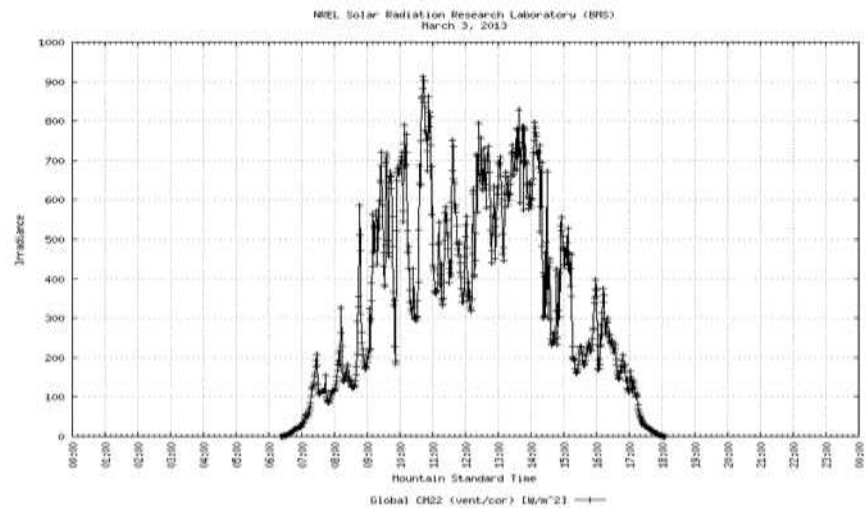
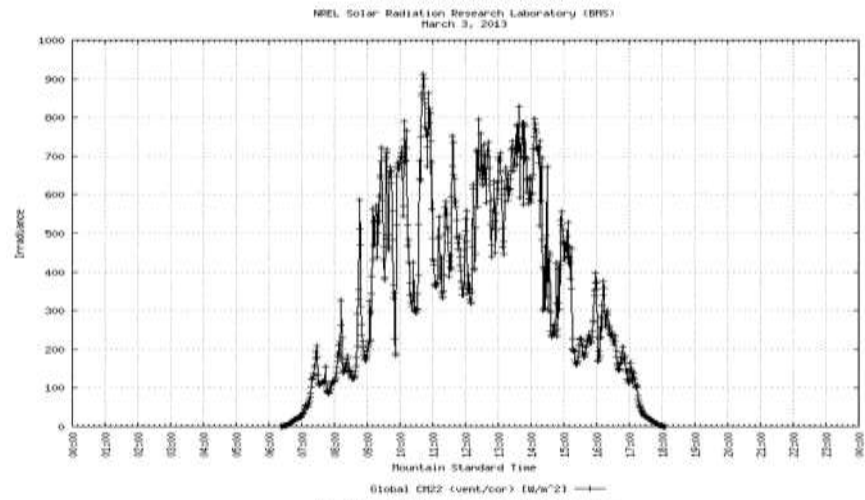
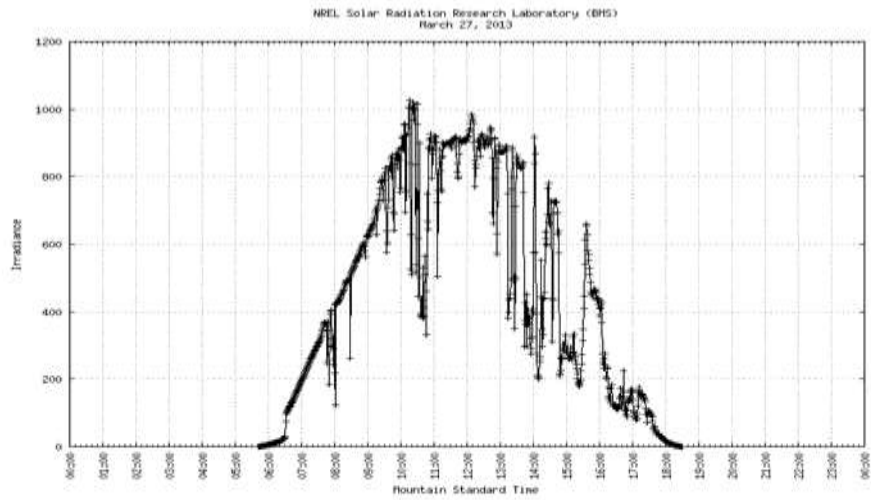


Figure 3-3 Solar Irradiance Curves – Cloudy Days

3.2 Significance of Weighted Efficiency for PV Inverters

In the previous section, it was established the available solar power is highly variable and function of myriad of parameters like

1. Length of Day.
2. Time of the Day.
3. Time of the Year.
4. Location Co-ordinates
5. Cloud Cover.
6. Partial Shading due to leaves.
7. Dust.

Based on the solar irradiance measurements done by NREL which are shown in Figure 3-2 and 3-3, it can be concluded that PV inverter is required to operate over its entire load curve for fair share of time. In order to justify the high investment cost required in PV as compared to conventional sources of energy, it is of utmost importance to extract every single watt of power at the best possible conversion efficiency.

Typically, every power converter has an optimal operating load point at which the converter's power conversion efficiency peaks. At other load points, the conversion efficiency deteriorates for the reasons explained in the next section of this chapter. If a converter is required to operate at a fixed load, then it can be designed such that the peak conversion efficiency load point of the converter intersects with the fixed operating load point at which converter is specified to operate. However, for PV applications, as

the available power to be converted is constantly varying, the Power Converters for PV applications are evaluated at Weighted Efficiency rather than peak efficiency. Weighted efficiency is a performance index which is widely used in PV applications as it generates the efficiency index based on the efficiency performance of the inverter over its entire load range.

Depending upon the geography, two sets of weighted efficiency performance indices are available [3.2]. These two efficiency indices vary in terms of weights assigned to different load points.

1. European Weighted Efficiency.

$$\eta_{EUR} = 0.03\eta_{5\% Load} + 0.06\eta_{10\% Load} + 0.13\eta_{20\% Load} + 0.1\eta_{30\% Load} + 0.48\eta_{50\% Load} + 0.2\eta_{100\% Load} \quad (3.3)$$

2. California Energy Commission Weighted Efficiency (US).

$$\eta_{CEC} = 0.04\eta_{10\% Load} + 0.05\eta_{20\% Load} + 0.12\eta_{30\% Load} + 0.21\eta_{50\% Load} + 0.53\eta_{75\% Load} + 0.05\eta_{100\% Load} \quad (3.4)$$

In order to achieve a higher weighted efficiency for Three Phase Inverters for Grid Tied PV applications, a control technique, *Phase Skipping Control* is proposed to improve the light load efficiency performance of the inverter. This control technique has been implemented for Three Phase Half Bridge PWM Inverter; however, it can be easily extended to any class of Three Phase Inverters.

3.3 Efficiency Behavior in Power Converters

Typically every power converter has an optimal operating point at which its efficiency peaks. Figure 3-4 shows the efficiency curve of such a typical power converter. Efficiency is low at light loads, it recovers with increase in load and reaches its maximum at around 70%-80% of its full load capacity and droops slightly at full load.

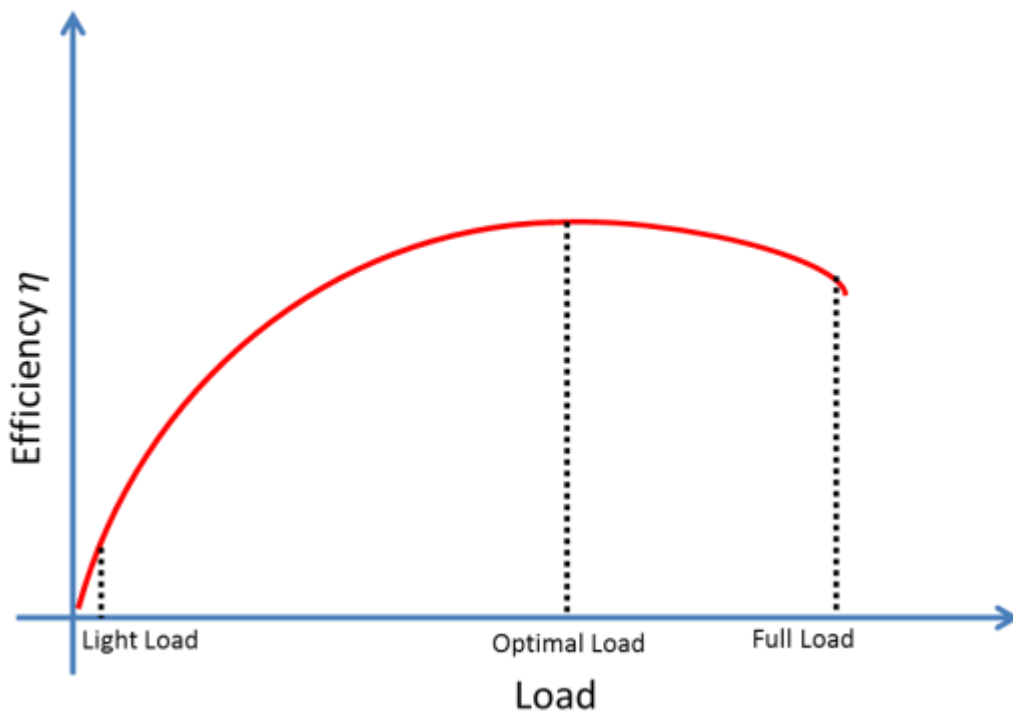


Figure 3-4 Efficiency Curve of a Typical Power Converter

Losses in a power converter are composed of two factors which causes the above mentioned efficiency curve of power converters [3.3].

$$P_{Loss} = P_{Load\ Dependent\ Loss}(I_{load}) + P_{Load\ Independent\ Loss} \quad (3.5)$$

1. **Load Dependent Losses:** These are losses in power converters which are dependent on the load like conduction losses in switches, copper losses in magnetics.
2. **Load Independent Losses:** These losses are not a function of load current. They are a function of supply voltages, switching frequency and ripple current through the magnetics. These losses are switching losses, magnetic core losses, high frequency AC copper losses magnetics due to high frequency ripple current and diode recovery losses.

Efficiency of a power converter can be represented by following equation:

$$\eta = 1 - \frac{P_{Loss}}{P_{in}} \quad (3.6)$$

Combining equation (3.6) and (3.7) together and expressing them as a function of load current we get:

$$\eta = 1 - \frac{P_{Load\ Dependent\ Loss}(I_{Load}) + P_{Load\ Independent\ Loss}}{P_{in}(I_{Load})} \quad (3.7)$$

As $P_{Load\ Independent\ Loss}$ is not a function of load current, at lighter loads it dominates the losses as well as tends to keep the numerator constant in equation (3.7). As denominator comprises of P_{in} which is a function of load current, it becomes smaller at lighter loads, thereby, deteriorating the efficiency at lighter loads. At heavier loads, the conduction loss tends to dominate the total losses. As conduction losses are mostly I^2R losses, they are a square law function of load current whereas P_{in} is a linear function of load current. This causes the efficiency to slightly droop at higher loads. The variation in losses with load current and its impact on efficiency is qualitatively represented in figure 3-5.

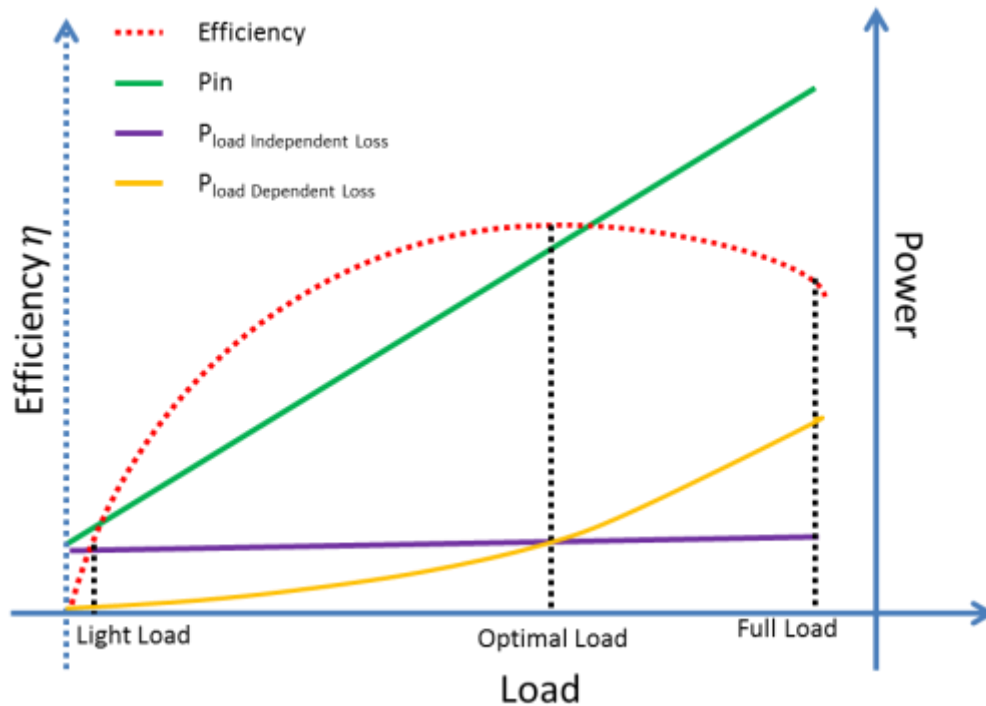


Figure 3-5 Impact of Losses on Efficiency as a Function of Load Current

In order to achieve a better weighted efficiency, the inverter must have a flat efficiency response over its entire load range. Various methods like variable switching frequency control, phase shedding, burst mode operation, using energy storage, bulk voltage reduction have been proposed in the literature for DC-DC Converters[3.3 – 3.9]. In order to improve light load efficiency for inverters, techniques like “Pulse Skipping” and different modulation techniques are proposed in the literature [3.10-3.12, 3.15]. Pulse Skipping causes the inverter to operate in burst mode which tends to create instability into the grid. Modulation Technique proposed in [3.10] [3.11] are topology specific.

Phase Skipping Control is a topology independent control technique which improves the light load efficiency for multiphase inverters. In order to establish a proof of concept, this technique has been implemented on a Half Bridge Three Phase PWM Inverter and analysis for this topology is given.

3.4 Half Bridge PWM Inverter

Half Bridge PWM Inverter is essentially a Sinusoidally Modulated Synchronous Buck Converter with a bipolar bus voltage. Figure 3-6 illustrates the topologies of Synchronous Buck Converter and Half Bridge Inverter.

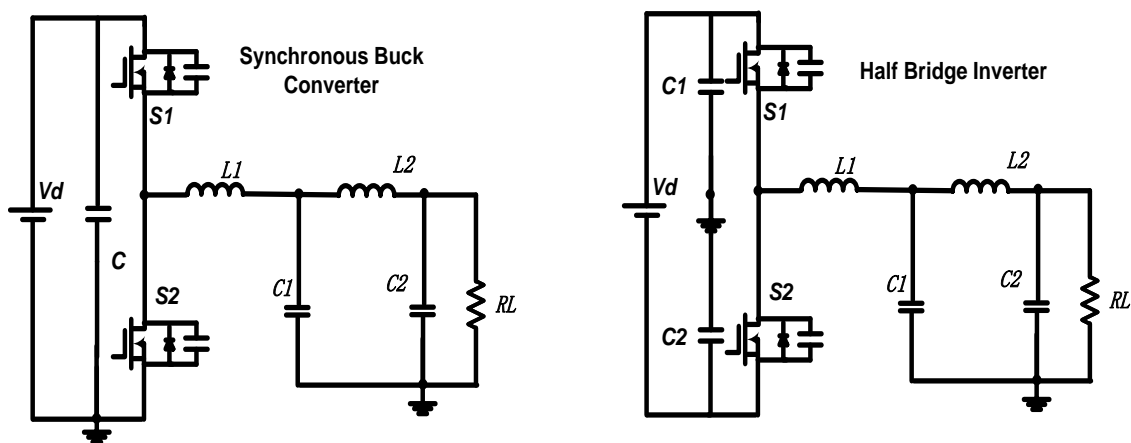


Figure 3-6 Comparison of Synchronous Buck Converter and Half Bridge Inverter

The gate drive signals for the MOSFET's of Half Bridge PWM Inverter are generated by modulating Saw Tooth Carrier Signal with Sinusoidal Reference. Frequency of carrier signal defines the switching frequency of the inverter and frequency of the modulating sinusoidal signal controls the frequency of the output voltage. Figure 3-7 illustrates the

gate drive signals for the Half Bridge Inverter. The Top Side MOSFET and Bottom Side MOSFET signals are complementary PWM Signals with dead-time (t_d) between them to avoid cross conduction of the two switches.

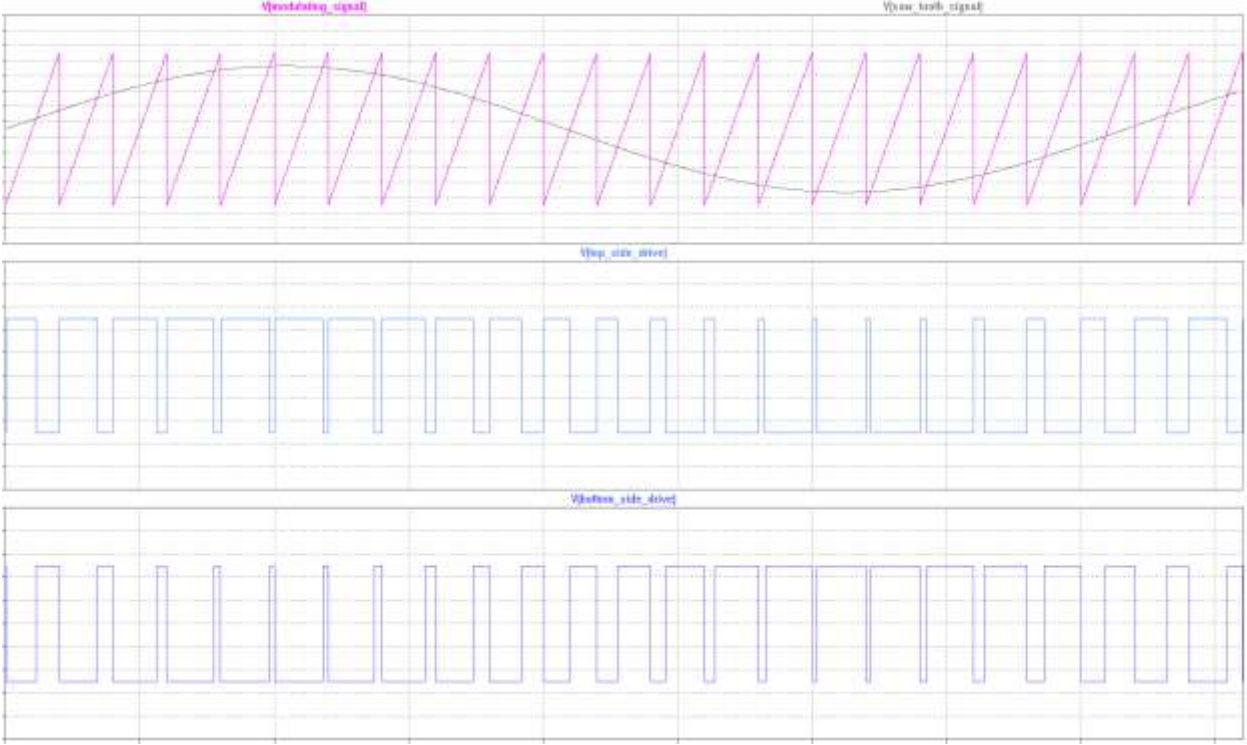


Figure 3-7 Gate Drive Signal for Half Bridge Inverter

Output voltage of the Half Bridge Inverter is a function of the modulation index (m). The modulation index is calculated as:

$$m = \frac{V_{modulating}}{V_{carrier}} \tag{ 3.8 }$$

For a proper sinusoidal output voltage, the modulation index m is less than unity. If m exceeds more than unity, then it leads to clipping of the output voltage.

3.4.1 Half Bridge Inverter Operation:

The operation of Half Bridge Inverter is divided into eight operation modes, four for each half cycle of the line voltage. Figure 3-8 illustrates all eight operation modes using the topology diagrams. Figure 3-9 and Figure 3-10 describe the operation mode waveforms of positive and negative half cycle respectively.

Mode 1(t₀-t₁):

This mode occurs during the positive line half cycle. Top side MOSFET S1 is turned ON while bottom side MOSFET S2 is turned OFF at t₀. In this mode, MOSFET S1 is hard switched while turning ON. Due to hard switch turn ON, discharge of Drain to Source Capacitor of S1 and reverse recovery of body diode of S2, there is a current spike at the start of this mode. V_{GS}(S1) exhibits a plateau region which occurs because of increase in C_{oss}(S1) caused due to collapse of drain to source voltage. Once the MOSFET is completely turned ON, the V_{DS} (S1) drops to I_L²R_{DS(ON)} voltage drop across S1. Current through inductor (L1) rises linearly with the slope given by:

$$\Delta I_{L1} = \frac{V_{BUS} - V_0(t)}{L_1} \quad (3.9)$$

where V_{BUS} = Bus voltage w.r.t Neutral

V₀(t) = Instantaneous Output Voltage

The inductor current continues to rise with the slope given in (4.9) until t₁ where this mode ends.

Mode 2 (t_1-t_2):

This mode occurs in positive line half cycle. This mode starts at t_2 at which turn OFF process of top side MOSFET S1 begins. Bottom side MOSFET S2 is still OFF. This mode is the dead-time interval between turning OFF of top side MOSFET S1 and turning ON of bottom side MOSFET S2. Turning OFF of MOSFET S1, blocks the existing inductor current path. As inductor does not allow sudden change in current through it; the current needs to find an alternate path. This alternate path is created by turning ON of body diode of bottom side MOSFET S2 and current freewheels through this body diode. Turning ON of body diode of S2 cause the $C_{DS}(S2)$ to discharge through the diode and the voltage across $V_{DS}(S2)$ drops to negative diode voltage drop. This mode ends at t_2 i.e. at the end of dead-time.

Mode 3 (t_2-t_3):

This mode occurs during the positive line half cycle. This mode begins with turn ON of bottom side MOSFET S2. Due to turn ON of body diode of S2 during MODE 2, the voltage across the drain to source terminal of the S2 is negative diode voltage diode drop. This enables ZVS turn ON of S2. Turn ON of S2 creates a low resistance path for the inductor current to flow through S2. With turn ON of S2, the bus voltage in series with instantaneous output voltage is applied across the inductor. This leads to voltage reversal across the inductor, thereby causing it to discharge. The inductor current begins to fall with the slope given by:

$$\Delta I_{L1} = \frac{-(V_{BUS} + V_0(t))}{L_1} \quad (3.10)$$

where V_{BUS} = *Bus voltage w.r.t Neutral*

$V_0(t)$ = *Instantaneous Output Voltage*

$V_{GS}(S2)$ does not exhibit an plateau region like top side MOSFET. This is because before turn ON of S2, the $V_{DS}(S2)$ is already negative voltage drop. Turning ON of S2 makes the voltage across drain to source terminals less negative and clamps it to $I_L^2 R_{DS(ON)}$ drop. Thus, there is no large change in voltage thereby leading to no significant change in $C_{oss}(S2)$.

This mode ends with start of turning OFF process of bottom side MOSFET S2 occurring at t_3 .

Mode 4 (t_3 - t_4):

This is the last mode occurring in positive line half cycle. This mode is exactly similar to Mode 2. Start of turn OFF process of bottom side MOSFET S2 brings the inverter in this mode. As the current through S2 begins to decrease, this causes the discharging inductor current which is still positive to turn ON the body diode of S2 in the search of alternate path to flow. Turning ON of body diode clamps the $V_{DS}(S2)$ to negative diode drop voltage thus enabling ZVS Turn OFF of bottom side MOSFET.

During entire positive half cycle, the bottom side MOSFET is completely soft switched.

Mode 5 – Mode 8 (t_5-t_9):

Mode 5 – Mode 8 are similar to Mode 1- Mode 4. The only difference is that the all the voltage and current transitions occurring on S1 and S2 which was explained in Mode 1- Mode 4 is swapped i.e. S2 in Mode 5-Mode 8 behaves like S1 behaves in Mode 1- Mode 4 and S1 in Mode 5-Mode 8 behaves like S2 behaves in Mode 1-Mode 4. Another difference between these two sets of Modes is that direction if inductor current is negative. Figure 3-10 illustrates the waveforms of Mode 5- Mode 8.

During Mode 5 and Mode 7 the inductor charges and discharges in the negative direction with slopes given in (3.9) and (3.10) respectively. During Mode 6 and Mode 8, the inductor current freewheels through top side MOSFET's body diode.

During Mode 5 – Mode 8, top side switch is completely soft switched.

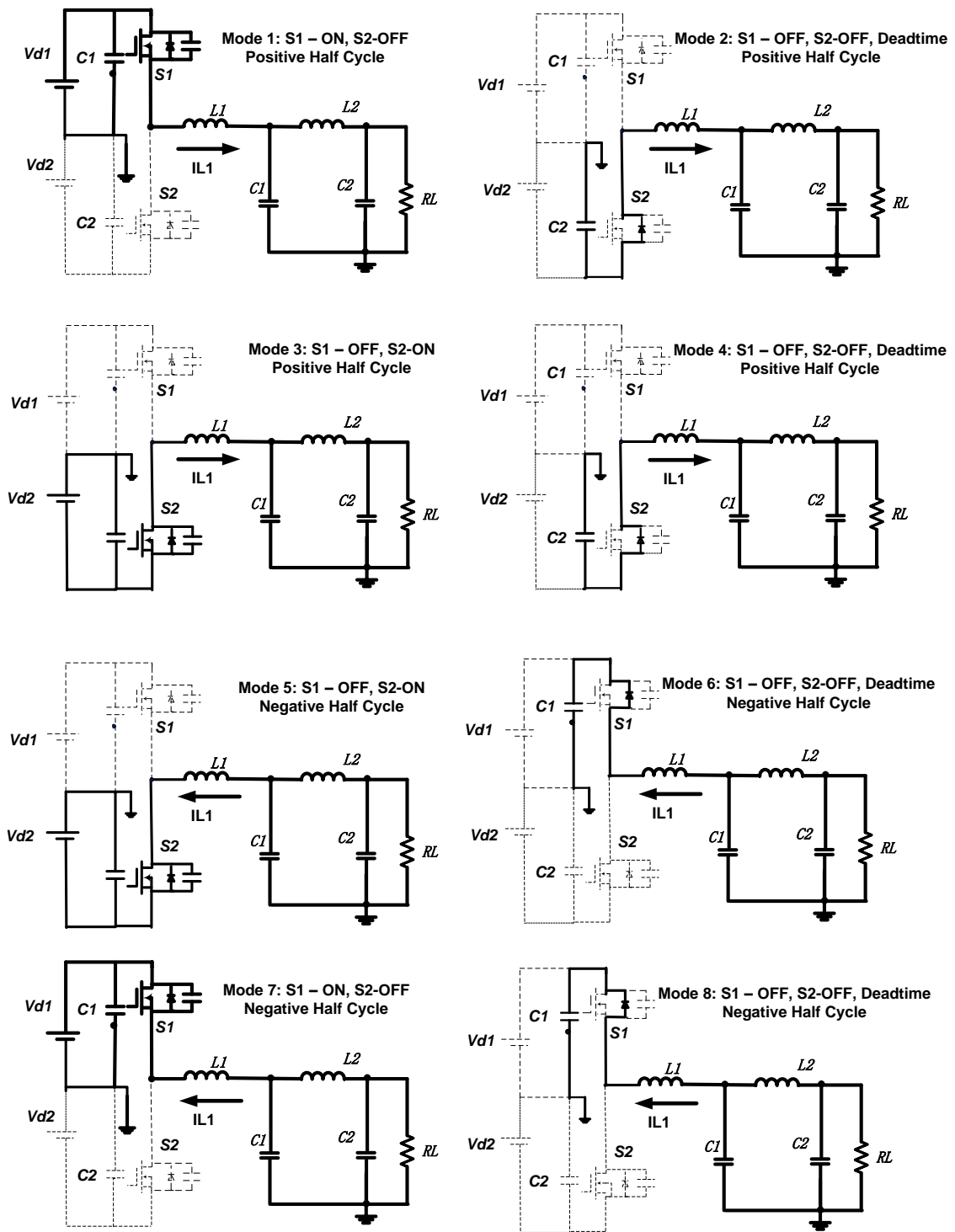


Figure 3-8 Half Bridge Inverter - Operation Modes - Topology

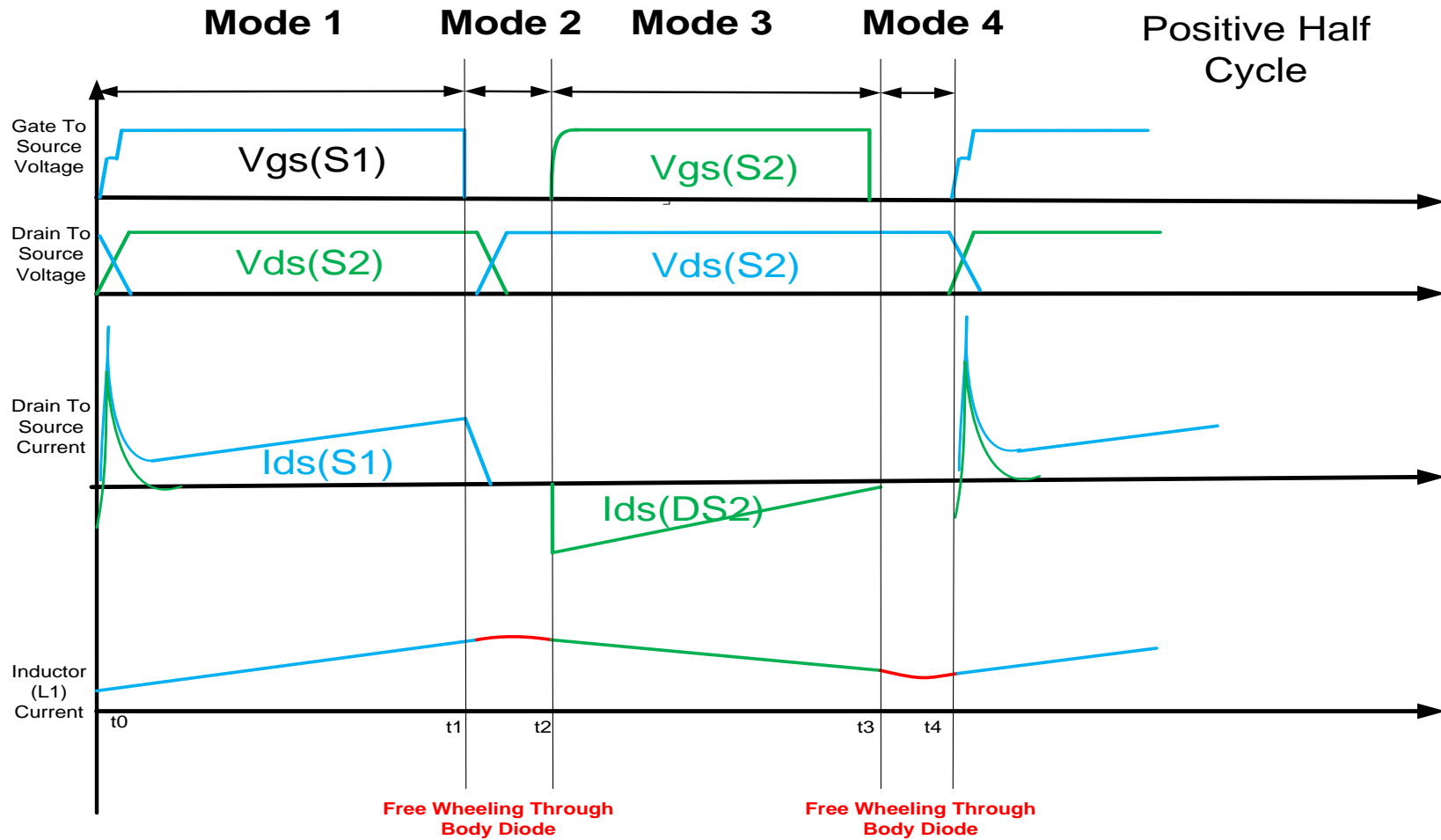


Figure 3-9 Half Bridge Inverter - Operation Mode Waveforms - Positive Half Cycle

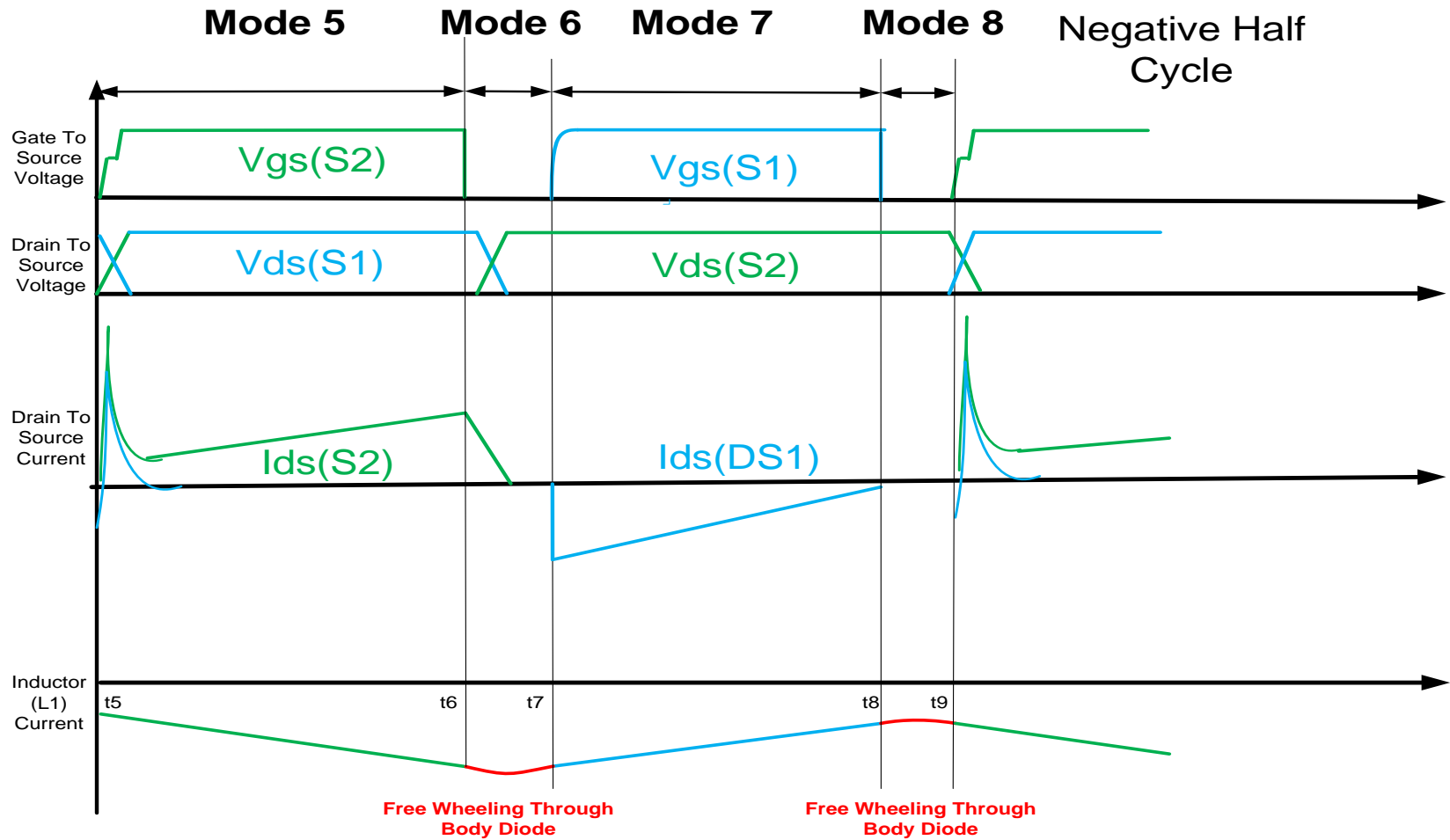


Figure 3-10 Half Bridge Inverter - Operation Mode Waveforms- Negative Half Cycle

3.4.2 Loss Analysis of Half Bridge Inverter:

Following are the main losses occurring in a Half Bridge Inverter:

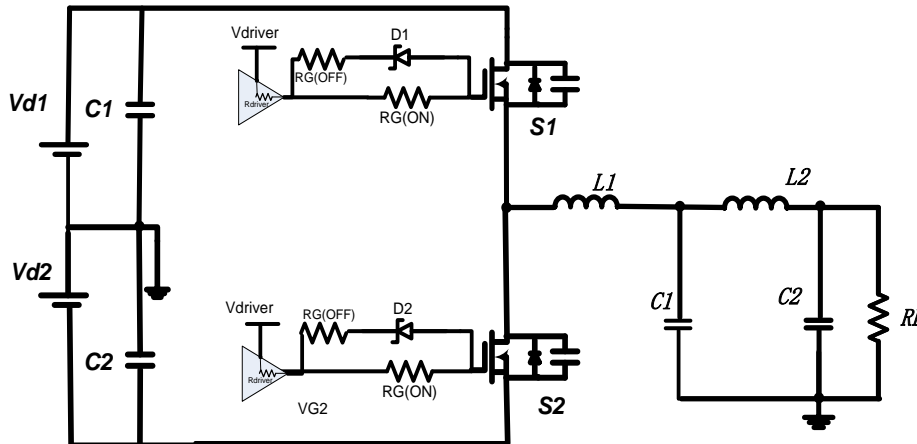


Figure 3-11 Half Bridge Inverter - With Drive Circuit

1. Losses in MOSFETs:

Losses in MOSFETs can be divided into two parts:

a. Switching Losses:

Switching Losses in MOSFETs are composed of 3 entities:

i. Cross Over Losses occurring due to hard switching of the MOSFET:

As one of the two MOSFET is completely soft switched, this loss occurs only in one of the MOSFETS.

Figure 3-12 illustrates the V_{DS} and I_D waveforms during switching transitions in the MOSFET. Looking at the waveform, the cross over losses can be estimated by the following equation in [3.12-3.13]

$$P_{SW \text{ CROSS OVER LOSS}} = 0.5 * V_{BUS \text{ TOTAL}} * I_{OUT \text{ avg}} * (T(ON) + T(OFF)) * f_{SW} \quad (3.11)$$

$$T(ON) = \frac{Q_G}{I_{G \text{ ON}}} \quad (3.12)$$

$$I_{G \text{ ON}} = \frac{V_{Driver} - V_{PL}}{R_{Driver \text{ PULL UP}} + R_{G(ON)}} \quad (3.13)$$

$$T(OFF) = \frac{Q_G}{I_{G \text{ OFF}}} \quad (3.14)$$

$$I_{G \text{ OFF}} = \frac{V_{PL}}{R_{Driver \text{ PULL DOWN}} + R_{G(OFF)}} \quad (3.15)$$

$$I_{OUT \text{ avg}} = \frac{2}{\pi} * I_{OUT \text{ peak}} \quad (3.16)$$

V_{PL} can be extracted from the datasheet of the MOSFET.

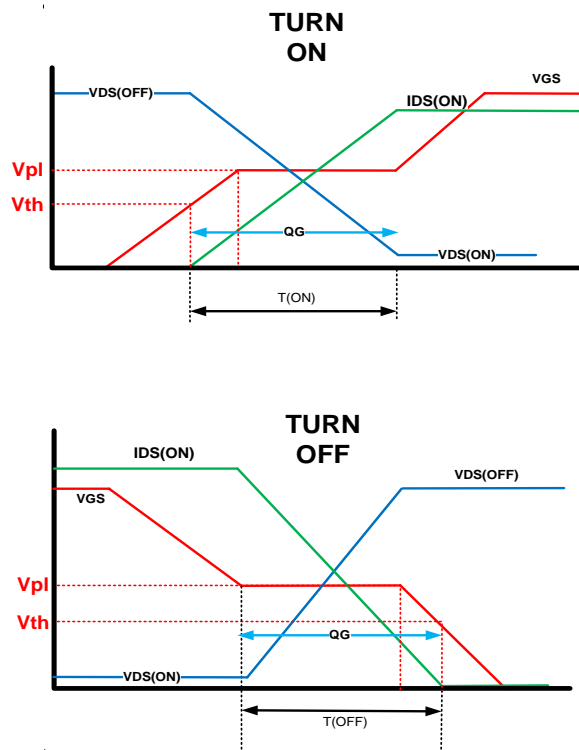


Figure 3-12 MOSFET Switching Waveform

ii. **Conduction Losses:**

Conduction Losses occurring in both MOSFETs are $I^2 R_{DS(ON)}$ losses. These losses can be estimated by:

$$P_{Conduction Loss} = 2 * D_{avg} * I^2_{OUT avg} * R_{DS(ON)} \quad (3.17)$$

$$D_{avg} = 2 * \frac{m}{\pi} \text{ where } m = \text{modulation index} \quad (3.18)$$

b. **Losses occurring due to discharge C_{OSS} :**

This loss occurs due to charge stored in C_{OSS} of the MOSFETs. If both MOSFETs are identical then losses occurring in both MOSFETs due to C_{OSS} discharge can be estimated by the following equation [3.12-3.15]:

$$P_{C_{OSS} Loss} = C_{OSS} * V_{BUS TOTAL}^2 * f_{sw} \quad (3.19)$$

c. Recovery Losses of Body Diode:

One of the body diode turns ON during the dead-time period; turning OFF of this body diode leads to reverse recovery losses. Figure 3-13 shows the reverse recovery phenomenon during positive line half cycle. During positive half cycle, bottom side MOSFET's body diode turns ON during the dead-time. The inverter is operating in MODE4 (refer to figure 3-8). During the transition from MODE 4 to MODE1, the body diode of bottom side MOSFET is turned OFF and it goes through reverse recovery.

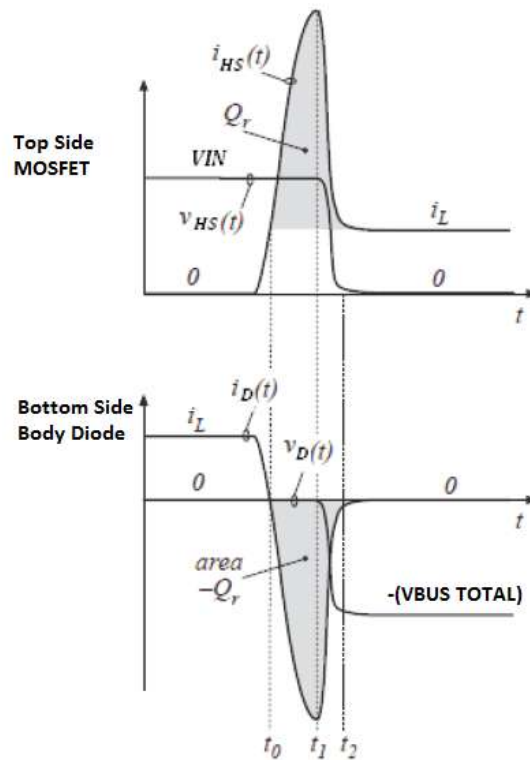


Figure 3-13 Diode Reverse Recovery Waveforms

At any point in the line cycle, body diode of only one of the MOSFETs turns ON. Thus, reverse recovery losses occur in the body diode of only one of the MOSFETs. If both MOSFETs are identical then power loss occurring during the reverse recovery phenomenon can be estimated by a common equation. From figure 3-13 [3.13], it can be seen that reverse recovery phenomenon occurs between t_0 - t_2 , however, the power loss occurs only between t_1 - t_2 as prior t_1 the voltage across the body diode is equal to forward diode voltage drop. Thus, recovery losses can be estimated by

$$P_{Reverse Recovery Loss} = V_{BUS TOTAL} * \frac{I_{rr}}{6} * (t_2 - t_1) * f_{SW} \quad (3.20)$$

2. Drive Losses:

Charging and discharging of input gate capacitance of the MOSFET's causes some dissipation of power across the resistances between the driver and the gate of the MOSFET. This drive loss P_{DRIVER} can be calculated as [3.14]:

$$P_{GATE} = Q_G * V_{DRIVER} * f_{SW} \quad (3.21)$$

3. Body Diode Conduction Loss:

Dead-time is introduced between the complementary gate drives to avoid cross conduction between two switches. During this dead-time, depending upon the half cycle, current is flowing through either of the MOSFET's body diode conducts. Dead-time losses can be estimated by [3.13]:

$$P_{Body Diode Conduction Loss} = Dead - Time * f_{SW} * V_{SD} * I_{OUT avg} \quad (3.22)$$

4. Losses in Magnetics:

Losses occurring in the filter inductor can be divided into 3 entities:

a. Line Frequency Copper Loss:

This is the line frequency conduction loss occurring in the filter inductor. This loss can be estimated by:

$$P_{Line\ Frequency\ Copper\ Loss} = I_{OUT(RMS)}^2 * R_{AC_{L1}(Line\ Frequency)} \quad (3.23)$$

b. Switching Frequency Copper Loss:

This is the switching frequency conduction loss occurring in the filter inductor. This loss can be estimated by:

$$P_{Switching\ Frequency\ Copper\ Loss} = I_{RIPPLE(RMS)}^2 * R_{AC_{L1}(f_{SW})} \quad (3.24)$$

$$where\ I_{RIPPLE(RMS)} = \sqrt{\left(\frac{1}{T} \int_0^T (I_{inductor}(t) - I_{out}(t))^2\right)} \quad (3.25)$$

c. Line Frequency Core Losses:

This is the hysteresis loss occurring in the inductor at line frequency. This loss can be estimated using Steinmetz Relationship as given below:

$$P_{Line\ Freq\ Core\ Loss} = k * f_{line\ freq}^\alpha * B_{peak\ line\ freq}^\beta * V_e \quad (3.26)$$

where k, α, β are function of core material, $V_e =$ Core Volume in cm^3

$$B_{peak\ line\ freq} = \frac{L * I_{OUT\ peak} * 10^{-2}}{N * A_e} \quad (3.27)$$

where $N =$ number of turns,

$A_e =$ Window Area in cm^2 , $L =$ Inductance in μH .

d. Switching Frequency Core Loss:

This is the hysteresis loss occurring in the inductor at switching frequency.

This loss can be estimated using Steinmetz Relationship as given below:

$$P_{\text{Switching Freq Core Loss}} = k * f^{\alpha}_{\text{Switching freq}} * B^{\beta}_{\text{peak switching freq}} * Ve \quad (3.28)$$

where k, α, β are function of core material, $Ve = \text{Core Volume in cm}^3$

$$B_{\text{peak switching freq}} = \frac{L * I_{\text{Ripple(pk)}} * 10^{-2}}{N * A_e} \quad (3.29)$$

where $I_{\text{Ripple(pk)}} = \text{Peak}(I_{\text{inductor}}(t) - I_{\text{OUT}}(t))$, $N = \text{number of turns}$

$A_e = \text{Window Area in cm}^2$, $L = \text{Inductance in } \mu\text{H}$.

3.4.3 Loss Model of Half Bridge Inverter:

Based on the loss analysis in the previous, a loss model for Half Bridge Inverter can be created. This loss model will consist of two entities:

$$P_{\text{Loss}} = P_{\text{Load Independent Loss}} + P_{\text{Load Dependent Loss}} \quad (3.30)$$

1. Load Independent Losses:

Load Independent losses comprises of the losses which are not a function of load current. The losses which fall under this category are:

- a. Diode Recovery Losses $-P_{\text{Reverse Recovery Loss}}$.
- b. C_{OSS} Discharge Losses $P_{\text{Coss Loss}}$.
- c. Drive Losses $P_{\text{DRIVE LOSS}}$.
- d. Switching Frequency Copper Loss $P_{\text{Switching Freq Copper Loss}}$.

e. Switching Frequency Core Loss $P_{\text{Switching Freq Core Loss}}$.

$$P_{\text{Load Independent Loss}} = P_{\text{Reverse Recovery Loss}} + P_{\text{Coss Loss}} + P_{\text{Drive Loss}} + P_{\text{Switching Freq Loss}} + P_{\text{Switching Freq Core Loss}} \quad (3.31)$$

Substituting equations (3.19), (3.20), (3.21), (3.24), (3.28) in equation (3.31) we

get :

$$P_{\text{Load Independent Loss}} = (V_{\text{BUS TOTAL}} * \frac{I_{rr}}{6} * (t_2 - t_1) * f_{sw}) + C_{oss} * V_{\text{BUS Total}}^2 * f_{sw} + I_{\text{RIPPLE(RMS)}}^2 * R_{AC L1}(f_{sw}) + (k * f_{\text{Switching freq}}^\alpha * B_{\text{peak switching freq}}^\beta * Ve) + (Q_G * V_{\text{DRIVER}} * f_{sw}) \quad (3.32)$$

2. Load Dependent Losses:

Load dependent losses are a function of load current. These losses vary with load current. Following losses fall under this category:

- Cross Over Switching Loss $P_{\text{Cross over Switching Loss}}$.
- Switch Conduction Losses $P_{\text{Switch Conduction Loss}}$
- Body Diode Conduction Losses $P_{\text{Body Diode Conduction Loss}}$.
- Line Frequency Core Loss $P_{\text{Line Freq Core Loss}}$.
- Line Frequency Copper Loss $P_{\text{Line Freq Copper Loss}}$.

$$P_{\text{Dependent Loss}} = P_{\text{Cross over Switching Loss}} + P_{\text{Switch Conduction Loss}} + P_{\text{Body Diode Conduction Loss}} + P_{\text{Line Freq Core Loss}} + P_{\text{Line Freq Copper Loss}}. \quad (3.33)$$

Substituting equations (3.11), (3.17), (3.22), (3.23), (3.26) in equation (3.33) we get

$$P_{\text{Dependent Loss}} = (0.5 * V_{\text{BUS TOTAL}} * I_{\text{OUT avg}} * (T(\text{ON}) + T(\text{OFF})) * f_{sw}) + (2 * D_{\text{avg}} * I_{\text{OUT avg}}^2 * R_{DS(\text{ON})}) + (\text{Dead - Time} * f_{sw} * V_{SD} * I_{\text{OUT avg}}) + (I_{\text{OUT(RMS)}}^2 * R_{AC(\text{Line Frequency})}) + (k * f_{\text{line freq}}^\alpha * B_{\text{peak line freq}}^\beta * Ve) \quad (3.34)$$

From equation (3.33) and (3.34) we can get a total loss equation as follows:

$$\begin{aligned}
P_{Loss} = & (V_{BUS\ TOTAL} * \frac{I_{rr}}{6} * (t_2 - t_1) * f_{SW}) + (C_{oss} * V_{BUS\ Total}^2 * f_{SW}) + (I_{RIPPLE(RMS)}^2 * \\
& R_{AC\ L1}(f_{SW})) + (k * f_{switching\ freq}^\alpha * B_{peak\ switching\ frequency}^\beta * Ve) + (0.5 * V_{BUS\ TOTAL} * \\
& I_{OUT\ avg} * (T(ON) + T(OFF)) * f_{SW}) + (2 * D_{avg} * I_{OUT\ avg}^2 * R_{DS(ON)}) + (Dead - \\
& Time * f_{SW} * V_{SD} * I_{OUT\ avg}) + (I_{OUT(RMS)}^2 * R_{AC(Line\ Frequency)}) + (k * \\
& f_{line\ freq}^\alpha * B_{peak\ line\ freq}^\beta * Ve) \tag{3.35}
\end{aligned}$$

Where $D_{avg} = 2 * \frac{m}{\pi}$; $m =$ modulation index

$$I_{RIPPLE(RMS)} = \sqrt{\left(\frac{1}{T} \int_0^T (I_{inductor}(t) - I_{out}(t))^2\right)}$$

k, α, β are function of core material

$$B_{peak\ line\ freq} = \frac{L * I_{OUT\ peak} * 10^{-2}}{N * A_e}$$

where $N =$ number of turns

$A_e =$ Window Area in cm^2 , $L =$ Inductance in μH .

$$B_{peak\ switching\ freq} = \frac{L * I_{Ripple(pk)} * 10^{-2}}{N * A_e}$$

where $I_{Ripple(pk)} =$ Peak($I_{inductor}(t) - I_{OUT}(t)$), $N =$ number of turns

$A_e =$ Window Area in cm^2 , $L =$ Inductance in μH .

$$T(ON) = \frac{Q_G}{I_{G\ ON}}$$

$$I_{G\ ON} = \frac{V_{Driver} - V_{PL}}{R_{Driver\ PULL\ UP} + R_{G(ON)}}$$

$$T(OFF) = \frac{Q_G}{I_{G\ OFF}}$$

$$I_{G\ OFF} = \frac{V_{PL}}{R_{Driver\ PULL\ DOWN} + R_{G(OFF)}}$$

$$I_{OUT\ avg} = \frac{2}{\pi} * I_{OUT\ peak}$$

3.4.4 Verification of Loss Model

The above mentioned loss model was applied to a single phase half bridge inverter with following specifications:

1. Input DC Voltage = 400V.
2. Maximum Power = 130W.
3. Output AC Voltage = 110V (rms).
4. $f_{sw}=20\text{kHz}$.

Following circuit components were used:

1. S1,S2 – FCB20N60F
2. $L1= 3.6\text{mH}$, $R_{AC(60\text{Hz})}=0.273\Omega$, $R_{AC(20\text{kHz})}=12.4\Omega$.
3. L1 Core type – Ferroxcube 42/29 Pot Core, Core Material – PC95.
4. $L2=470\mu\text{F}$, $R_{AC(60\text{Hz})}= 80\text{m}\Omega$.
5. $C1=C2=1\mu\text{F}$.
6. Driver IC – HCPL-3180-360E, $V_{DRIVER}=12\text{V}$, $R_{G(ON)}=22\Omega$, $R_{G(OFF)}=0.05\Omega$.
7. Dead-time = 800nS.
8. Modulation Index = 0.83.
9. $I_{RIPPLE(RMS)}=300\text{mA}$, $I_{RIPPLE(PEAK)}=0.65\text{A}$.

Figure 3-14 and 3-15 shows the load independent and load dependent losses respectively based on application of the proposed loss model to the above mentioned single phase half bridge inverter. Figure 3-17 shows the calculated efficiency single phase half bridge inverter with the above mentioned specifications; obtained from the loss model. In order to verify the accuracy of the model, the calculated results are

compared with the experimental efficiency measurements. From figure 3-17, it can be concluded that loss model calculations closely follow the experimental results and thereby the loss model can be deemed accurate. In this loss analysis and efficiency measurement, drive losses are not accounted for.

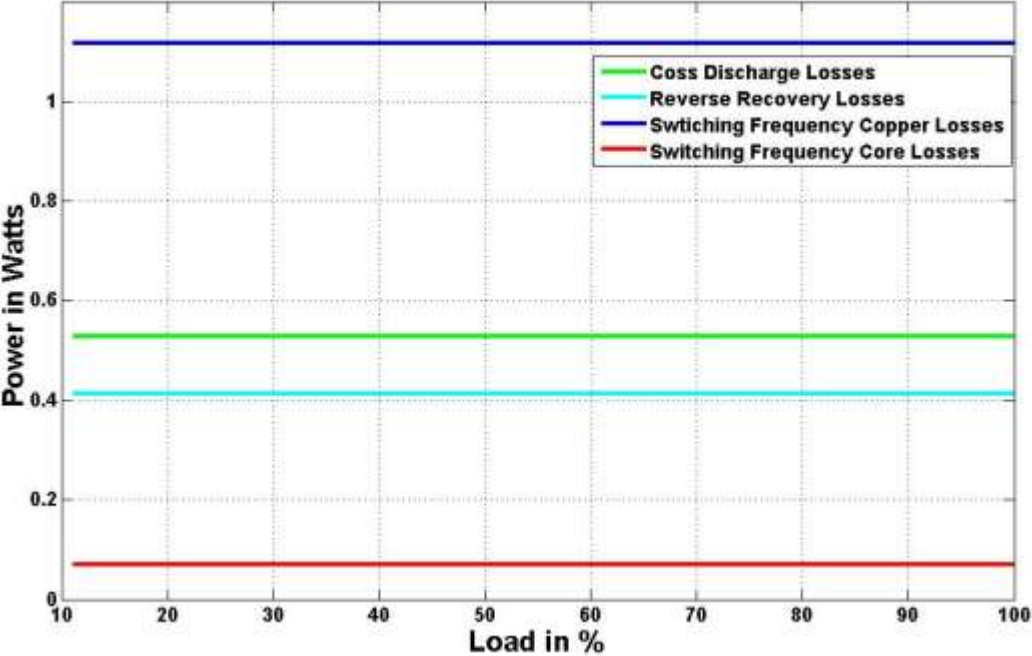


Figure 3-14 Load Independent Losses based on Loss Model, design example

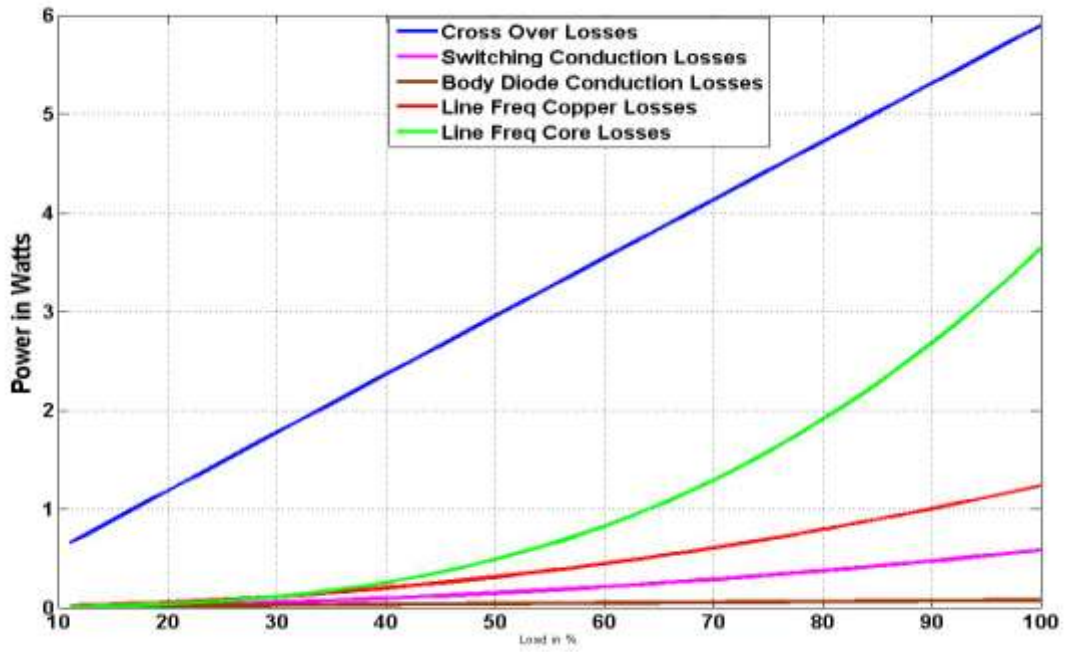


Figure 3-15 Load Dependent Losses based on Loss Model, design example.

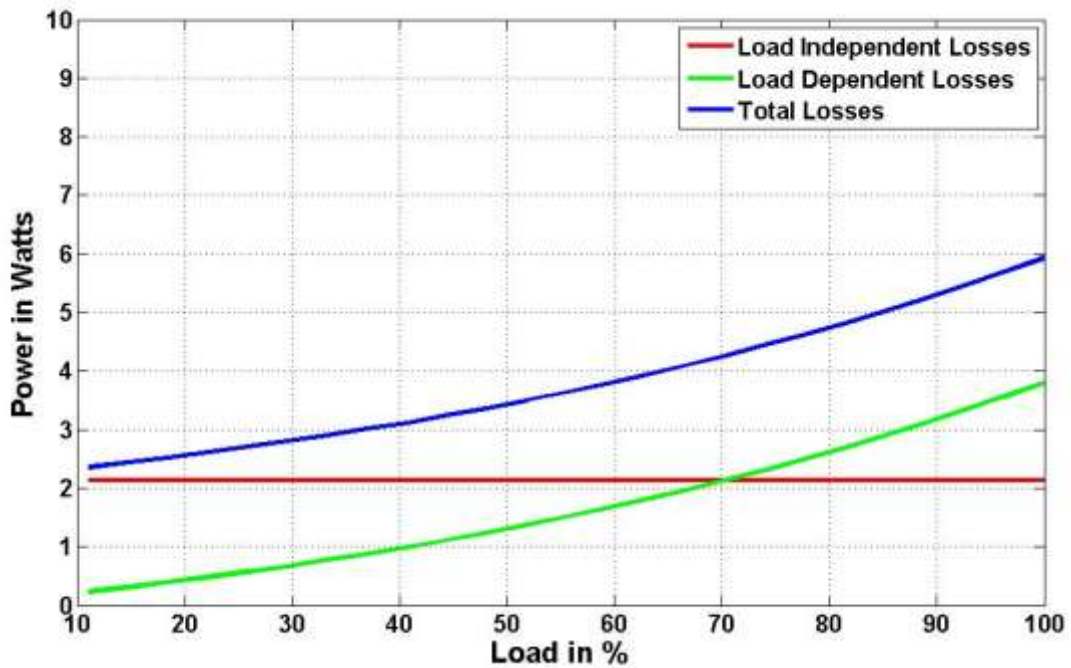


Figure 3-16 Losses in Half Bridge Inverter, design example

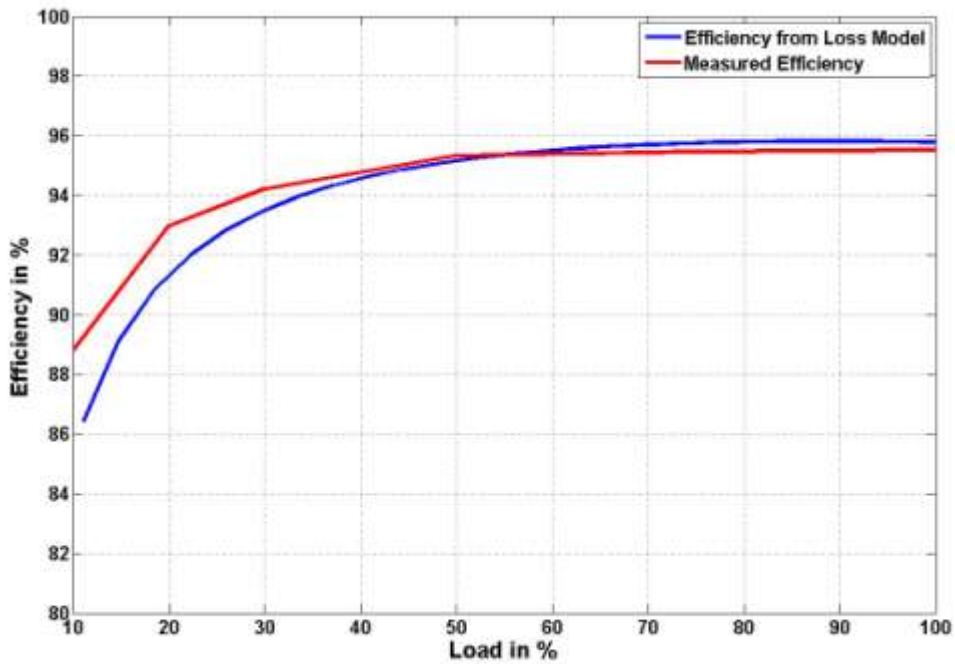


Figure 3-17 Efficiency of Half Bridge Inverter - Loss Model Calculated vs. Experimental

The loss model proposed in the previous section can be easily extended to a Three Phase PWM Half Bridge inverter as shown in figure 3-18.

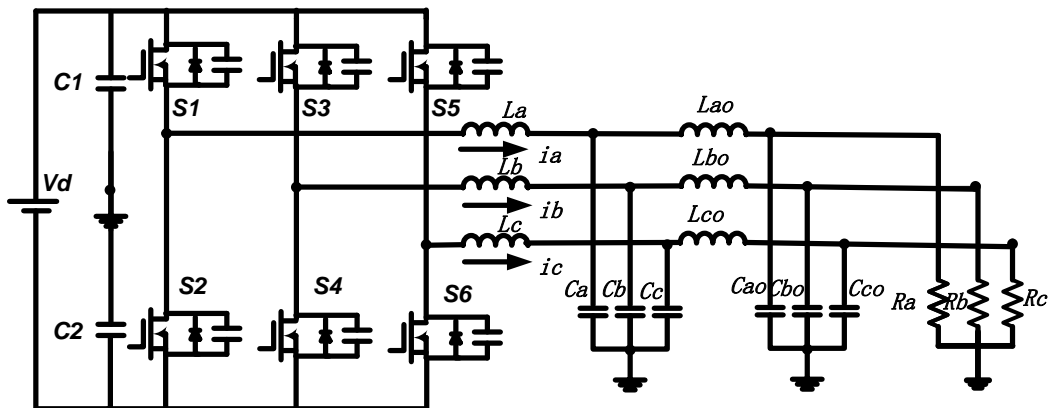


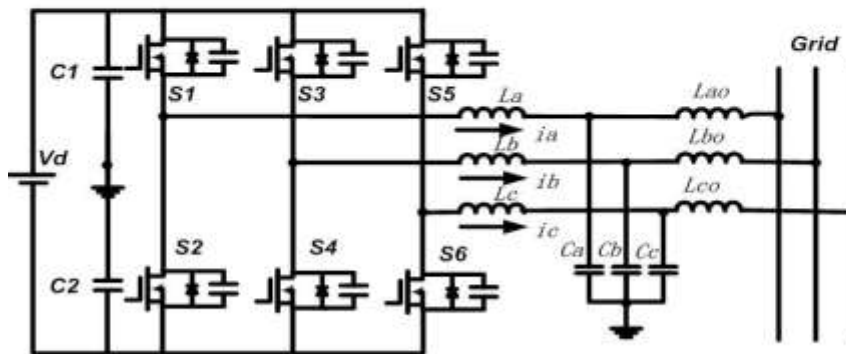
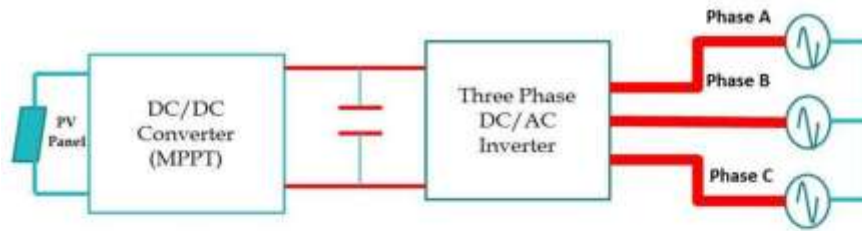
Figure 3-18 Half Bridge Three Phase PWM Inverter

3.5 Phase Skipping Control of Three Phase Micro-Inverter

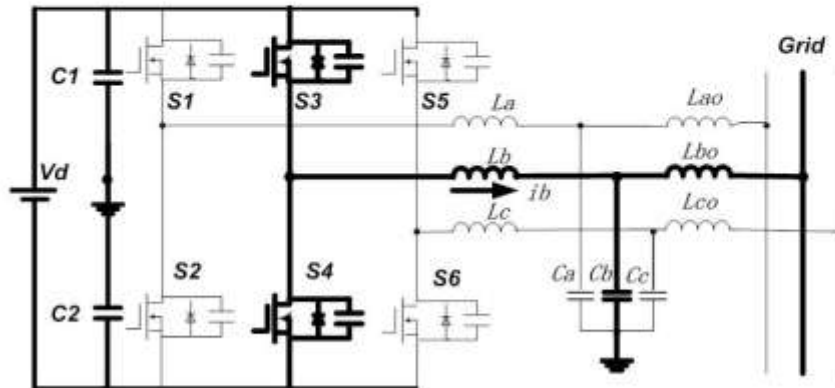
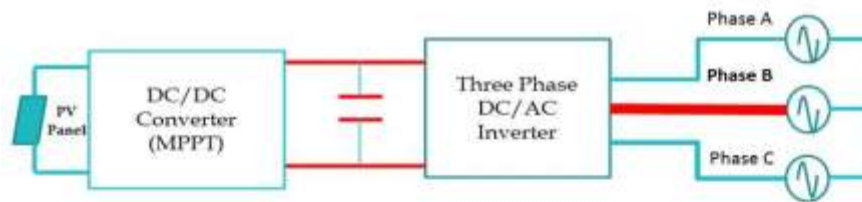
In the previous section, it was proved using theoretical calculations as well as experimental results that efficiency of a Half Bridge Three Phase PWM Inverter drops dramatically at lighter loads. This dramatic drop in the efficiency at lighter loads is caused because of the load independent losses in the inverter. In order to improve the light load efficiency of Grid Tied Three Phase Micro-inverter, *Phase Skipping Control Technique* is proposed.

3.5.1 Concept

Phase Skipping Control technique employs selective injection of power through individual phases depending upon the power available from the PV panel. The micro-controller continuously monitors the power being injected into the grid. Once the power falls below a predetermined threshold, in this case it is 30% of the total power capacity; the micro-controller shuts down two out of three phases. This shutting down of two phases diverts the power from other two phases onto a single phase which now operates at up to 90% instead of 30% of its per phase load capacity. Thus, now the entire available power is converted using only single phase which is operating at up to 90% of its per phase capacity and thereby at efficiency corresponding to up to 90% load. This mode of operation is called *Phase Skipping*. Figure 3-19 describes conceptual operation of *Phase Skipping*. As Grid-Tied Inverters do not have a dedicated load to drive them, selective phase power injection can be applied to them.



(a) Normal Mode – $30\% \leq \text{Load} \leq 100\%$



(b) Phase Skipping Mode – $\text{Load} \leq 30\%$

Figure 3-19 Conceptual Diagram - Normal Mode - Phase Skipping Mode

3.5.2 Implementation of Phase Skipping Control for Three Phase Grid Tied Micro-Inverters

In order to implement the phase skipping control, available input power from the front end MPPT controller is constantly monitored. Once the available power drops below a predefined power level $P_{\text{PHASE SKIPPING}}$ i.e. 30% Load, the on board controller disables the PWM drive to 2 out of 3 phases.

Figure 3-20 shows the implementation scheme for Phase Skipping Control, it can be seen from the figure, that the digital micro-controller constantly monitors the available input power from the MPPT controller. Depending upon the available input power, the micro-controller drives all the 3 phases when available power is greater than 30% of P_{MAX} i.e. Normal Mode of operation or just 1 phase when the available power is less than 30% of P_{MAX} . Figure 3-21 shows the flowchart of the software implementation of Phase Skipping Control Scheme.

Phase Skipping Mode can also be implemented in two stages. Inverter enters into Stage 1 of operation when input power is less than 66% of P_{MAX} . During Stage 1, power is injected through 2 out of 3 phases and thereby disabling only 1 out of 3 phases. When the available power further drops less than 30% of the P_{MAX} , the inverter enters into Stage 2 of operation. During Stage 2, power is injected using just one phase. Efficiency curve of the inverter under consideration determines whether the phase skipping mode is implemented in one stage or two stages. If the efficiency of the inverter starts dropping significantly after 65% load than two stage implementation of

phase skipping mode can be justified. However, if the efficiency drop up to 30% load is not significant enough then the phase skipping mode is implemented using single stage.

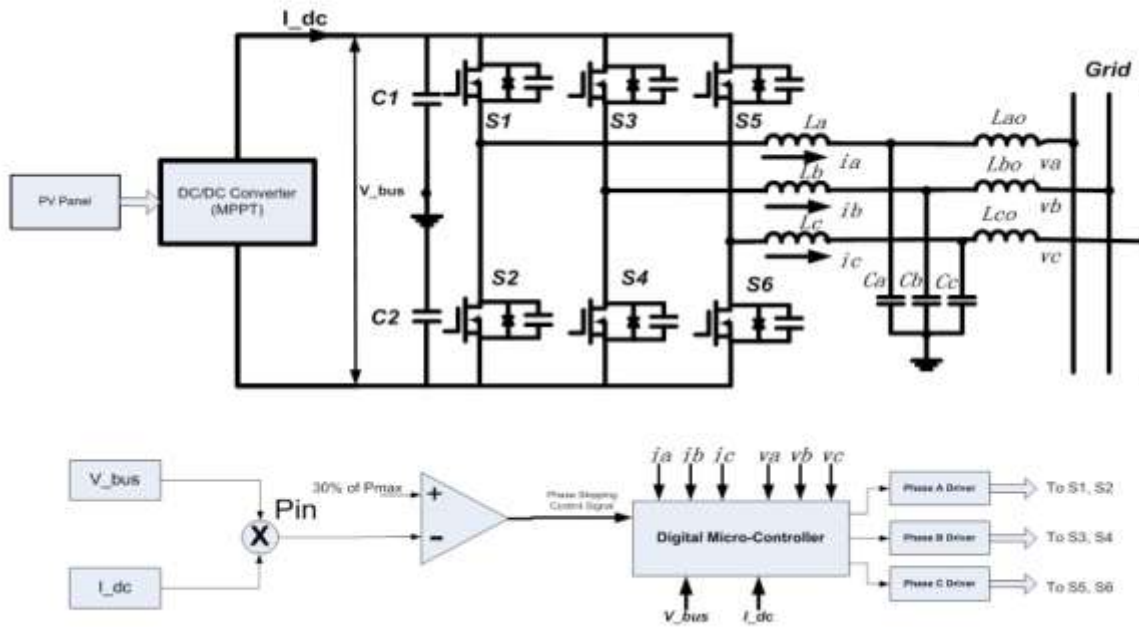


Figure 3-20 Implementation of Phase Skipping Control Scheme- Single Stage

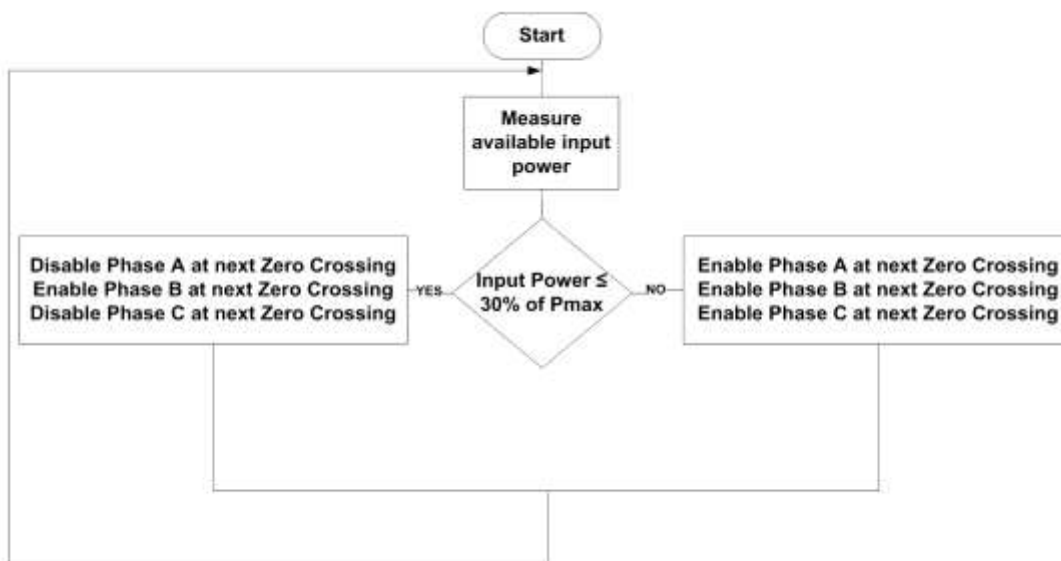


Figure 3-21 Flow Chart of Phase Skipping Control Algorithm-Single Stage

3.5.3 Experimental Results of Phase Skipping Control

Phase Skipping Control is a generic control technique independent of the topology. In order to establish the proof of concept, this control technique was implemented on a DC-AC stage of the prototype as shown in figure 3-22. DC-AC stage is implemented using a Three Phase Half Bridge Inverter with following specifications:

1. Input DC Voltage = 400V.
2. Maximum Output Power = 400W.
3. Output AC Voltage = 110V (rms).
4. $f_{sw}=20\text{kHz}$.

Following circuit components were used:

1. S1, S2, S3, S4, S5, S6 – FCB20N60F
2. $L_a=L_b=L_c= 3.6\text{mH}$, $R_{AC(60\text{Hz})}=0.273\Omega$, $R_{AC(20\text{kHz})}=12.4\Omega$.
3. $L_a=L_b=L_c$ Core type – Ferroxcube 42/29 Pot Core, Core Material – PC95.
4. $L_{ao}=L_{bo}=L_{co}=470\mu\text{F}$, $R_{AC(60\text{Hz})} = 80\text{m}\Omega$.
5. $C_a=C_b=C_c=C_{ao}=C_{bo}=C_{co}=1\mu\text{F}$.
6. Driver IC – HCPL-3180-360E, $V_{DRIVER} = 12\text{V}$, $R_{G(ON)} = 22\Omega$, $R_{G(OFF)}=0.05\Omega$.
7. Dead-time = 800nS.
8. Modulation Index = 0.83.
9. $I_{RIPPLE(RMS)}/\text{phase}=300\text{mA}$, $I_{RIPPLE(PEAK)}/\text{phase}=0.65\text{A}$.

The schematic of the prototype is shown in figure 3-23.

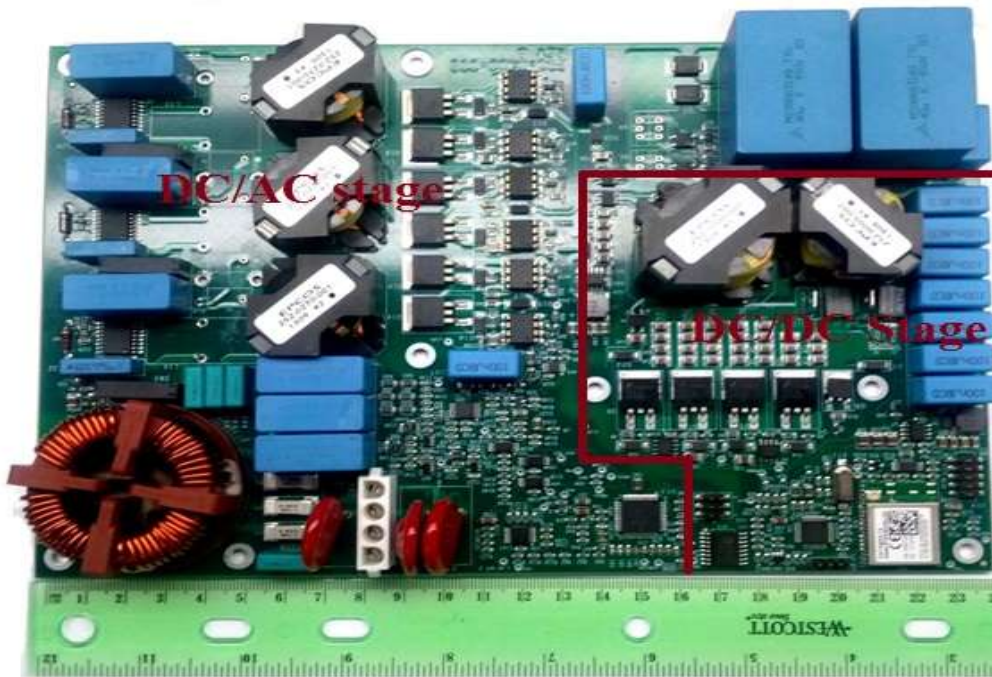


Figure 3-22 Prototype of 400W Three Phase Micro-Inverter

The prototype develop has a front end LLC DC-DC converter. This front-end converter is designed as per the design guidelines in chapter 2. Output of the front-end DC-DC stage is fed to Three Phase Half Bridge PWM Inverter.

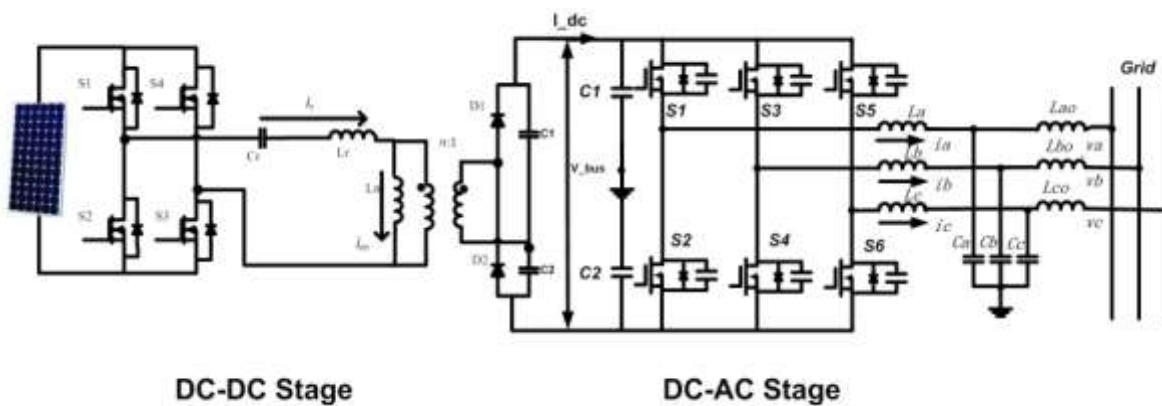


Figure 3-23 Schematic of Three Phase Micro-Inverter

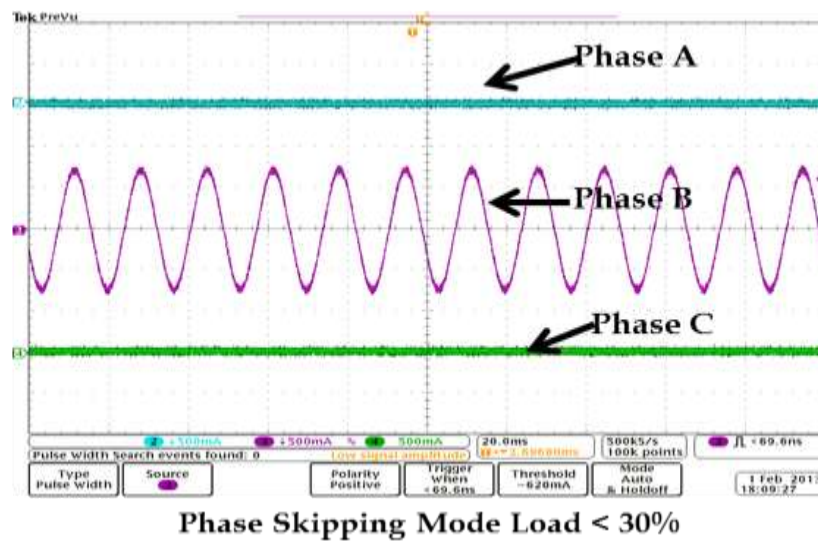
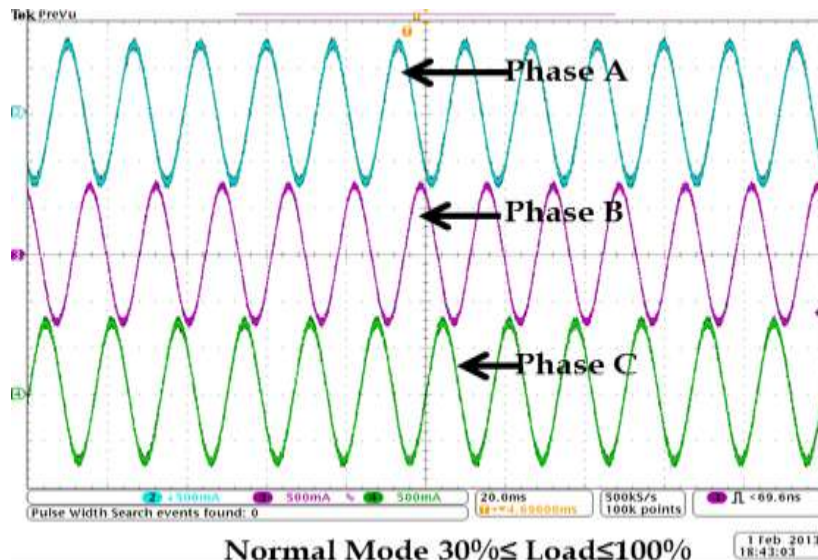
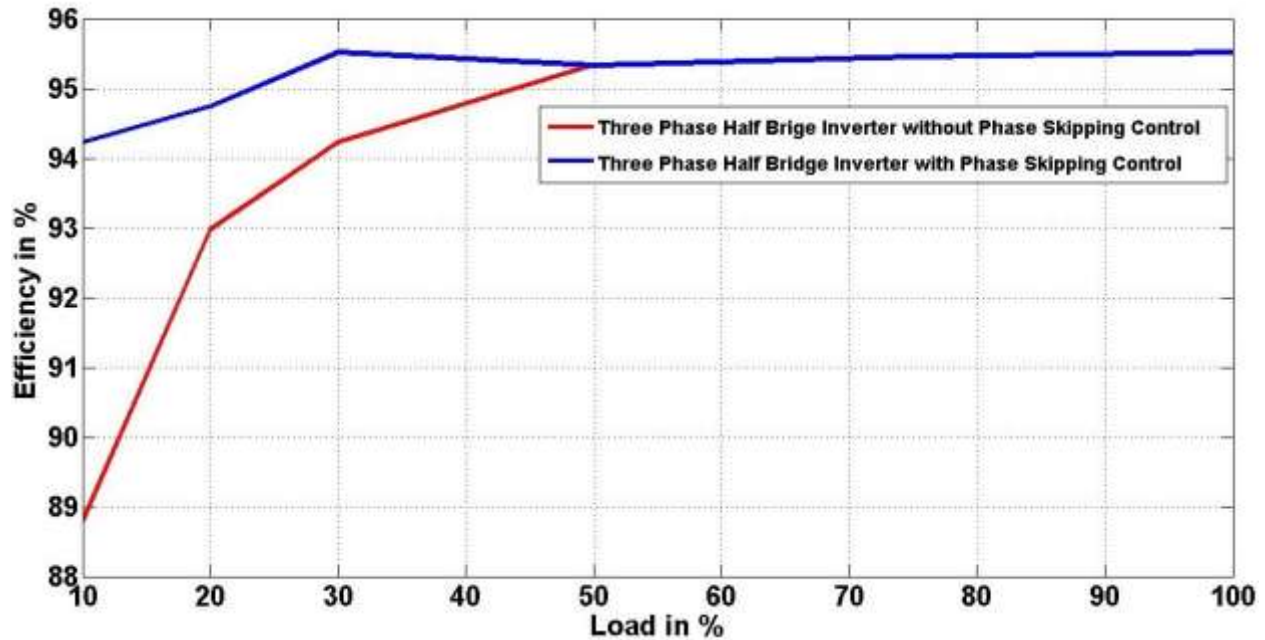


Figure 3-24 Operational Waveforms of Phase Skipping Control

Figure 3-25 shows the efficiency performance of DC-AC stage of the three phase micro-inverter with and without phase skipping control. It can be noted from the efficiency curve that phase skipping control helps to improve light load efficiency (10% load) by more than 5% and CEC efficiency by 0.5% in DC-AC Three Phase Half Bridge PWM Inverters. For PV applications, where inverters operate at less than 50% load for

significant length of their operation time, Phase Skipping Control proves to be a highly beneficial control technique.



1

Figure 3-25 Three Phase Half Bridge Inverter Efficiency with Phase Skipping Control ¹

3.5.4 Avoiding Phase Power Imbalance due to Phase Skipping

Due to selective phase injection of power in phase skipping control technique, when implemented on a Three Phase Micro-Inverter PV farm, there is a possibility of creating a power imbalance amongst the phases. Also according to National Electric Code 705.100 - *Three-phase inverters and 3-phase ac modules in interactive systems shall*

¹ For expediency purposes the efficiency measurements for three phase half bridge PWM inverter were extrapolated from the measurements of single phase. As all three phases are exactly identical, it is safe to assume that such an extrapolation would yield same results as the actual efficiency measurements on all three phases.

have all phases automatically de-energized upon loss of, or unbalanced, voltage in one or more phases unless the interconnected system is designed so that significant unbalanced voltages will not result. Figure 3-26 shows a conceptual diagram of a power imbalance avoidance scheme implemented on a Three Phase Micro-inverter based PV farm implementing Phase Skipping Control. As seen in Chapter 1, every micro-inverter available in the market comes with a communication module. Thus, having a communication module has become a de facto standard for micro-inverter. The proposed scheme to avoid this power imbalance utilizes this communication feature. As shown in figure 3-26, all modules communicate to a centralized controller for diagnostic and telemetry purposes. Under low light conditions, the controller can divide the farm into 3 clusters with each of them injecting power into a particular phase and thereby avoiding power imbalance. In the conceptual diagram, cluster 1 injects power into Phase A; cluster 2 injects power into Phase B and cluster 3 injects power into Phase C. This distributed injection of power ensures balance of the power at the overall farm level. Similar concept can be applied for commercial roof top applications in which case all the micro-inverters with certain distance having fairly uniform solar irradiance conditions are divided into 3 clusters with each of the injecting power into a particular phase during low irradiance conditions.

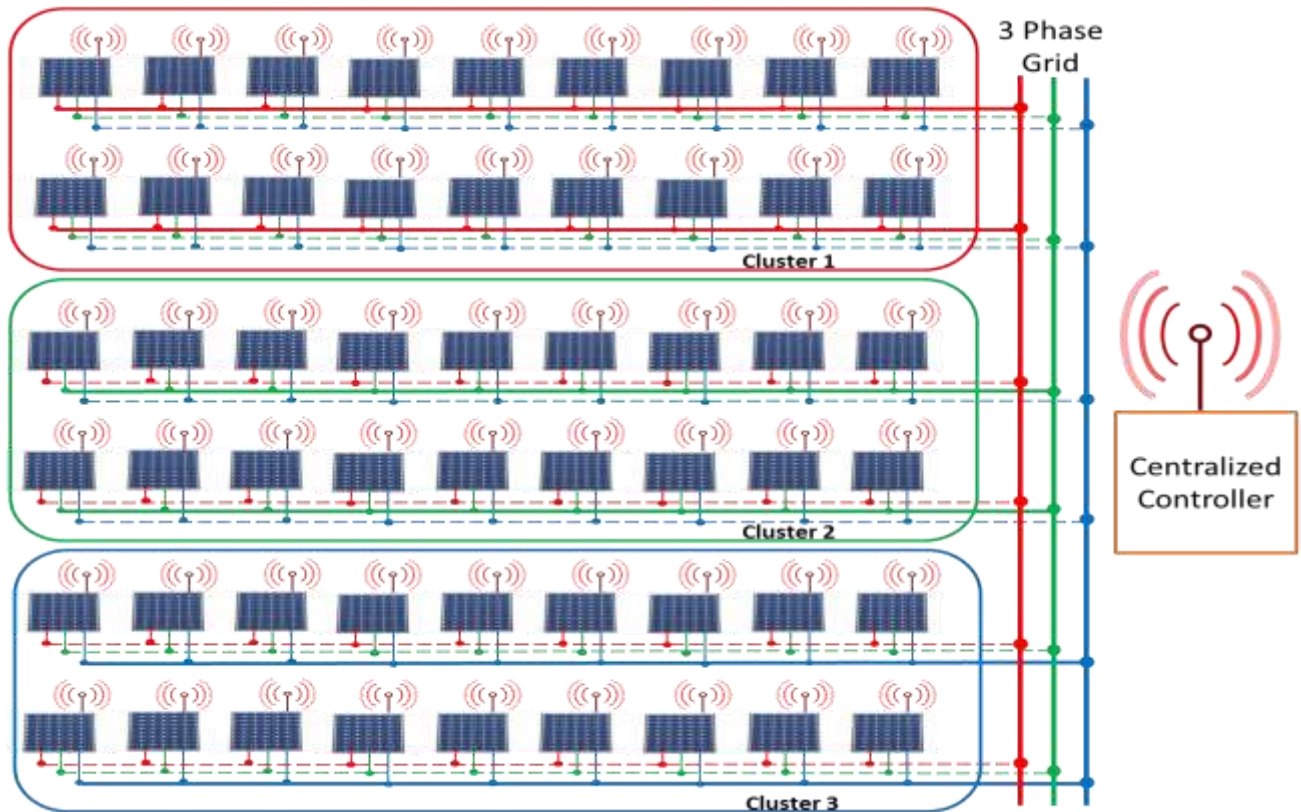


Figure 3-26 Avoiding Power Imbalance amongst Phases due to Phase Skipping Control – Concept

3.6 References

- 3.1 Matlab Documentation Center; *Function* : *Gausswin*. Retrieved from <http://www.mathworks.com/help/signal/ref/gausswin.html>
- 3.2 Overall Efficiency of Photovoltaic Inverters, EN50530.
- 3.3 Yungtaek Jang; Jovanovic, M.M.; Dillman, D.L., "Light-Load Efficiency Optimization Method," *Applied Power Electronics Conference and Exposition*,

2009. *APEC 2009. Twenty-Fourth Annual IEEE* , vol., no., pp.1138,1144, 15-19 Feb. 2009

- 3.4 H. S. Choi and D. Y. Huh, "Techniques to minimize power consumption of SMPS in standby mode," in *IEEE Power Electron. Spec. Conf. (PESC) Rec.*, 2005, pp. 2817–2822.
- 3.5 P. Vinciarelli, "Adaptive boost switching preregulator and method," U.S. Patent 5 289 361, Feb. 22, 1994.
- 3.6 S. W. Hobrecht and R. G. Flatness, "Multiple phase switching regulators with stage shedding," U.S. Patent 6 674 274, Jan. 6, 2004.
- 3.7 J. Choi, D. Huh, and Y. Kim, "The improved burst mode in the stand-by operation of power supply," in *Proc. IEEE Appl. Power Electron. Conf. (APEC)* 2004, pp. 426–432.
- 3.8 Mulligan, M.D.; Broach, B.; Lee, T.H., "A constant-frequency method for improving light-load efficiency in synchronous buck converters," *Power Electronics Letters, IEEE* , vol.3, no.1, pp.24,29, March 2005.
- 3.9 Byung-Duk Min; Jong-Pil Lee; Jong-Hyun Kim; Tae-Jin Kim; Dong-Wook Yoo; Eui-Ho Song, "A New Topology With High Efficiency Throughout All Load Range for Photovoltaic PCS," *Industrial Electronics, IEEE Transactions on* , vol.56, no.11, pp.4427,4435, Nov. 2009.
- 3.10 Zhe Zhang; Min Chen; Mingzhi Gao; Qiong Mo; Zhaoming Qian, "An optimal control method for grid-connected photovoltaic micro-inverter to improve the

efficiency at light-load condition," *Energy Conversion Congress and Exposition (ECCE), 2011 IEEE* , vol., no., pp.219,224, 17-22 Sept. 2011.

- 3.11 Lucia, O.; Burdio, J.-M.; Barragán, L.A.; Acero, J.; Carretero, C., "Series resonant multi-inverter with discontinuous-mode control for improved light-load operation," *IECON 2010 - 36th Annual Conference on IEEE Industrial Electronics Society* , vol., no., pp.1671,1676, 7-10 Nov. 2010
- 3.12 Klein, John;; *AN-6005 Synchronous Buck MOSFET loss calculations with Excel Model*; Fairchild Semiconductor Technical Application Note.
- 3.13 Jauregui, David; Wang, Bo; Chen, Rengang (July 2011); *Power Loss Calculation with Common Source Inductance Consideration for Synchronous Buck Converters*; Texas Instruments Application Report.
- 3.14 Depew, Joseph; *AN 1471 - Efficiency Analysis of Synchronous Buck Converter using Microsoft Excel Based Loss Calculator*; Microchip Application Note.
- 3.15 Haibing Hu; Al-Hoor, W.; Kutkut, N.H.; Batarseh, I.; Shen, Z.J., "Efficiency Improvement of Grid-Tied Inverters at Low Input Power Using Pulse-Skipping Control Strategy," *Power Electronics, IEEE Transactions on* , vol.25, no.12, pp.3129,3138, Dec. 2010

CHAPTER 4: CHAPTER FOUR: CONCLUSIONS AND FUTURE WORK

This chapter summarizes and concludes the findings of this thesis. Essence of each chapter is summarized and findings of each chapter are stated. Based on the findings presented in the thesis, further opportunities of research are identified and stated under the section of future work.

4.1 Conclusions

Growing population and growing GDP is continuously driving the demand of energy. Limited nature of fossil fuel reserves, environmental impacts of burning of fossil fuels and political conflicts with oil producing nations have led humankind to evaluate non-conventional sources of energy. Based on investment trends in different non-conventional sources of energy it can be stated that Solar Energy is the most popular clean energy alternative pursued by the world. Apart from corroborating the above claims with statistical data, Chapter 1 gives an overview of types of Solar PV systems in operation. It focuses on Grid Tied Inverter PV system and illustrates different types of Grid Tied PV System architectures. After a relative comparison of four different types of Grid Tied PV System architectures, this chapter focuses on the most recent and upcoming PV system architecture for high power roof top and low power PV farm applications i.e. AC Module Type Inverter or Micro-Inverters. Furthermore, the existing single phase micro-inverters in the market are evaluated and the trends in micro-inverter business are listed. Having evaluated single phase micro-inverters and their

implementation in three phase systems, the need of a true Three Phase Micro-Inverter is established.

The two most important blocks of a Three Phase Micro-Inverter are:

1. Front End DC-DC Converter.
2. Output Side DC-AC Inverter.

Chapter 2 deals with Front End DC–DC Converter. This chapter states the I-V behavior of PV Panel under different irradiance and temperature conditions. From PV panel's I-V characteristics it is concluded that every PV panel has an optimal voltage level known as Maximum Power Point Voltage (V_{MPP}), at which maximum power can be extracted from the PV panel. This maximum power point voltage has a minimum variance with respect to irradiance levels but varies significantly with change in temperature. Thus, in other words it can be said that at a constant operating temperature the voltage at which maximum power can be extracted is independent of the available power. This behavior in PV panels establishes an optimal design factor of front-end DC-DC converter i.e. at a constant temperature the input voltage of the front end DC-DC converter is fairly independent (variation is very small) of the load.

Resonant LLC Converter is evaluated as a front end DC-DC converter. Based on the operation modes of the LLC Converter, it is established that

1. Resonant frequency operating point is the most efficient operating point of LLC converter.
2. DC gain at resonant frequency is independent of the load current.

From the operational characteristics of LLC converter and the observations from I-V characteristics of PV panel, an optimal design procedure for resonant parameters of the LLC converter as a front end DC-DC converter for PV applications is proposed. It is proved using mathematical model of PV panel and gain model of LLC converter that resonant parameters obtained using the proposed design procedure ensures operation of LLC converter at resonant frequency while operating at maximum power point at room temperature of 25°C.

Chapter 3 focuses upon the output DC-AC stage of the micro-inverter. In this chapter, based on Solar Irradiance patterns obtained from National Renewable Energy Laboratory, it is established that a PV micro-inverter operates at less than 50% of its maximum power capacity for a significant period of time. In order to maximize the extraction of power from PV panels, it is of utmost importance to convert this power at highest possible efficiency. Typically a power converter has higher efficiency at heavier loads and poorer efficiency at lighter loads. The factor degrading the light load efficiency is the constant load independent losses occurring in a power converter. This claim has been proved by analyzing the losses of a half bridge PWM inverter using the proposed loss model. A prototype of half bridge PWM

inverter is developed and is analyzed using the proposed loss model. The accuracy of the proposed loss model has been verified by comparing the efficiency results of the loss model with experimental results obtained from the efficiency measurement performed on the prototype.

Since solar micro-inverters are expected to operate over its entire load range there is a need to boost the light load efficiency of the micro-inverters. *Phase Skipping Control* technique has been proposed to improve the light load efficiency of the DC-AC stage of the Three Phase Micro-Inverter. Phase Skipping Control selectively shuts down 2 out of 3 phases of the DC-AC stage of the Three Phase Micro-Inverter at lighter loads. This shutting down of phases diverts the available power flow from other phases onto a single phase, thereby causing a single phase to operate at higher per phase load capacity which converts the available power at higher efficiency corresponding to heavier load rather than operating all three phases at lighter load and correspondingly at a lower efficiency. In other words, Phase Skipping Control eliminates the load independent losses of the two phases at lighter loads.

Phase Skipping Control is a generic control technique independent of the topology. In order to establish the proof of concept, this control technique has been implemented on a Three Phase Half Bridge PWM Inverter. Experimental results demonstrate an improvement in light load efficiency(10% Load) of the three phase

half bridge PWM inverter by 5% and an improvement in the CEC efficiency of the DC-AC stage by 0.5%. Furthermore, the chapter introduces a technique at conceptual level to avoid power imbalance between the phases due to selective injection of power into one of the three phases caused due to implementation of Phase Skipping Control on three phase micro-inverters.

4.2 Future Work

In this thesis, techniques to improve efficiency of both stages of micro-inverter i.e. front end DC-DC Converter and Output DC-AC inverter have been proposed. Based on the conclusions of the findings of this thesis, opportunities for the future research can be stated.

4.2.1 Future Work for LLC Converter as front end DC-DC Converter

An optimal design procedure for LLC Converter as front end DC-DC converter for PV applications has been proposed. However based on this design procedure, the converter operates at highest possible efficiency only at fixed input voltage or in other words at a constant panel temperature. Further optimization needs to be done in order to operate LLC converter at high efficiency over its entire operating temperature range.

4.2.2 Future Work for Phase Skipping Control

In order to avoid power imbalance amongst phases due to selective injection of power in phase skipping control, a technique has been suggested at a conceptual level in chapter 3. Detailed implementation of proposed technique or some other technique is needed to avoid power imbalance amongst phases caused by selective injection of power in phase skipping control of three phase micro-inverters.